

**NOVEL RUTHENIUM COMPLEXES FOR DYE
SENSITIZED SOLAR CELL**

CHONCHANOK TALODTHAISONG

A THESIS SUBMITTED IN PARTIAL FULFILLMENT OF THE REQUIREMENTS

FOR THE DEGREE OF MASTER OF SCIENCE

MAJOR IN CHEMISTRY

FACULTY OF SCIENCE

UBON RATCHATHANI UNIVERSITY

ACADEMIC YEAR 2015

COPYRIGHT OF UBON RATCHATHANI UNIVERSITY



UBON RATCHATHANI UNIVERSITY
THESIS APPROVAL
MASTER OF SCIENCE
IN CHEMISTRY FACULTY OF SCIENCE

TITLE NOVEL RUTHENIUM COMPLEXES FOR DYE SENSITIZED SOLAR CELL

AUTHOR MR. CHONCHANOK TALODTHAISONG

EXAMINATION COMMITTEE

PROF. DR. SUJITTRA YOUNGME

CHAIRPERSON

ASST. PROF. DR. RUKKIAT JITCHATI

MEMBER

ASST. PROF. DR. KITTIYA WONGKHAN

MEMBER

ADVISOR

Rukkiat Jitchati
.....

(ASST. PROF. DR. RUKKIAT JITCHATI)

Utith Inprasit
.....

(ASSOC. PROF. DR. UTITH INPRASIT)
DEAN, FACULTY OF SCIENCE

A. Pongrat
.....

(ASSOC. PROF. DR. ARIYAPORN PONGRAT)
VICE PRESIDENT
FOR ACADEMIC AFFAIRS

COPYRIGHT OF UBON RATCHATHANI UNIVERSITY

ACADEMIC YEAR 2015

ACKNOWLEDGMENTS

I would like to acknowledge my advisor, Asst.Prof.Dr.Rukkiat Jitchati, for allowing me to undertake this project, all the brilliant ideas, his enthusiasm, advice and guiding me throughout the years. Thank for his support, patience, and encouragement throughout my graduate studies. It is not often that one finds an advisor and colleague that always finds the time for listening to the little problems and roadblocks that unavoidably crop up in the course of performing research. His technical and editorial advice was essential to the completion of this dissertation and has taught me innumerable lessons and insights on the workings of academic research in general. His advice was most valuable to understand the obtained results and to determine the next steps for the research presented in this thesis.

I would like to thanks many people who contributed their time and their advice. Thank to Asst. Prof. Dr. Kittiya Wongkhan for advice and support me in every problem especially in English and for writing my publication. Asst. Prof. Dr. Taweesak Sudyoadsuk, who set the instruments for the device measurement and for his guidance on the DSSCs fabrication. Assoc. Prof. Dr. Sayant Saengsuwan for TGA and DSC data. Dr. Pongsathorn Tongkasee and Dr.Narid Prachumrak are responsible for the device on the fabrication of all DSSCs presented in my work as well as for sharing their chemistry with me. I am very thankful to Department of Physics, Faculty of Science Ubon Ratchathani University for XRD and AFM measurement. I want to acknowledge The National Research Council of Thailand (NRCT), Science Achievement Scholarship of Thailand (SAST) and Ubon Ratchathani University for providing financial support for this work.

Special thanks to everyone in our group for contributed and helped me to make this research work possible at Ubon Ratchathani University. In particular, thanks outside of chemistry goes to my best friend. Finally, I must thank my family for their love and personal support during my study.

Chonchanok Talodthaisong

Chonchanok Talodthaisong

Researcher

บทคัดย่อ

เรื่อง : สารเชิงซ้อนของโลหะรูทีเนียมชนิดใหม่เพื่อเป็นสีย้อมไวแสงสำหรับเซลล์พลังงานแสงอาทิตย์

ผู้วิจัย : ชนม์ชนก ตลอดไธสง

ชื่อปริญญา : วิทยาศาสตรมหาบัณฑิต

สาขาวิชา : เคมี

อาจารย์ที่ปรึกษา: ผู้ช่วยศาสตราจารย์ ดร.รักเกียรติ จิตคตติ

คำสำคัญ : DSSC, N3, เซลล์แสงอาทิตย์

วิทยานิพนธ์เล่มนี้ เป็นการศึกษาสารเชิงซ้อนของโลหะรูทีเนียมสำหรับเซลล์พลังงานแสงอาทิตย์ชนิดสีย้อมไวแสง โดยแบ่งออกเป็นสองส่วน คือ ส่วนที่ 1 ศึกษาสารสีย้อม N3 ที่สังเคราะห์ (N3-2 ถึง N3-5) เปรียบเทียบกับ N3 มาตรฐาน (N3-1) สำหรับการพิสูจน์เอกลักษณ์ทางโครงสร้างของ N3 พบสัญญาณ ^1H NMR ของอะโรมาติกที่เหมือนกัน อย่างไรก็ตาม ค่าร้อยละของน้ำหนักที่หายไปที่อุณหภูมิต่ำกว่า $100\text{ }^{\circ}\text{C}$ (%WL₁₀₀) ของ N3 ทุกตัว ได้รับการยืนยันจากการวิเคราะห์สมบัติความเสถียรทางความร้อน โดยมีลำดับของ %WL₁₀₀ ดังนี้ N3-1 > N3-5 > N3-3 > N3-2 > N3-4 ซึ่งสอดคล้องกับค่าอัตราส่วนของ OH/C=O ที่ได้จากการวิเคราะห์ด้วยเทคนิค FTIR ประสิทธิภาพรวมของเซลล์แสงอาทิตย์ของ N3 มีค่าที่แตกต่างกัน ตั้งแต่ร้อยละ 4.54 ถึง 5.92 ลำดับของค่าประสิทธิภาพนี้สอดคล้องกับลำดับข้อมูลที่ได้จาก TGA และ FTIR ซึ่งสรุปได้ว่า เมทานอลและน้ำที่ตกค้างใน N3 ช่วยเพิ่มสมบัติการละลายอันส่งผลต่อจำนวนโมเลกุลของ N3 ที่เกาะบนผิว TiO₂ นำไปสู่ค่าประสิทธิภาพที่มากขึ้น ส่วนที่ 2 ของวิทยานิพนธ์ คือ ศึกษาสารเชิงซ้อนรูทีเนียมชนิดใหม่ที่มีสายโซ่แอลคิลในลิแกนด์ของสารเชิงซ้อนรูทีเนียมที่ยาวแตกต่างกัน ได้แก่ เมทิล (CLC-C01), เฮกซิล (CLC-C06) และ ออกทิล (CLC-C08) ประสิทธิภาพเซลล์แสงอาทิตย์จาก CLC-C01, CLC-C06 และ CLC-C08 ให้ค่าเท่ากับร้อยละ 3.08, 3.18 และ 3.14 ตามลำดับ เทียบกับสารมาตรฐาน N719 ซึ่งมีค่าเท่ากับร้อยละ 7.80 นอกจากนี้ยังพบว่าสายโซ่เฮกซิล และออกทิล ของสีย้อมไวแสงชนิดใหม่ แสดงความเสถียรที่ดีต่ออายุการใช้งานของเซลล์แสงอาทิตย์ (1000 ชั่วโมง)

ABSTRACT

TITLE : NOVEL RUTHENIUM COMPLEXES FOR DYE SENSITIZED
SOLAR CELL
AUTHOR : CHONCHANOK TALODTHAISONG
DEGREE : MASTER OF SCIENCE
MAJOR : CHEMISTRY
ADVISOR : ASST. PROF. RUKKIAT JITCHATI, Ph.D.
KEYWORDS : DSSC; N3; SOLAR CELL

This thesis shows the study of ruthenium complexes for DSSCs which are spitted into two parts. Part I is the study of synthesized N3s (N3-2 to N3-5) compared with the commercial N3 (N3-1). For N3s characterization, the same aromatic ¹H NMR spectra were observed. However, the different %weight loss below 100 °C (%WL₁₀₀) in all N3s were confirmed from the thermogravimetric analysis (TGA). The order of %WL₁₀₀ are N3-1 > N3-5 > N3-3 > N3-2 > N3-4 that corresponds to OH/C=O ratio determined from FTIR. The DSSCs power conversion efficiencies (η) are varied from 4.54% to 5.92%. The order of the efficiency is in agreement with the TGA and FTIR data. It was concluded that methanol and water residuals in N3s improved the solubility that affected to the number of N3 molecules on the TiO₂ surface leading to high efficiency. Part II is the study of new ruthenium complexes with different alkyl chains length in the ligands of ruthenium complex, which are methyl (CLC-C01), hexyl (CLC-C06) and octyl (CLC-C08). The DSSCs efficiency for CLC-C01, CLC-C06 and CLC-C08 are 3.08%, 3.18% and 3.14%, respectively, compared with standard N719 (7.80%). The hexyl and octyl chains of new dyes show excellent long term stability (1000 h).

CONTENTS

	PAGES
ACKNOWLEDGMENTS	I
ABSTRACT IN THAI	II
ABSTRACT IN ENGLISH	III
CONTENTS	IV
LIST OF TABLES	VI
LIST OF FIGURES	VII
LIST OF ABBREVIATIONS	XI
CHAPTER 1 INTRODUCTION	
1.1 Importance in research and development	1
1.2 Dye-sensitized solar cells	1
1.3 Compositions of DSSC	2
1.4 Principle of DSSCs	5
1.5 The performances of DSSC	6
1.6 Type of dye sensitizer	7
1.7 Objectives of thesis	14
CHAPTER 2 LITERATURE REVIEWS	
2.1 Literature reviews	15
CHAPTER 3 EXPERIMENTAL	
3.1 Chemicals	23
3.2 Instruments and general chemical characterization techniques	25
3.3 Experimental section	27
3.4 Ligand and ruthenium(II)cymene synthesis	28
3.5 The synthesis of bis(4,4'-dicarboxy-2,2'-bipyridine) dithiocyanato ruthenium(II), (N3s)	29
3.6 The synthesized a new ruthenium complexes dye by using new ligands for DSSC	30

CONTENTS (CONTINUED)

	PAGES
3.7 The synthesis a new ruthenium complexes dye	34
3.8 Fabrication of DSSC devices using N3s as sensitizer	37
3.9 Fabrication of DSSC devices using N719, CLC-C01, CLC-C006 and CLC-C08 as sensitizer	41
3.10 DSSCs characterization	41
CHAPTER 4 RESULTS AND DISCUSSIONS	
4.1 The study of N3s (N3-2 to N3-5) in DSSC as the dyes sensitizer	42
4.2 Synthesis a new of ruthenium complexes dye using new ligands for DSSCs	50
4.3 Optical properties	63
4.4 The photovoltaic performance characteristics of DSSCs	65
4.5 The photovoltaic performance characteristics for stability test of DSSCs	67
CHAPTER 5 CONCLUSIONS	70
REFERENCES	73
APPENDICES	
A Characterization data	82
B Publications	95
VITAE	100

LIST OF TABLE

TABLE		PAGES
3.1	Chemicals for the synthesis of new ligands and ruthenium complexes	23
3.2	Chemicals for DSSCs devices	24
3.3	Instruments for characterization techniques	25
4.1	%WL ₁₀₀ of N3s from evaporation of water and methanol	47
4.2	FTIR data for OH/C=O ratio of N3-1 to N3-5	48
4.3	Photovoltaic efficiencies parameter of the synthesized and commercial N3 dyes	49
4.4	The absorption of N719, CLC-C01, CLC-C06 and CLC-C08 in ethanol solution	64
4.5	The photovoltaic parameters of N719, CLC-C01, CLC-C06 and CLC-C08	67
4.6	The photovoltaic parameters of N719, CLC-C01, CLC-C06 and CLC-C08 for stability test during 1000 h	69
5.1	The photovoltaic parameters of ruthenium(II) complexes	71
5.2	The photovoltaic parameters of N719, CLC-C01, CLC-C06 and CLC-C08 for stability test during 1000 h	72

LIST OF FIGURES

FIGURE	PAGES
1.1 Schematic of the DSSC	2
1.2 Schematic representation of interfacial electron transfer following light absorption for dye-sensitized	3
1.3 Schematic picture of working principle of DSSCs	5
1.4 The <i>I-V</i> characteristic curves of DSSC	6
1.5 D-π-A structures of organic dyes	7
1.6 Chemical structures of C343 , NKX-2311 and NKX-2677	8
1.7 Chemical structures of D102 and D149	8
1.8 Chemical structures of 1P-PSP , 1N-PSP , C219 , XS29 and HKK-BTZ4	9
1.9 A; Molecular structure of porphine, B; represents the generic structure of a metallo-porphyrin	10
1.10 Chemical structures of Zn-1a dye	10
1.11 Chemical structures of YD-0 and DTBC dyes	11
1.12 Chemical structures of YD-2 dye	11
1.13 The molecular structures of N3 , black dye and N719	12
1.14 The molecular structures of C101 dye	13
1.15 The molecular structures of Z991 dye	13
2.1 The molecular structure of Z907 dye	16
2.2 The molecular structures of the dyes with different chain lengths	16
2.3 A: The molecular structure of Z910 , B: absorption spectra of Z910 , N719 , and Z907 anchored on nanocrystalline TiO ₂ film	17
2.4 A: the molecular structure of K19 , B: absorption spectra of K19 and the Z907 anchored on an 8 μm thickness transparent nanocrystalline TiO ₂ film	18
2.5 The molecular structure of K77 dye	19

LIST OF FIGURES (CONTINUED)

FIGURE	PAGES
2.6	The molecular structure of JK-92 and S8 19
2.7	The structure of C101 dye 20
2.8	The structure of CYC-B1 dye 21
2.9	The molecular structures of B11 and B19 sensitizers 22
2.10	The structure of Z991 dye 22
3.1	Experimental flow chart model of this work 27
3.2	The picture of DSSCs based on N3s 37
3.3	The picture of burning electrodes 38
3.4	The picture of N3s dye solution 38
3.5	The picture of the completed the working electrode 38
3.6	The picture of counter electrodes 39
3.7	The heating step for device assembling 39
3.8	The injection step of electrolyte into the cell 40
3.9	The completed dye-sensitized solar cells 40
3.10	The dye solution of N719 , CLC-C01 , CLC-C06 and CLC-C08 41
4.1	The synthetic route for the preparation of N3s dye 42
4.2	The synthesis of Ru-cymene 43
4.3	The ¹ H NMR of Ru-cymene in CDCl ₃ 43
4.4	The synthesized of CR-01 44
4.5	The ¹ H NMR spectra of CR-1 in CDCl ₃ 44
4.6	The synthetic route of ligand substitution reaction to N3s 45
4.7	The aromatic ¹ H NMR of N3s in CD ₃ OD 46
4.8	The TGA of N3s 46
4.9	The FTIR spectra for OH/C=O ratio of N3s 47
4.10	A: XRD pattern of N3s , B: AFM of FTO coated on bare TiO ₂ and TiO ₂ coated by N3s 48
4.11	The <i>I-V</i> curves of N3s 49

LIST OF FIGURES (CONTINUED)

FIGURE	PAGES
4.12 The structures of new dyes	50
4.13 The synthetic route of new dyes	51
4.14 The synthesis of CLC-01	52
4.15 The mechanism of MC-1	53
4.16 The ^1H NMR of MC-1 in CDCl_3	53
4.17 The mechanism of the formation of CLC-01 synthesis	54
4.18 The ^1H NMR of the CLC-01 in CDCl_3	55
4.19 The mechanism for the synthesis of CL-06	55
4.20 ^1H NMR of the CL-06 in CDCl_3	56
4.21 Synthesis procedure of the CLC-06	56
4.22 ^1H NMR of the CLC-06 in CDCl_3	57
4.23 The synthesis of CLC-08	58
4.24 The ^1H NMR of the CL-08 in CDCl_3	58
4.25 The ^1H NMR of the CLC-08 in CDCl_3	59
4.26 The synthesis of CLC-C01 dye	60
4.27 The ^1H NMR spectrum of the CLC-C01 in CD_3OD	61
4.28 ^1H NMR of the CLC-C06 in CD_3OD	62
4.29 The ^1H NMR spectrum of the CLC-C08 in CD_3OD	63
4.30 UV-vis spectra of N719 , CLC-C01 , CLC-C06 and CLC-C08 in ethanol solution	64
4.31 Incident photon to current conversion efficiency (IPCE) of N719 , CLC-C01 , CLC-C06 and CLC-C08	65
4.32 The $I-V$ curve of DSSCs based on N719 , CLC-C01 , CLC-C06 and CLC-C08	66
4.33 The efficiencies variations with aging time (1000 h) for the device based on CLC-C01 , CLC-C06 , CLC-C08 and N719	67

LIST OF FIGURES (CONTINUED)

FIGURE	PAGES
4.34 Photocurrent density variations with aging time (1000 h) for the device based on CLC-C01 , CLC-C06 , CLC-C08 and N719	68

LIST OF ABBREVIATIONS

ABBREVIATION	DEFINITION
A	Ampere
AR.	Analysis reagent
aq.	Aqueous
AM.	Air mass
anh.	Anhydrous
Ar	Aromatic
bipy	Bipyridine
conc	Concentrated
cm ⁻¹	Reciprocal centimeter (unit of wavenumber)
¹³ C NMR	Carbon nuclear magnetic resonance
°C	Degree Celsius
cb	Conduction band
cm	Centimeter
cm ³	Centimeter cubic unit
d	Doublet (for NMR spectral data)
dd	Double of doublet (for NMR spectral data)
DCM	Dichloromethane
DMF	Dimethylformamide
DMSO	Dimethyl sulfoxide
DSSCs	Dye-Sensitized Solar Cells
Eg	Energy gap
eV	Electron volt
ESI-MS	Electrospray ionization mass spectrometry
EtOAc	Ethyl acetate
<i>ff</i>	Fill factor
FTIR	Fourier transforms infrared spectroscopy
FTO	Fluorine doped tin oxide
g	Gram
h	Hour

LIST OF ABBREVIATIONS (CONTINUED)

ABBREVIATION	DEFINITION
HOMO	Highest occupied molecular orbital
^1H NMR	Proton nuclear magnetic resonance
hv	High voltage
Hz	Hertz
IPCE	Incident Photon to Current Conversion Efficiency
J	Coupling constant (for NMR spectral data)
J_{max}	Maximum current
J_{sc}	Short circuit current density
LUMO	Lowest unoccupied molecular orbital
M	Molarity
m	Multiplet (for NMR spectral data)
mA	Milliampere
mL	Milliliter
MLCT	Metal to ligand charge transfer
mM	Millimolar
mmol	Millimol
m.p.	Melting point
mV	Millivolt
nm	Nanometer
ppm	Part per million
Pt	Platinum
q	Quintet (for NMR spectral data)
Ra	Average roughness
Ru	Ruthenium
s	Singlet (for NMR spectral data)
s	Second
t	Triplet (for NMR spectral data)
TBA	Tetra butyl ammonium hydroxide
TGA	Thermal gravimetric analysis

LIST OF ABBREVIATIONS (CONTINUED)

ABBREVIATION	DEFINITION
UV	Ultra violet
v	Volt
V_{\max}	Maximum voltage
V_{oc}	Open circuit voltage
W	Watt
%WL ₁₀₀	%weight loss below 100 °C
XRD	X-ray Diffractometer
δ	Chemical shift (for NMR spectral data)
η	Power conversion efficiency
μm	Micrometer
μL	Microliter
α	Alpha
p	Para
ε	Molar absorptivity
λ	Wavelength

CHAPTER 1

INTRODUCTION

1.1 Importance in research and development

One of the many challenges that we face today is the increasing energy consumption. The power consumption is expected to double within the next 30 years. Now a day, the main energy resource is the fossil fuels such as coal, oil and natural gas. These types of energy are non-renewable energy source. They also are the main reason to global warming and environmental pollution; for example, produce greenhouse gases, generate air pollution, aid in acid rain and deplete the ozone.

To overcome these problems, the development of renewable and clean energy sources is imperative common challenges for main future energy. Solar energy is one of the best renewable energy because it granted from the sun, clean, non-polluting and sustainable. Sun light can be converted directly to electricity which is call photovoltaic cell or solar cell. To date, the common and commercial solar cells are silicon-based which deploy solar-energy conversion efficiencies of about 18-25% [1]. However, the synthesis steps of this type require high-purity silicon and skilled manufacturing techniques, which resulted in the construction and installation costs. Therefore, widespread using in our life has been limited. To overcome this problem, dye-sensitized solar cells provides a technically and economically credible alternative concept to present day p-n junction photovoltaic devices. The dye-sensitized solar cells (DSSCs) was invented by O'Regan and Grätzel in 1991 [2] because it is easy to fabricate. Low production cost, flexible and easy model, the designer can use for decoration.

1.2 Dye-sensitized solar cells

The DSSC was first reported by O'Regan and Grätzel group. They reported the solar harvesting device, yielding a solar energy conversion to electricity of 7%. Now a day, the DSSC shows efficiency of 13 % based on a porphyrin dye [3]. The DSSC contains several different components; a conducting glass substrate, a mesoporous

semiconductor film, a sensitizer, an electrolyte and a counter electrode, show in Figure 1.1.

1.3 Compositions of DSSC

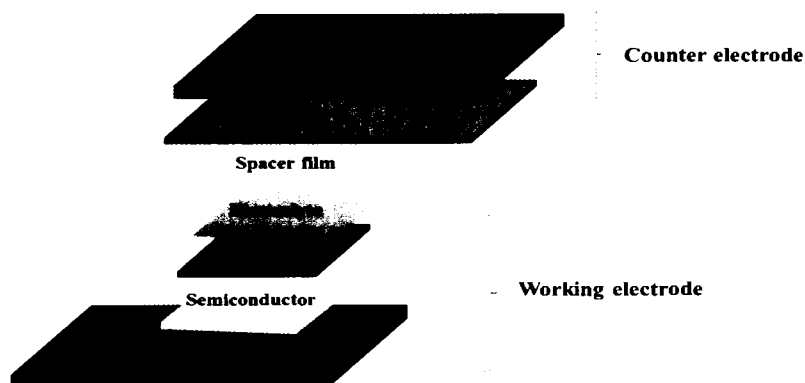


Figure 1.1 Schematic of the DSSC

1.3.1 Conductive glass

Conductive glass is optically transparent and electrically conductive glass. The optoelectronic devices are widely fabricated from the glass doped metal oxides which are indium tin oxide (ITO) and fluorine doped tin oxide (FTO) [4, 5]. The ITO is high transparency and electrical conductivity at room temperature, the latter property is severely spoiled under high temperature. Therefore, in DSSC popularly used the FTO as a transparent electrode because it is stable under atmospheric conditions, chemically inert, less expensive and stable at high temperature.

1.3.2 Semiconductor

Semiconductor oxides used in dye-sensitized solar cells include TiO_2 , ZnO , SnO_2 and Nb_2O_5 [6]. However, the most popular is TiO_2 nanoparticle. TiO_2 is a stable, non-toxic oxide, the well-known minerals rutile, anatase and brookite. Rutile is the thermodynamically most stable form. However, anatase form is the preferred structure in DSSCs, because of its larger bandgap (3.2 eV vs 3.0 eV for rutile), and its high conduction band edge. This leads to a high Fermi level and V_{oc} (open-circuit voltage, which is the difference between the semiconductor Fermi level and the redox potential of the electrolyte).

1.3.3 Dye sensitizer

Dye sensitizers serve as solar energy absorbers in DSSC, which control the light harvesting efficiency and the power conversion efficiency. An ideal sensitizer should absorb all light below a threshold wavelength of about 920 nm. They firmly grafted to the semiconductor oxide surface and inject electrons into the conduction band with a steady rate. They can be regenerated rapidly *via* electron donation from the electrolyte system and high stable in the oxidation state. There are many types of dyes, for example organic dyes [7, 8], porphyrin dyes [9, 10] and ruthenium complex dyes [11]. Molecular designs of dyes for DSSCs are as follows:

The structure dyes have one or more anchoring group (e.g., -COOH, -SO₃H, -PO₃H₂, -OH) for adsorption on the TiO₂ surface (see in Figure 1.2). Especially, a carboxyl group can form an ester linkage with the TiO₂ surface to provide a strongly bound dye and good electron communication between them.

The electrons from the excited dye can be injected to the conduction band (CB) of the TiO₂. The energy level of the lowest unoccupied molecular orbital (LUMO) of the dye must be higher (more negative) than the conduction band of the TiO₂ electrode. On the other hand, the ground state can receive electron back from I₃⁻/I⁻ redox couple in the electrolyte, the energy level of the highest occupied molecular orbital (HOMO) of the dye must be lower (more positive) than the I₃⁻/I⁻ redox potential.

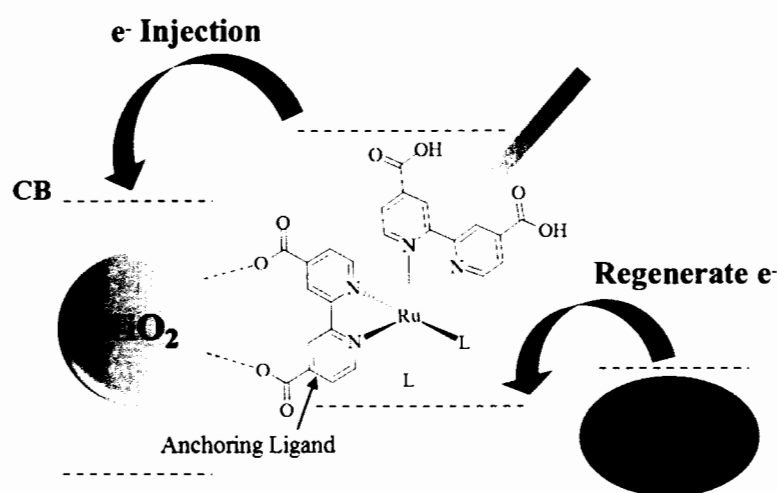


Figure 1.2 Schematic representation of interfacial electron transfer following light absorption for dye-sensitized

1.3.4 Electrolyte system

In 1991, M. Grätzel reported using organic liquid electrolyte containing LiI/I_2 , which obtained an overall light-to-electricity conversion efficiency of about 7.1% under irradiation of AM 1.5, 1000 W. m^{-2} . Later, many kinds of liquid electrolytes containing iodide/triiodide redox couple and high dielectric constant organic solvents such as acetonitrile (AcN), ethylene carbonate (EC), 3-methoxypropionitrile (MePN), propylenecarbonate (PC), γ -butyrolactone (GBL) and *N*-methylpyrrolidone (NMP) were investigated and some DSSCs with high photovoltaic performance were obtained [2, 12]. Currently, two different kinds of electrolytes have been used in real DSSCs.

The most commonly used is a liquid electrolyte such as I_3^-/I^- system in acetonitrile (CH_3CN) [13, 14]. This kind of electrolyte show rapid dye regeneration process to keeping high efficiency of DSSCs. However, the limitations such as the volatility of the electrolyte can lead to long term stability issues due to difficulties in sealing the device.

Ionic liquids (IL) exhibit a negligible vapor pressure and a high electric conductivity at room-temperature. Combined with the low-flammability and a wide electrochemical window, ILs is a promising candidate to replace the liquid electrolyte. At the moment derivatives of imidazolium salts are exclusively applied in DSSC [15]. However, pure IL usually give higher viscosity than that of organic solvent, which limits the iodide/triiodide transport speed and the restoration of oxidized dye, so the photovoltaic performance of these DSSCs is not as well as that of DSSCs using liquid electrolyte-containing organic solvents [16].

1.3.5 Counter electrode

Counter electrodes in DSSCs are usually constructed of conducting glass substrates coated with metal films. The roles of the counter electrode are to transfer electrons arriving from the external circuit back to the redox electrolyte and to catalyze the reduction of the redox couple. The popular metal which is platinum, the platinum serves as an excellent electro catalyst for triiodide reduction. Other counter electrodes such as carbon black and polymers have also been tested [8-9].

1.4 Principle of DSSCs

The principle working of DSSCs are shown in Figure 1.3.

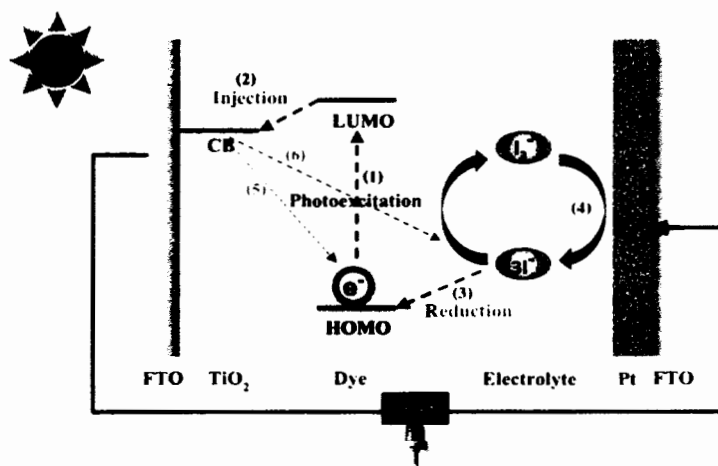
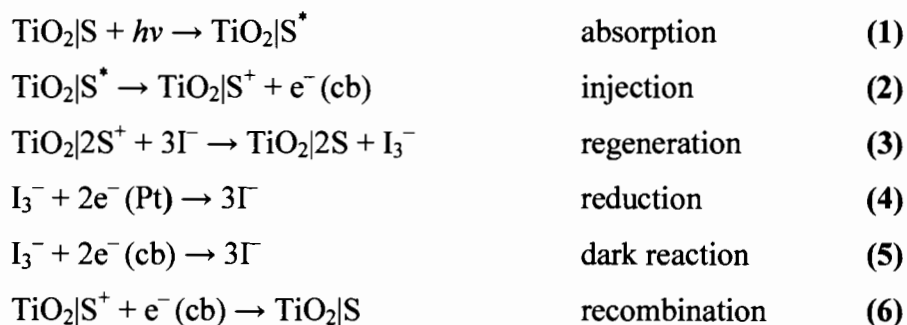


Figure 1.3 Schematic picture of working principle of DSSCs

From Figure 1.3, the dye sensitizer absorbs a photon (sun light) to generate the photo excited state of the dye (1) and injects electrons into the conduction band (CB) of TiO_2 (2). The injected electrons move through the network of interconnected TiO_2 nanoparticles to arrive at the transparent conducting oxide (FTO). After that, the electrons transfer through the external circuit to the counter electrode (Pt-coated glass). At the same time, the oxidized dye is regenerated by iodide/triiodide couple (3). The iodide is regenerated by the reduction of triiodide at the counter electrode (4) through the donation of electrons from the external and then the circuit is completed.



However, there are undesirable side reactions: the injected electrons may recombine either with oxidized sensitizer, (dark reaction (5)) or with the oxidized

redox couple at the TiO₂ surface, (recombination (6)), resulting losses in the cell efficiency.

1.5 The performances of DSSC

The performances of the solar cell depend on these major parameters:

1.5.1 Incident Photon to Current Conversion Efficiency (IPCE)

IPCE is one of the basic measurements for DSSC performance. It is also known as the “external quantum efficiency” and describes how efficiently the light of a specific wavelength is converted to current, *i.e.* (electrons out) / (photons in). The IPCE can be calculated according to equation (1).

$$\text{IPCE (\%)} = \frac{1240 \text{ (eV nm)} J_{sc} \text{ (mA cm}^{-2}\text{)}}{\lambda \text{ (nm)} I \text{ (mW cm}^{-2}\text{)}} \times 100 \quad (1)$$

When J_{sc} is the short-circuit photocurrent density for monochromatic irradiation, λ and I are the wavelength and the intensity of the monochromatic light, respectively.

1.5.2 Photocurrent/Voltage Curve (I/V curve)

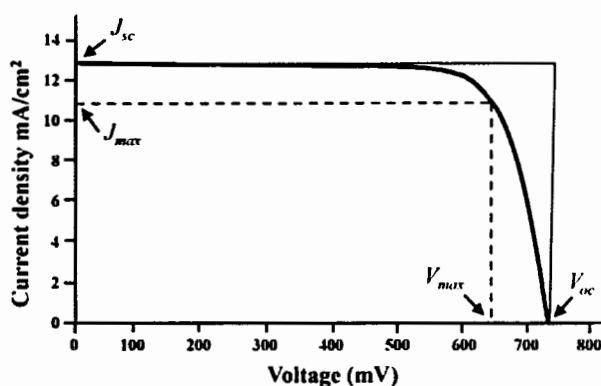


Figure 1.4 The I/V characteristic curves of DSSC

Measurement of the I/V curve is useful method for the evaluation of the DSSC performance. The parameters determine from the I/V curve:

Open-circuit photovoltage (V_{oc})

Short circuit photocurrent density (J_{sc})

Fill factor (ff)

$$ff = \frac{J_{max} \cdot V_{max}}{J_{sc} \cdot V_{oc}} \quad (2)$$

1.5.3 Solar energy to electricity conversion yield or power conversion efficiency (η)

The most discussed performance parameter of a solar cell is the power conversion efficiency. It is defined as the percentage of incident irradiance (light power per unit area) that converts into output power. Because the point where the cell operates on the I - V curve changes depending on the load, the output power depends on the load. For consistency, the maximum output power is used for calculating efficiency. In equation form, efficiency is written as shown in equation (3).

$$\eta = \frac{J_{sc} (\text{mA.cm}^{-2}) V_{oc} (\text{V}) ff}{I (\text{mW.cm}^{-2})} \quad (3)$$

1.6 Type of dye sensitizer

The sensitizers used in DSSCs are divided into three types, *viz.*, organic dyes, porphyrin dyes and organometallic dyes according to the structure.

1.6.1 Organic sensitizers

A common way to design organic dyes is the **D- π -A** strategy, where the molecule is built up of an electron donor (**D**), a conjugated linker (π), and an electron acceptor (**A**), as illustrated in Figure 1.5.



Figure 1.5 D- π -A structures of organic dyes

Organic dyes with large π -aromatic system such as coumarin [17], phenothiazine [18], benzothiadiazole [19], triphenylamine [20], thiophene [21], and perylene, have been investigated as sensitizers in DSSCs.

The performances of DSSCs based on organic dyes have been greatly improved by several groups. The first transient studies on a coumarin dye in DSSCs

coded as **C343** (Figure 1.6) was reported in 1996 by Grätzel et al. The **C343** has a narrow absorption spectrum. So, the conversion efficiency of this specific compound was low. **NKX-2311** was developed for expanded absorption spectrum by increase the π -system. which improved the conversion efficiency of 5.6% [22]. Next, **NKX-2677** was developed by extending the thiophene unit as π -linker. The **NKX-2677** shows the power conversion efficiency of 7.4% and a high stability for DSSC [23].

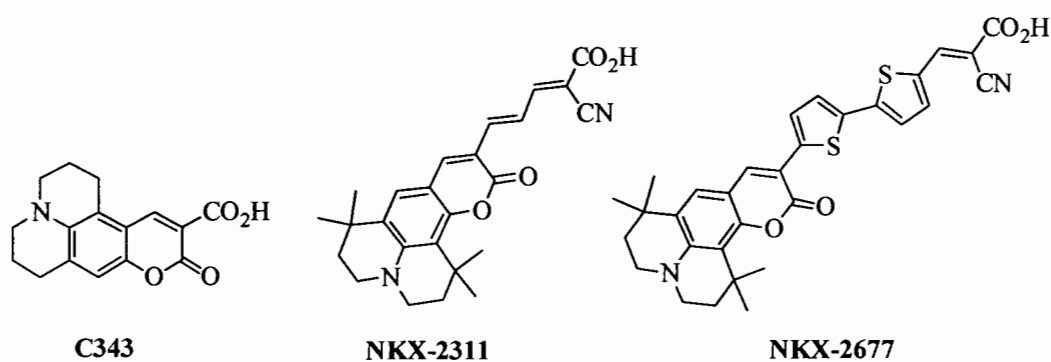


Figure 1.6 Chemical structures of C343, NKX-2311 and NKX-2677

An indoline dye which is **D102** and **D149** (Figure 1.7) were discovered by Ito and co-worker [24]. They gave energy conversion efficiency of 6 and 9%, respectively.

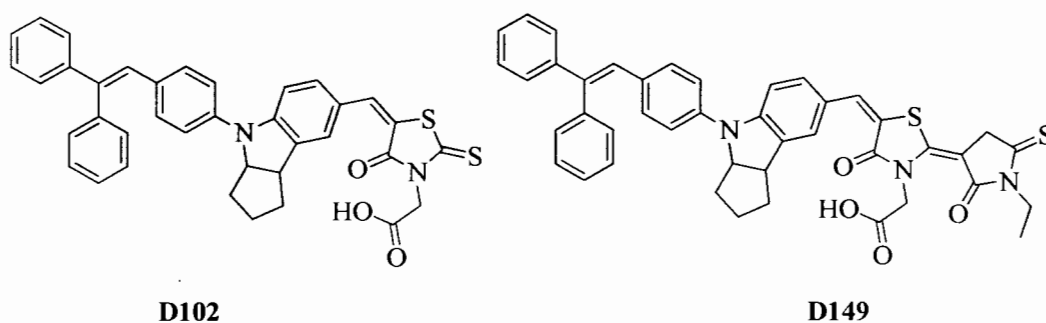


Figure 1.7 Chemical structures of D102 and D149

The efficiency and stability of dyes were improved by triphenylamine or *N,N'*-diphenylnaphthalen-1-amine moiety as the electron donor and cyanoacrylic acid moiety as the electron acceptor; for example, **1P-PSP**, **1N-PSP**, **C219**, **XS29** and **HKK-BTZA**. Their structures are shown in Figure 1.8. They show the energy conversion efficiency about 5 to 10% [16, 25-28].

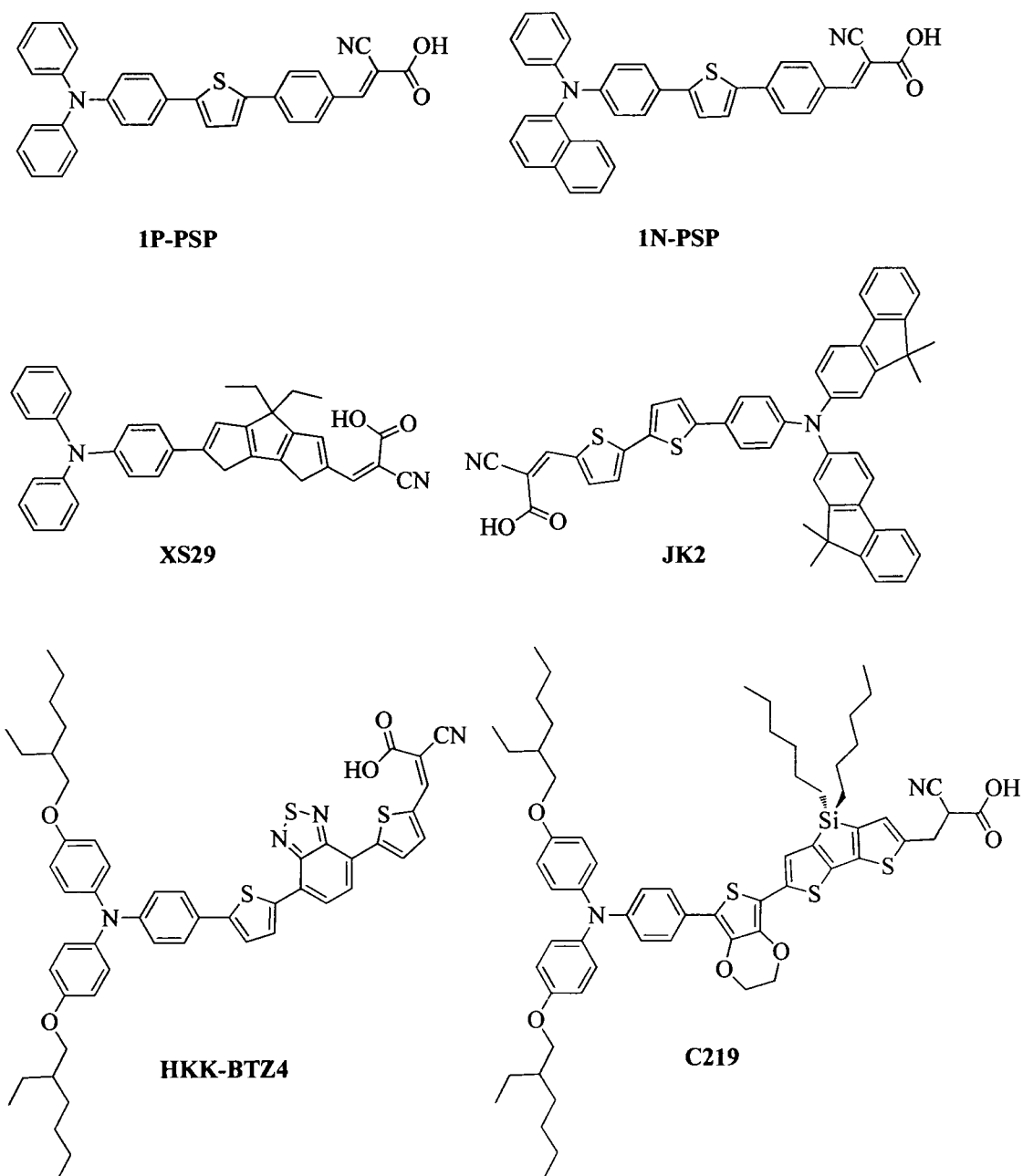


Figure 1.8 Chemical structures of 1P-PSP, 1N-PSP, C219, XS29 and HKK-BTZ4

1.6.2 Porphyrin sensitizer

Porphyrin dyes are a highly colored compounds due to the 22 π -electrons delocalized over the macrocycle. A number of naturally occurring pigments contain a tetrapyrrol structure with various substituents at the eight β -positions of the pyrroles, and the meso-positions between the pyrrol rings [29, 30]. The simplest porphyrin is porphine, in which all positions on the periphery of the macrocycle are taken by hydrogen atoms. Chemical modifications of the basic porphine structure can easily be

performed by substitutions on the β - and meso-carbons (Figure 1.9). The inner four nitrogen atoms of the deprotonated free-based porphyrin can act as ligand and strongly coordinate metal ions.

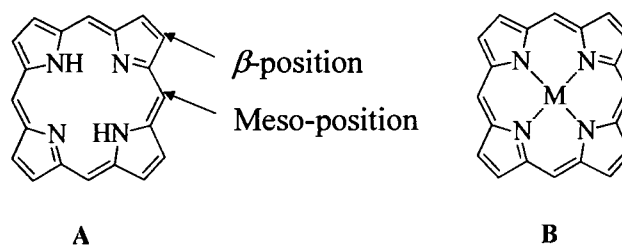


Figure 1.9 A: Molecular structure of porphyrin, B: represents the generic structure of a metallo-porphyrin

In 2004, Campbell synthesized meso-linked porphyrin dye, **Zn-1a** ($\eta = 4.2\%$), in Figure 1.10. After that the various structure of Zn metal was developed; for example, **YD0** ($\eta = 3.5\%$) [31] and **DTBC** ($\eta = 5.2\%$) [32], as shown in Figure 1.11 [10, 33].

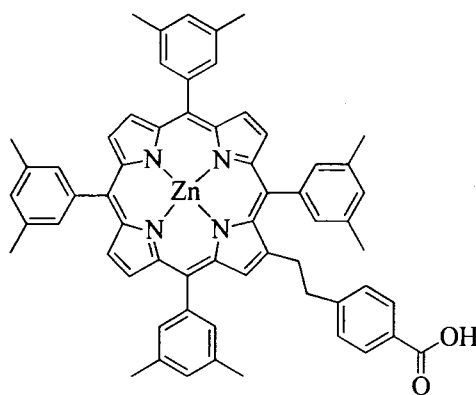


Figure 1.10 Chemical structures of Zn-1a dye

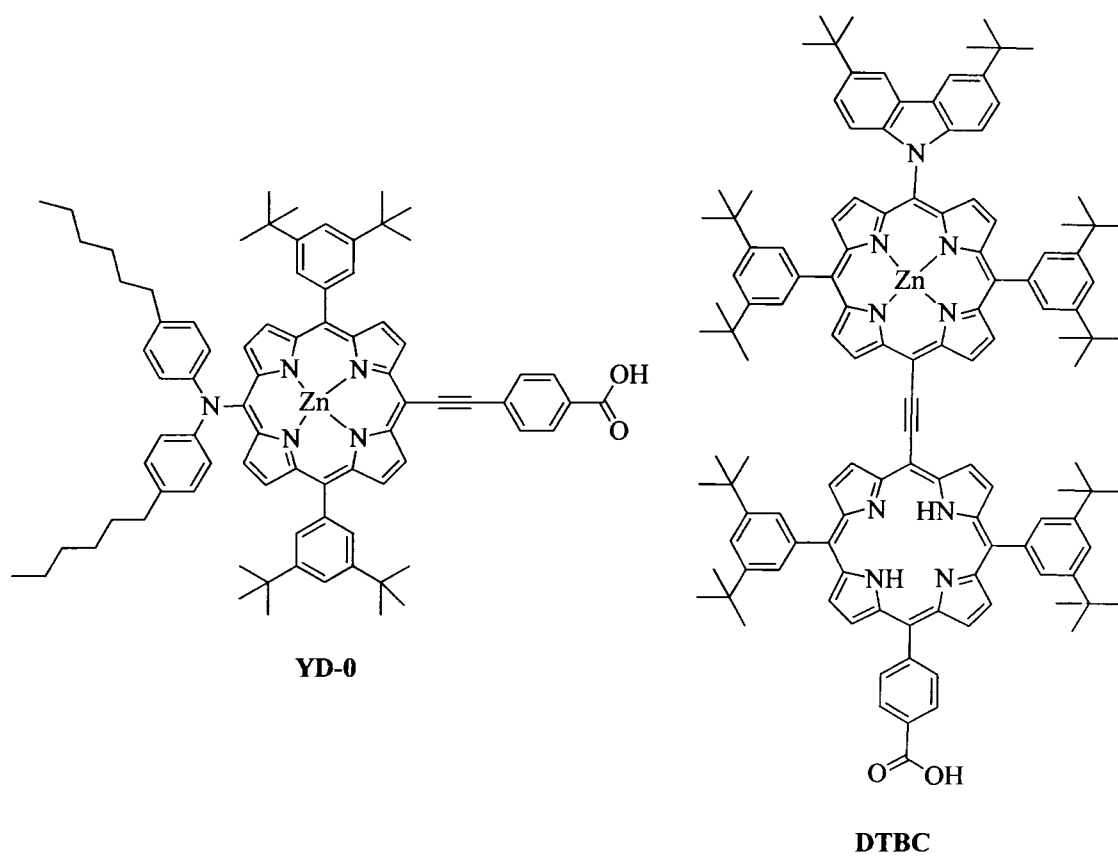


Figure 1.11 Chemical structures of YD-0 and DTBC dyes

In 2010, T. Bessho and co-worker reported the D- π -A porphyrin dye, which is **YD2** (Figure 1.12). The **YD2** show a power conversion efficiency of 11% when used with iodide/triiodide redox electrolyte.

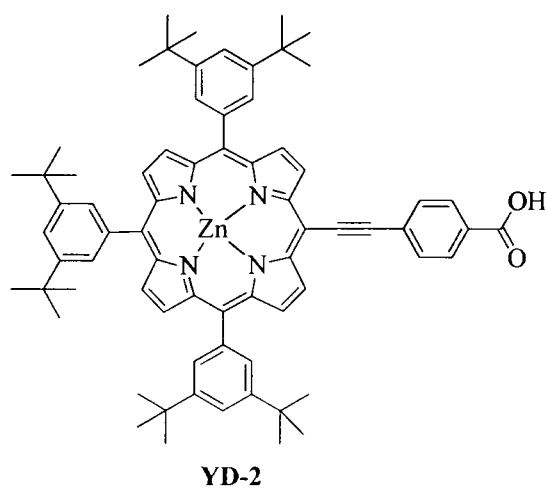


Figure 1.12 Chemical structures of YD-2 dye

1.6.3 Ruthenium sensitizer

Ruthenium (II) complexes dye are the most popular of organometallic complex dyes, because they show high solar light to conversion efficiency and good property for sensitizer such as absorb solar energy, transfer electron to metal oxide, stability in the oxidation state and easily modify structure. The common and efficient ruthenium sensitizers are *cis*-di(thiocyanato)-*N,N'*-bis(4,4'-dicarboxy-2,2'-bipyridine) ruthenium(II) (**N3**) [2, 34], tri(thiocyanato)(4,4',4''-tricarboxy-2,2':6',2''-terpyridine)ruthenium(II) (**black dye**) [35, 36], di-tetrabutyl ammonium *cis*-bis(isothiocyanato)-bis(2,2'-bipyridyl-4,4'-dicarboxylato)ruthenium(II) (**N719**) [37]. The three dyes show efficiency more than 10%. They have an intense and wide-range absorption of visible light, mainly due to metal to ligand charged transfer (MLCT) transition that moves the electrons from d orbital of ruthenium to the π orbital of diimine which is directly attached to TiO_2 . The structures are shown in Figure 1.13.

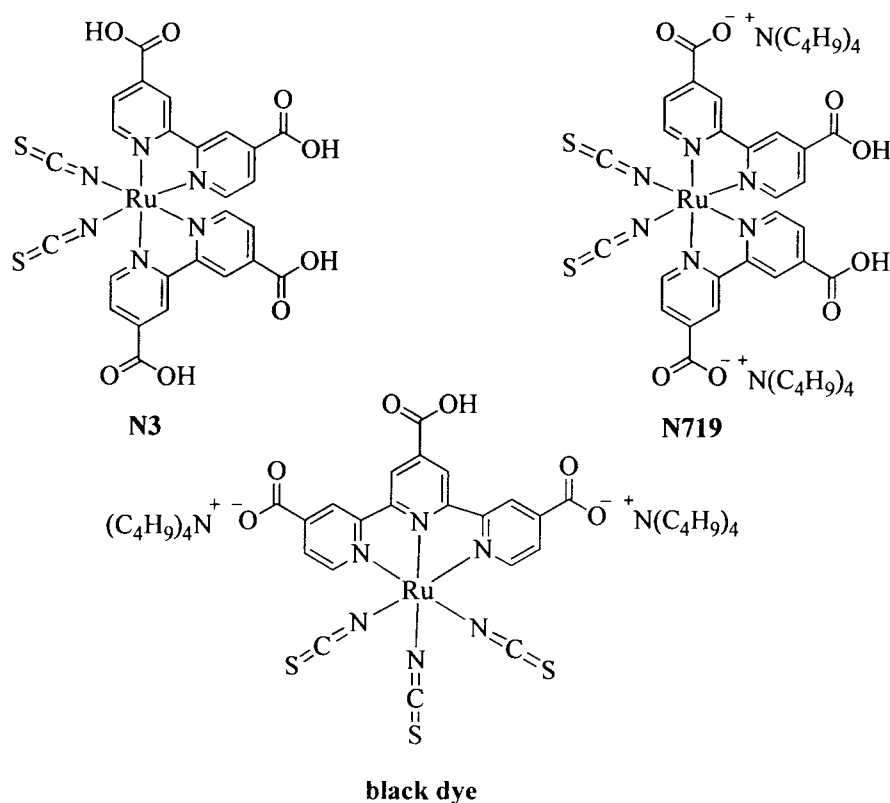
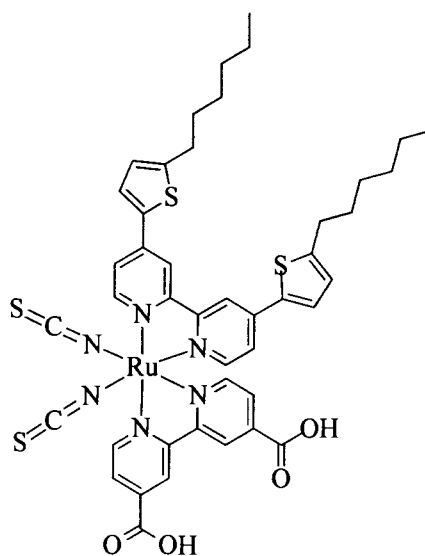


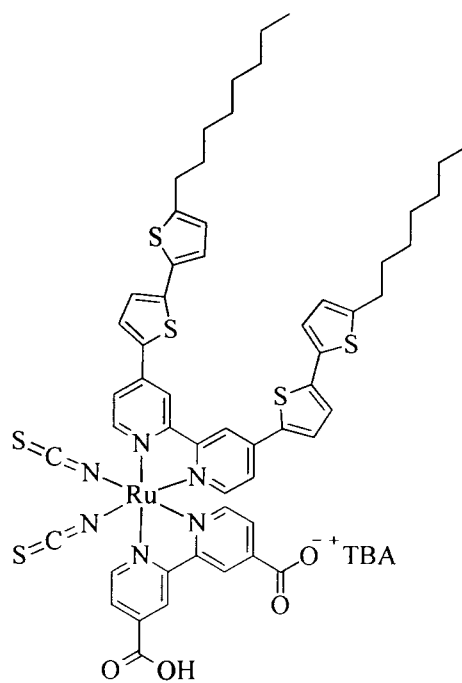
Figure 1.13 The molecular structures of N3, black dye and N719

Recently, the Grätzel's group reported the DSSCs with efficiencies of 11.3% [38] and 12.3% [39] containing the dyes **C101** (Figure 1.14) and **Z991** (Figure 1.15), respectively.



C101

Figure 1.14 The molecular structures of **C101** dye



Z991

Figure 1.15 The molecular structures of **Z991** dye

This project studied the ruthenium complexes for dye sensitizer in DSSCs. We started with the N3 which is well known as the standard dye. In addition, we synthesized new dye sensitizers to study power conversion efficiency and long term stability.

1.7 Objectives of thesis

1.7.1 To synthesize N3s

1.7.2 To synthesize new ruthenium dyes

1.7.3 To characterize the molecular structure of ligands and the target complexes by ^1H and ^{13}C NMR, Fourier transform infrared spectroscopy (FTIR) and mass spectroscopy (MS)

1.7.4 To study UV-Vis absorption

1.7.5 To study performance and stability of synthesized ruthenium complexes for DSSCs



CHAPTER 2

LITERATURE REVIEWS

2.1 Literature reviews

Ruthenium complexes show effective charge separation at the metal to ligand (Ru-bpy) and ligand to metal (SCN-Ru) absorption bands in the visible light region. The DSSCs based on ruthenium dyes which is **Z991** [39], produced solar energy to electricity conversion efficiency of up to 12.3 %. The ruthenium complexes are divided into 3 groups which are;

2.1.1 Homoleptic ruthenium complex

Over the last 15 years, the homoleptic ruthenium complex with 4,4'-dicarboxylic acid-2,2'-bipyridine (**dc bpy**) ligands has been considered as the best anchoring ligand in ruthenium sensitizers, reported by Grätzel and coworkers, such as *cis*-dithiocyanatobis(4,4'-dicarboxylic acid-2,2'-bipyridine)ruthenium(II), (**N3**) (Figure 1.13). The carboxylic groups form a bond with the TiO₂ surface. The dye molecules absorb photon *via* an excitation between the electronic states of the molecule. The **N3** dye shows two absorption maxima in the visible region at 518 nm and at 380 nm. The **N3** showed power conversion efficiency of 10.4% [2, 40].

2.1.2 Heteroleptic ruthenium complex

Dyes attached to TiO₂ through carboxylic acid groups are susceptible to desorption from the surface under the action of trace quantities of water, thus they are serious consequences on the long-term stability of the resultant solar cells. In 2003, P. Wang and co-worker presented a new amphiphilic heteroleptic dyes, [RuLL'(NCS)₂], (L=4, 4'-dicarboxylic acid-2, 2'-bipyridine, L'=4, 4'-dinonyl-2, 2'-bipyridine) in which the hydrophobic long chains referred to **Z907** [41, 42] (Figure 2.1). The fact that more alkyl chains for **Z907** lead to higher hydrophobicity in the surface of dye-sensitized mesoporous TiO₂ because it can reduce the charged recombination with the electrolyte. It can display an enhanced stability towards desorption from TiO₂ induced by water in the liquid or gel electrolyte. A cell based on **Z907** using a volatile electrolyte gives power conversion efficiency of 6.2 %

under AM 1.5 G simulated sunlight. The device also showed excellent stability under light soaking at 55 °C for 1,000 h.

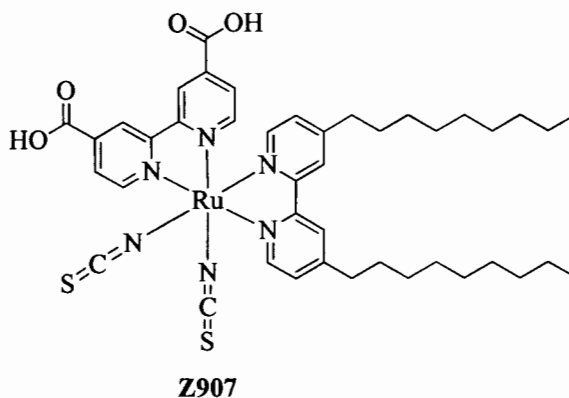


Figure 2.1 The molecular structure of Z907 dye

The influence of the hydrophobic hydrocarbon chain length of amphiphilic ruthenium dyes on the device performance was reported by L. Schmidt-Mende and co-worker, in 2005 [43]. They varied the hydrocarbon chain length of an amphiphilic ruthenium dye (Figure 2.2). The result shows that chain length of the dye lead to a long distance between TiO₂ and the hole conductor. The dyes with a hydrophobic chain on the other end, give more effectively as a spacer and blocking layer between TiO₂ and the hole conductor to avoid recombination. A chain length between C₉ (Z907) and C₁₃ seems to be ideal for this system. It is assumed that, this is in general for reducing the recombination in mechanism.

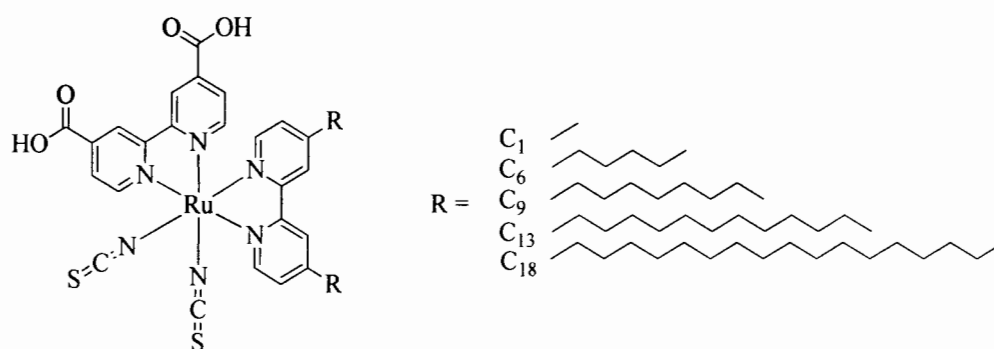


Figure 2.2 The molecular structures of the dyes with different chain lengths

Although, the **Z907** showed stable under prolonged thermal stress at 80 °C and soaking with light. However, the molar extinction coefficient of this sensitizer is somewhat lower than that of the standard **N719** dye. Therefore, P. Wang and coworker have developed a new ruthenium complex sensitizer with high molar extinction coefficient by extending the π -conjugation. Enhancing the absorption of sensitizers has been demonstrated to improve the photovoltaic performance of dye sensitize solar cells. The molecular structure of ruthenium(4,4'-dicarboxylic acid-2,2'-bipyridine)(4,4'-di(3-methoxystyryl)-2,2'-bipyridine)(NCS)₂, coded as **Z910** [44], which is shown in Figure 2.3A. The MLCT absorption bands of new dye presented in Figure 2.3B shows two maxima at 410 and 543 nm, which are about 20 nm red-shifted compared to those of **Z907** and its analogues. In addition, the molar extinction coefficient of **Z910** is higher than those of **N719** and **Z907**, respectively. The power conversion efficient of device based **Z910** is 10.2% using liquid electrolyte. Moreover, it shows higher stability after 1000 h of light soaking.

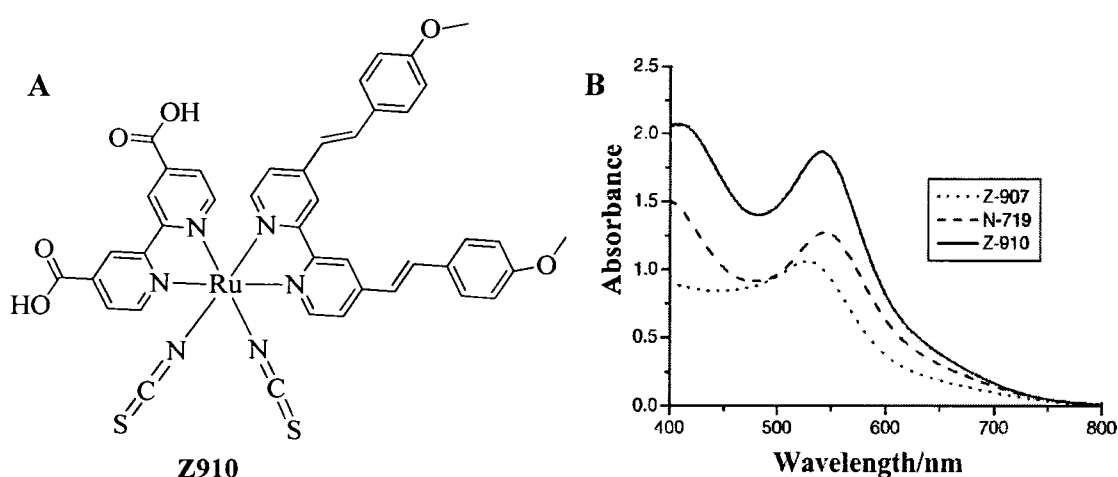


Figure 2.3 A: The molecular structure of Z910, B: Absorption spectra of Z910, N719 and Z907 anchored on nanocrystalline TiO₂ film

Next year, P. Wang and co-worker synthesized the new an amphiphilic heteroleptic polypyridyl ruthenium(II) complex, ruthenium(4,4'-dicarboxylic acid-2,2'-bipyridine)(4,4'-bis(*p*-hexyloxystyryl)-2,2'-bipyridine)(NCS)₂, coded as **K19** [45] (see Figure 2.4A). This dye is related to the analogous amphiphilic dye **Z907** but comprises additional stilbene units conjugated onto the hydrophobic ligand for

enhanced harvesting of visible light. Consequently, this dye show higher molar extinction coefficient than that **Z907**, as shown Figure 2.4B. **K19** also retains the high stability to thermal stress and light soaking displayed which was attributed to the hydrophobic spectator ligand. Furthermore, a cell based on the **K19** sensitizer show power conversion efficiency of 7% using liquid electrolyte and also shows excellent stability under light soaking after 1000 h of light soaking at 60 °C, no drop in efficiency was observed for cells covered with an ultraviolet absorbing polymer film.

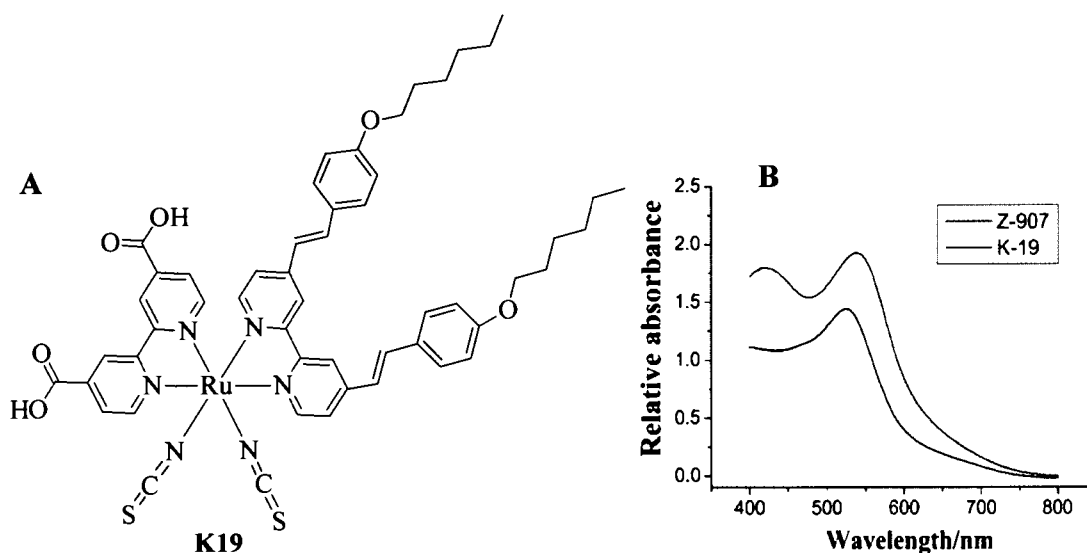
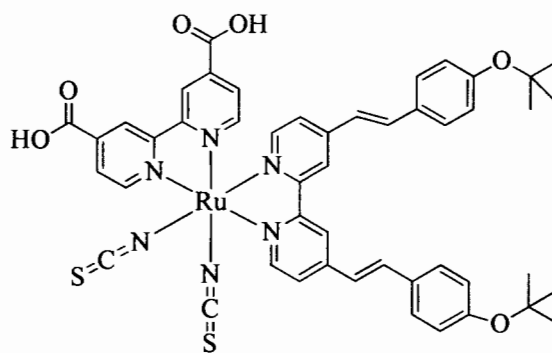


Figure 2.4 A: The molecular structure of K19, B: Absorption spectra of K19 and the Z907 anchored on an 8 μm thickness transparent nanocrystalline TiO₂ film

In order to improve the power conversion efficiency and stability of DSSCs, the research was focused on the synthesis of new highly efficient sensitizers. A new sensitized dye name is ruthenium(2,2'-bipyridine-4,4'-dicarboxylic acid)(4,4'-bis(2-(4-tert-butylphenoxy)ethenyl)-2,2'-bipyridine)(NCS)₂, denoted **K77** [46] (Figure 2.5). The DSSCs with more than of 10.5% photoelectrical conversion efficiency were obtained utilizing the designed high molar extinction coefficient sensitizer (**K77**) in conjunction with a volatile electrolyte. Highly efficient DSSCs (up to 9.5%) show unprecedented long-term stability (1000 h) under both light soaking and thermal stressing.



K77

Figure 2.5 The molecular structure of K77 dye

The ruthenium (II) complex, **JK-92** ($\eta = 6.22\%$) [47] was developed by extending the π -conjugation of bipyridine ligand using phenyl triazole moieties and endowing with alkoxy groups. The dioctyl 2,2'-bipyridine-4,4'-dicarboxylate moieties of complex **S8** ($\eta = 5.36\%$) [48] and 4,4'-bis(1-(4-(hexyloxy)phenyl)-1H-1,2,3-triazol-4-yl)-2,2'-bipyridine moieties of **JK-92** (Figure 2.6) improved the molar extinction coefficient of sensitizers and furthermore to provide directionality in the excited state by fine tuning the LUMO level of the ligands with the electron donating alkoxy group. The **JK-92** and **S8** dyes have several advantages over the conventional N3 dye such as, higher binding capacity onto the TiO₂ surface than N3 dye and hydrophobic group in the complex increasing the stability of cells towards water induced desorption.

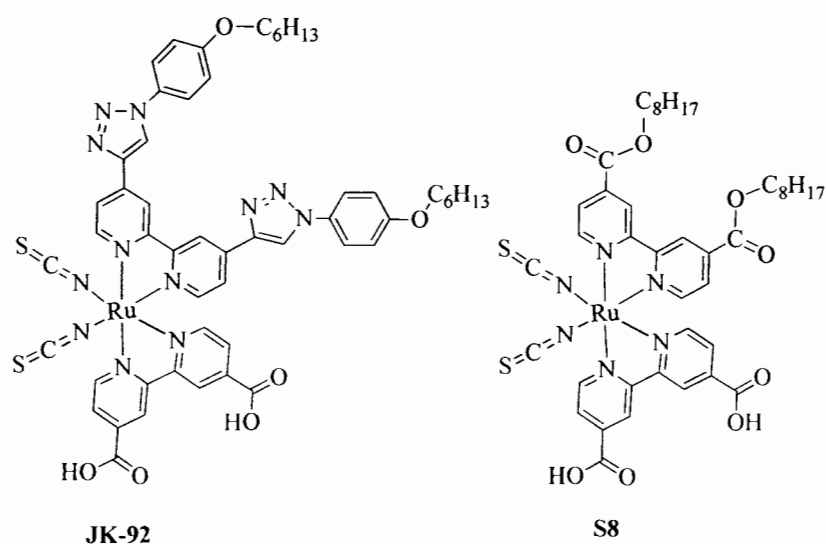


Figure 2.6 The molecular structure of JK-92 and S8

The heteroleptic polypyridyl ruthenium complex dye, coded **C101** with high power conversion efficiency was reported by F. Gao and co-worker. The molecular structure of **C101** is shown in Figure 2.7. The **C101** was developed with high molar extinction coefficients by extending the π -conjugation of spectator ligands, with a motivation to enhance the optical absorptivity of mesoporous titania film and charge collection yield in a dye-sensitized solar cell. Along with an acetonitrile-based electrolyte, the **C101** sensitizer has already achieved a strikingly high efficiency of 11.0-11.3% [38].

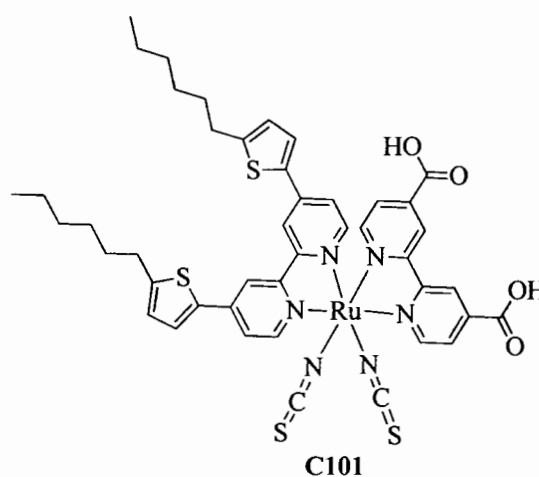


Figure 2.7 The structure of **C101** dye

In 2006, C.Y. Chen and co-worker reported the ruthenium photo-sensitizer, **CYC-B1** [49]. In which one of the **dc bpy** ligands in **N3** was replaced with **abtpy**, a bipyridine ligand substituted with alkyl bithiophene groups (**abtpy**). **CYC-B1** shows power-conversion efficiency at 10% higher than that of **N3** under the same cell fabrication and measuring procedures. The **CYC-B1** enhances the absorption coefficient by increasing the conjugation length of the ancillary ligand. Moreover, the alkyl group on the **abtpy** ancillary ligand can prevent the complexes from water-induced desorption of the dye molecules from the TiO_2 surface, exhibit good stability. The structure of **CYC-B1** is shown in Figure 2.8.

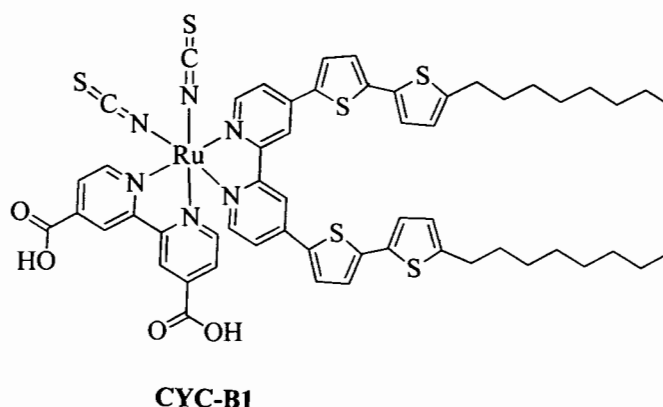


Figure 2.8 The structure of CYC-B1 dye

2.1.2 Homoleptic and heteroleptic ruthenium complex with ammonium salt

In 1993, Nazeeruddin and co-worker developed the ruthenium(II) complex based on structure of **N3** sensitizer, two carboxylic acid groups of **N3** were deprotonated and replaced by two ammonium salt (Figure 1.13). The ruthenium complex dye name is bis(tetrabutyl ammonium)-*cis*-di(thiocyanato)-*N,N'*-bis(4-carboxylato-4'-carboxylic acid-2,2'-bipyridine)ruthenium(II) (**N719**). The **N719** shows high solubility in ethanol and high power conversion efficiency of 11% [50].

In 2009, Chen and co-worker studied the dyes by increases π -conjugate and hydrocarbon long chain for increases the stability of the dye, which are **B11** [51] and **B19** [52]. They contain hexylthio-bithiophene in ancillary ligand and the vinyl-conjugation on anchoring ligand for **B19**. The molecular structures of the two sensitizers are shown in Figure 2.9. The **B11** using a volatile electrolyte gives power conversion efficiency of 11.5% which higher than the **B19**, shows power conversion efficiency of 8.4%. These results supported that the dye containing ammonium base can improve the efficiency. In addition, they found that the extending π -conjugation in ancillary ligand (**B11**) improved efficiency, whereas the extending π -conjugation on anchoring ligand (**B19**) decreased the efficiency. This underway lead to the improvement of varies new dyes.

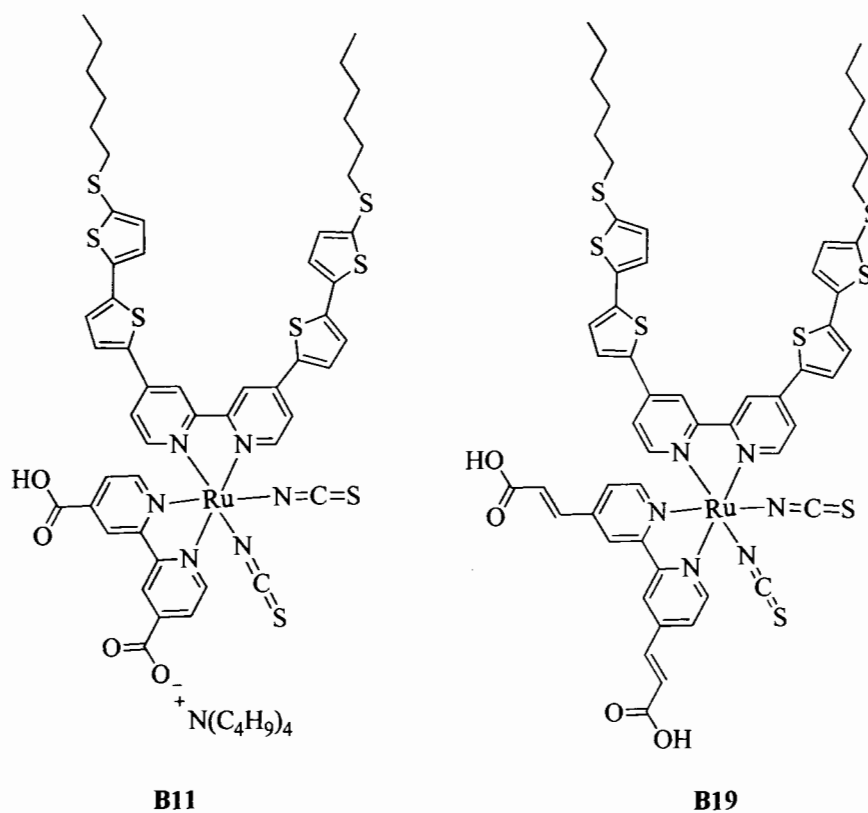


Figure 2.9 The molecular structures of B11 and B19 sensitizers

The high power conversion efficiency in the ruthenium complexes dye system is **Z991** dye, which achieved a conversion efficiency of 12.3% based using liquid electrolyte. The **Z991** was developed from **CYC-B1** dye (Figure 2.8) [49] by adding ammonium base, reported in 2009 [39] by the Grätzel group. The molecular structure of **Z991** is shown in Figure 2.2.

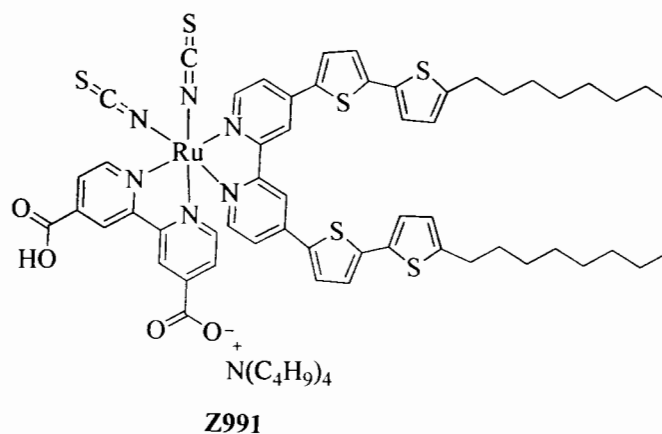


Figure 2.10 The structure of Z991 dye

CHAPTER 3

EXPERIMENTAL

3.1 Chemicals

All chemicals used in this project are shown in Table 3.1 and Table 3.2 for the synthesis and the DSSC devices, respectively.

Table 3.1 Chemicals for the synthesis of new ligands and ruthenium complexes

Chemicals	Formula	Grade	Manufacturer
Ammonium thiocyanate	NH ₄ SCN	ACS reagent, 97.5%	Acros
Anisole	C ₇ H ₈ O	99.7%	Acros
1-bromooctane	C ₈ H ₁₇ Br	99%	Acros
4,4'-dimethyl-2,2'-bipyridine	C ₁₂ H ₁₂ N ₂	99%	Acros
Calcium hydride	CaH ₂	93%	Acros
Dimethylformamide	C ₃ H ₇ NO	Organic synthesis	Acros
Diethyl ether	C ₄ H ₁₀ O	PA-ACS-ISO	Panreac
Ethanol	C ₂ H ₆ O	ACS-for analysis	CARLO ERBA
Hydrochloric acid	HCl	37%, for analysis	CARLO ERBA
Magnesium sulfate	MgSO ₄	Industrial Grade	Panreac
Methanol	CH ₄ O	ACS-for analysis	CARLO ERBA
Nitric acid	HNO ₃	67%, for analysis	CARLO ERBA
α -Phellandrene	C ₁₀ H ₁₆	$\geq 85\%$ GC	SAFC
<i>o</i> -Phenanthroline	C ₁₂ H ₈ N ₂	ACS-for analysis	CARLO ERBA
Phenol	C ₆ H ₆ O	Analytical Grade	CARLO ERBA
Ruthenium(III) trichloride trihydrate	RuCl ₃ .3H ₂ O	Hygroscopic	Pressure Chem.Co.
Sulfuric acid	H ₂ SO ₄	96% AR. Grade	CARLO ERBA
Sodium hydroxide	NaOH	ISO-ACS-for analysis	CARLO ERBA
Tetrabutyl ammonium hydroxide	C ₁₆ H ₃₇ NO	1 M solution in methanol	Acros

Table 3.2 Chemicals for DSSCs devices

Chemicals	Formula	Grade	Manufacturer
Acetonitrile	C ₂ H ₃ N	ACS-for analysis	CARLO ERBA
Bis(4,4'-dicarboxy-2,2'-bipyridine)dithiocyanato ruthenium(II) (N3)	C ₂₆ H ₁₆ N ₆ O ₈ RuS ₂	95% NMR	Sigma-Aldrich
Chloroplatinic acid	H ₂ PtCl ₆	40% Pt	Acros
Di-tetrabutylammonium <i>cis</i> -bis(isothiocyanato) - bis (2,2'-bipyridyl-4,4'- di carboxylato) ruthenium(II) (N719)	C ₃₈ H ₈₆ N ₈ O ₈ RuS ₂	95% NMR	Dyesol
Ethanol	C ₂ H ₆ O	ACS-for analysis	CARLO ERBA
Isopropanol	C ₃ H ₈ O	ACS-for analysis	CARLO ERBA
Iodine	I ₂	ACS-for analysis	CARLO ERBA
Lithium iodide	LiI	99%, pure analysis	Acros
3-Methoxy ethanol	C ₃ H ₈ O ₂	99.8% anhydrous	CARLO ERBA
Tetra propyl ammonium iodine	C ₁₂ H ₂₈ NI	98%	Acros
Titanium(IV) oxide	TiO ₂	Titanium nanoxide 20T/SP, D/SP	Solaronix
Titanium(IV) oxide	TiO ₂	Ti-Nanoxide R/SP	Solaronix
Titanium tetrachloride	TiCl ₄	0.09 M in 20% HCl	Sigma-Aldrich
4-Tertbutyl pyridine (TBP)	C ₉ H ₁₃ N	96%	Acros
Valeronitrile	C ₅ H ₆ N	98%	Acros

3.2 Instruments and general chemical characterization techniques

3.2.1 General instruments

Table 3.3 Instruments for characterization techniques

Instruments	Model	Company
Fourier Transform Infrared Spectrometer (FTIR)	Spectrum RX 1	Perkin Elmer
ALPHA FTIR Spectrometer	Diamond crystal ATR mode for Mid-IR range	Bruker
Perkin-Elmer Spectrum two FTIR spectrometer	Attenuated total reflectance (ATR)	Perkin-Elmer
UV-Visible Spectrometer	V-650 spectrophotometer	Jasco
Nuclear Magnetic Resonance (NMR)	Bruker AVANCE, 300 MHz	Bruker
Mass Spectroscopy (MS)	JMS-700	JEOL
LAB EQUIPMENT Buchi 530 (mp.)	Melting point TYPE-B-530	Buchi
Photocurrent voltage (I-V) and incident photon to electron conversion efficiency (IPCE)	Kiethley 2400	Oriel instruments

3.2.2 General chemical characterization techniques

The ruthenium complexes were purified by column chromatography technique using a LH-20 SephadexTM as stationary phase and using methanol as eluent. The structural of ligands were characterized by ¹H NMR, ¹³C NMR, melting point, FTIR and MS techniques. The ruthenium(II) complexes were characterized by ¹H NMR, ¹³C NMR, FTIR and MS techniques. The optical properties of the ruthenium(II) complexes were characterized by UV-Visible spectroscopy.

3.2.3 Fourier Transform Infrared Spectroscopy (FTIR)

The N3s dye were characterized by Fourier transform infrared spectrometer (FTIR). The FTIR spectra were recorded on NaCl pellets technique (100 mg of dried NaCl and 2 mg of samples) with a Perkin-Elmer Spectrum RX.I one Fourier transform infrared spectrophotometer over the 4000 - 400 cm^{-1} range, at the rate of 16 nm/s . The FTIR spectra are reported as wavenumber (cm^{-1}).

The methanol and water residual in the N3s dye were measured by Alpha FTIR spectrometer with diamond crystal, attenuated total reflectance (ATR) mode for Mid-IR 4000 - 550 cm^{-1} range (by broker optics), at the resolution of 4 cm^{-1} and number of scan at 64.

The FTIR spectra of ligands and ruthenium complexes dye were measured with Perkin-Elmer Spectrum by ATR technique. The data are reported as wavenumber (cm^{-1}).

3.2.4 Thermal gravimetric analysis (TGA)

The thermal property of polymer was analyzed by thermal gravimetric analysis (TGA) under a nitrogen atmosphere with a heating rate of 10 $^{\circ}\text{C}/\text{min}$.

3.2.5 UV-Visible spectroscopy

UV-Visible spectra were measured in a 1 cm path length quartz cell using a V-650 spectra high resolution UV-Vis for ruthenium(II) complex dyes. The samples were dissolved in DMF and diluted to a concentration of 1×10^{-5} M.

3.2.6 Nuclear magnetic resonance (NMR)

^1H NMR and ^{13}C NMR spectra were performed in CDCl_3 , DMSO-d_6 , Acetone- d_6 or CD_3OD recorded on Bruker AVANCE 300 MHz spectrometer, using TMS (0.00 ppm) as the internal reference. Data for NMR spectra are reported as followed: chemical shift (δ ppm), multiplicity, coupling constant (J , Hz) and integration.

3.2.7 Mass spectroscopy (MS)

Molecular weight of ruthenium(II) complexes dye were measured on Bruker micrOTOF II by electrospray ionisation techniques (ESI).

3.2.8 Melting point

Melting points was measured on Buchi 530 scientific melting point apparatus in open capillary method and are uncorrected and reported in degree Celsius.

3.3 Experimental section

This section describes the synthesis of ruthenium(II) complexes and the fabrication of the DSSCs. The organization of this thesis can be divided into two main parts, which are; I) the study of N3 dyes and II) the study of a new ruthenium complexes dye. From Figure 3.1, the experimental started from the synthesis of the ligand and the di- μ -chloro(*p*-cymene)chlororuthenium(II) precursors before forming the target ruthenium complex. Part I was divided into 5 steps. Step 1 is the synthesis of N3 dyes. Step 2 and 3 are the characterization and physical studied of the N3s. Step 5 is the photovoltaic performance studied of DSSCs. Part II was divided into 5 steps. Step 1 is the synthesis of CLC-C01, CLC-C06, CLC-C08 dyes. Step 2 and 3 are the characterization and electrochemical study. Step 4 and 5 are the photovoltaic performance study and long term stability study of DSSCs using new ruthenium complexes.

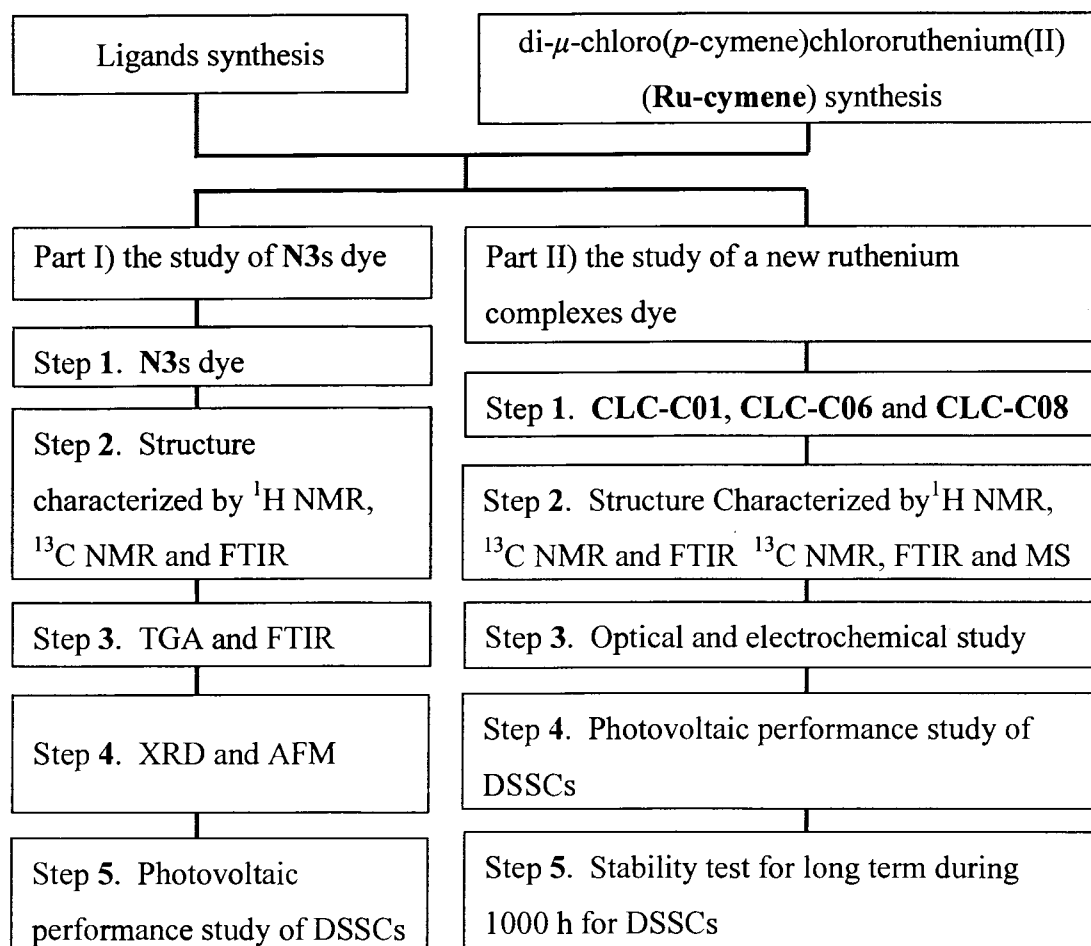
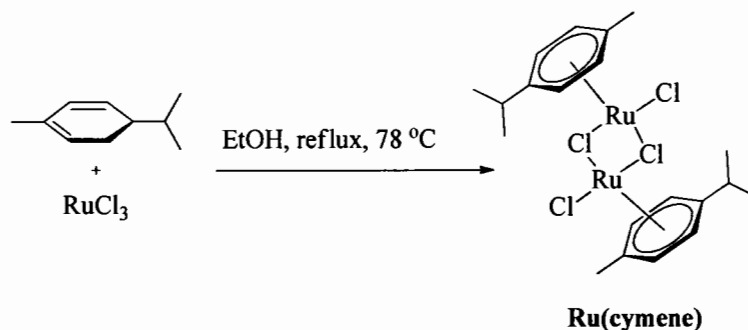


Figure 3.1 Experimental flowchart model of this work

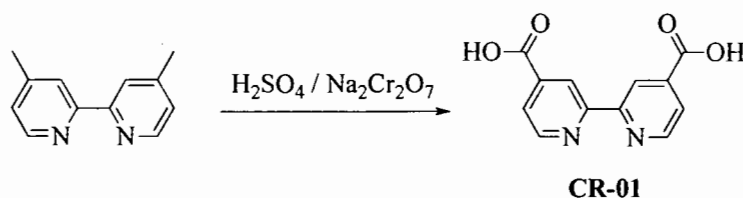
3.4 Ligands and di- μ -chloro(*p*-cymene)chlororuthenium(II) synthesis

3.4.1 Synthesis of di- μ -chloro(*p*-cymene)chlororuthenium(II)



Ruthenium(III) trichloride trihydrate (0.5 g, 2.41 mmol) was dissolved by 10 ml ethanol then α -phellandrene (2.6 ml) was added into round bottom flask. The reaction mixture was refluxed for 1 h. The solvent was removed by rotary evaporator then filtered and then washed the precipitate crude product with hexane. The product was obtained as red solid (1.16 g, 76%); m.p. 190 °C (decomposed); ESI-MS calcd for $C_{20}H_{26}C_{13}Ru_2$ ($M - Cl$) 572.9186, found 576.9185; 1H NMR (300 MHz, $CDCl_3$): 5.49 (d, $J = 6$ Hz, 4H), 5.35 (d, $J = 6$ Hz, 4H), 2.93 (q, $J = 6$ Hz, 2H), 2.71 (s, 6H), 1.29 (d, $J = 6$ Hz, 12H); ^{13}C NMR ($CDCl_3$, 75 MHz): δ 101.2, 96.7, 81.3, 80.5, 30.6, 22.1, 18.9; FTIR: (ATR) 3053, 2957, 2873, 2364, 1472, 1387, 878 cm^{-1} .

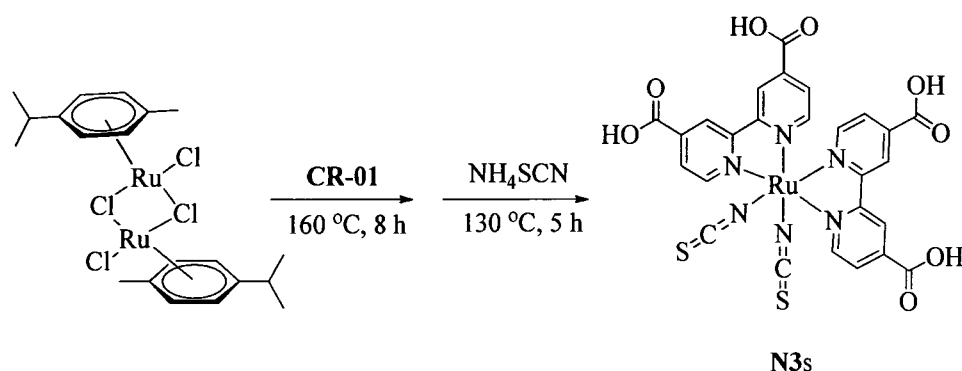
3.4.2 Synthesis of 4,4'-dicarboxy-2,2'-bipyridine ligand, (CR-1)



$Na_2Cr_2O_7$ (1.35 g, 8.69 mmol) was added to 25 ml of conc H_2SO_4 in 100 ml round bottom flask. Then, 4,4'-dimethyl-2,2'-bipyridine (0.40 g, 2.17 mmol) was added and stirred for 30 min (color changed from red to green) and then poured the mixture solution into 200 ml ice water and kept at 5 °C for 1 h. The yellow precipitate was filtered, then washed with ice water (10 ml x 3) and dissolved with 40% NaOH. The initial pH was adjusted to 2 by conc HCl and filtered again. The compound was

obtained as white solid (0.45 g, 84%); m.p. > 250 °C; ESI-MS calcd for C₁₂H₈N₂O₄ (M + H⁺) 245.0562, found 245.0779; ¹H NMR (300 MHz, DMSO-d₆): δ 7.89 (d, *J* = 6 Hz, 2H), 8.80 (s, 2H), 8.90 (d, *J* = 6 Hz, 2H); ¹³C NMR (75 MHz, DMSO-d₆): δ 166.4, 155.9, 151.1, 140.0, 120.0, 119.8; FTIR: (ATR) 3413, 3108, 2448, 1717, 1456, 1368, 1292, 1068, 1011 cm⁻¹.

3.5 The synthesis of bis(4,4'-dicarboxy-2,2'-bipyridine)dithiocyanato ruthenium(II)

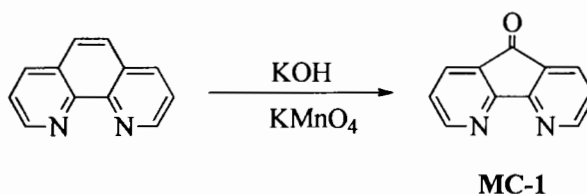


To a solution of **Ru(cymene)** (0.1 g, 0.15 mmol) in 25 mL dry DMF was added **CR-1** (0.15 g, 0.63 mmol) with stirring. The solution was heated at 160 °C under N₂ for 8 h in the dark. After that, the NH₄NCS (0.12 g, 1.57 mmol) was added and the reaction mixture was further heated at 130 °C for 5 h. DMF was removed on a rotary evaporator under vacuum to get a slurry mixture product. Then, the varied amount of DI water (18-20 mL) was added to induce the precipitation. The resulting solid was filtered off, washed with water and diethyl ether and dried under vacuum. The crude product was dissolved in basic methanol (with NaOH) and further purified on the sephadex LH-20 with methanol as an eluent. The main band was variously added DI water (18-20 mL) and was precipitated with 0.01 M HNO₃ to obtain **N3-2** (20%). The **N3-3**, **N3-4** and **N3-5** were synthesized using similar procedure as used for the synthesis of **N3-2**. The %yield of **N3** product for each reaction are **N3-3** (30%), **N3-4** (18%) and **N3-5** (22%) for third, fourth and fifth reaction set up, respectively; m.p. > 250 °C; ¹H NMR (300 MHz, CD₃OD) δ 9.44 (d, *J* = 5.7 Hz, 2H), 9.19 (s, 2H), 9.02 (s, 2H), 8.38 (d, *J* = 5.5 Hz, 2H), 7.80 (d, *J* = 5.6 Hz, 2H), 7.60 (d, *J* = 6.1 Hz, 2H); ¹³C NMR (75 MHz, CD₃OD): δ 165.9, 165.4, 159.0, 157.5, 153.4, 153.0, 140.6,

140.0, 134.8, 126.6, 125.7, 123.3, 122.9; FTIR: (ATR) 3500, 2900, 2500, 2300, 1700, 1491 cm^{-1} .

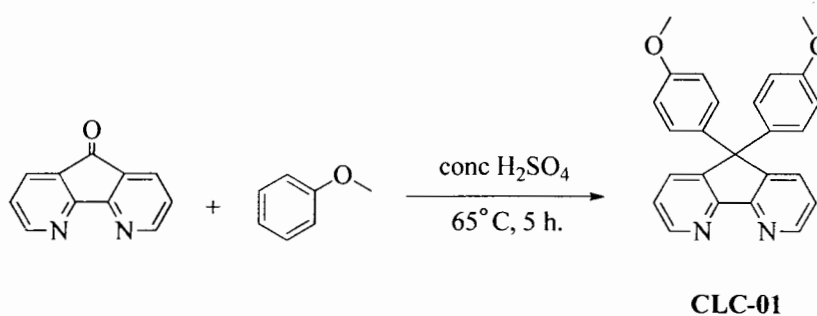
3.6 The synthesized a new ruthenium complexes dye by using new ligands for DSSC

3.6.1 The synthesized of 4,5-diazafluoren-9-one (MC-1)



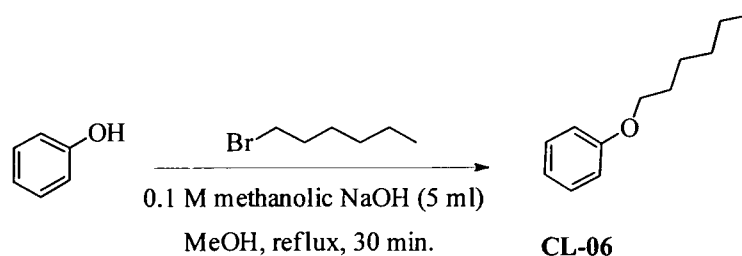
1,10-Phenanthroline (3.0 g, 16.6 mmol) was dissolved by 0.2 M of KOH in distilled water (100 mL). The reaction was refluxed until phenanthroline completely dissolved. A hot solution of KMnO_4 (6.6 g, 48.0 mmol) in distilled water (25 mL) was added to the reaction mixture over 1 h. After that, the reaction mixture was further refluxed for 10 min, and then the precipitate was filtered off. The filtrate was cooled to ambient temperature and extracted with ethyl acetate. The combined extracted organic solution was dried with Na_2SO_4 anhydrous and was concentrated by rotary evaporator. The residue was recrystallized by ethyl acetate: hexane to give MC-1 (1.21 g, 40%); m.p. > 250 °C; ^1H NMR (300 MHz, CDCl_3) δ 8.82 (d, $J = 4.7$ Hz, 2H), 8.02 (d, $J = 7.4$ Hz, 2H), 7.38 - 7.26 (m, 2H); ^{13}C NMR (75 MHz, CDCl_3): δ 183.5, 158.81, 156.8, 138.58, 133.85, 124.44; FTIR: (ATR) 3034, 2922 - 2853, 1713, 1555, 1397, 1259, 754 cm^{-1} .

3.6.2 The synthesized of 5,5'-bis(4-methoxyphenyl)-5H-cyclopenta (1,2-b:5,4-b')dipyridine (CLC-01)



MC-1 (0.5 g, 2.8 mmol) and anisole (0.7 ml) were added to round bottom flask. Conc H_2SO_4 (0.7 ml) was slowly added. After that, the reaction mixture was heated at 65 °C for overnight. The reaction mixture was cooled to room temperature and then water (20 ml) was added to the flask. The initial pH of the medium was adjusted with 1 M NaOH to give white precipitate. The solid was collected by suction filtration, washed with water and diethyl ether. This crude product was dissolved in dichloromethane and dried with Na_2SO_4 and was concentrated by rotary evaporator. The residue was recrystallized from EtOAc: hexane to give **CLC-01** (0.52 g, 50%); m.p. > 250 °C; ESI-MS calcd for $\text{C}_{25}\text{H}_{20}\text{N}_2\text{O}_2$ ($\text{M} + \text{Na}^+$) 403.1422, found 403.1408; ^1H NMR (300 MHz, CDCl_3) δ 8.87 - 8.59 (m, 2H), 7.86 - 7.67 (m, 2H), 7.37 - 7.22 (m, 4H), 7.17 - 6.96 (m, 3H), 6.90 - 6.66 (m, 3H), 3.77 (d, $J = 1.2$ Hz, 6H); ^{13}C NMR (75 MHz, CDCl_3): δ 158.9, 156.8, 149, 146, 135, 133.53, 128.89, 123.43, 113.91, 60, 55.23; FTIR: (ATR) 3074.32 - 3050.13, 3001.34, 2949.12, 2900.75, 2827.49, 1504.85, 1240.55, 1176.24, 811.28, 745.75 cm^{-1} .

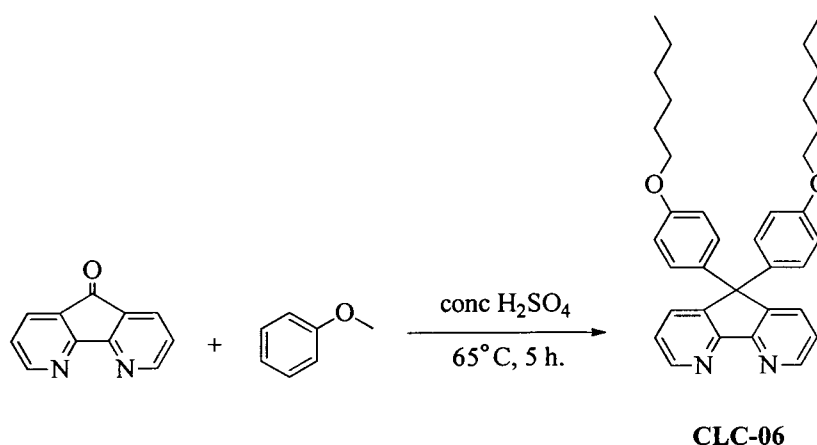
3.6.3 The synthesized of n-hexyl phenyl ether (CL-06)



A mixture of phenol (2 g, 21.25 mmol) was dissolved in MeOH (5 mL), 0.1 M methanolic NaOH (5 mL) and bromohexane (3 ml). The solution mixtures were refluxed for 1 h in a round bottom flask. The completed reaction was followed by TLC before extracted with ethyl acetate. The combined organic extracts were concentrated on rotary evaporator and the residue was purified by column chromatography using 3% ethyl acetate: hexane as eluent to get colorless liquid product **CL-06** (2.9 g, 82%); ESI-MS calcd for $\text{C}_{12}\text{H}_{18}\text{O}$ ($\text{M} + \text{Na}^+$) 201.1255, found 201.1257; ^1H NMR (300 MHz, CDCl_3) δ 7.45 - 7.24 (m, 2H), 7.09 - 6.84 (m, 3H), 4.11 - 3.97 (m, 2H), 1.92 - 1.81 (m, 2H), 1.62 - 1.27 (m, 6H), 1.01 (dd, $J = 8.9$, 4.7 Hz, 3H); ^{13}C NMR (75 MHz, CDCl_3) δ 158.9, 129.49, 120.55, 114.64, 67.94,

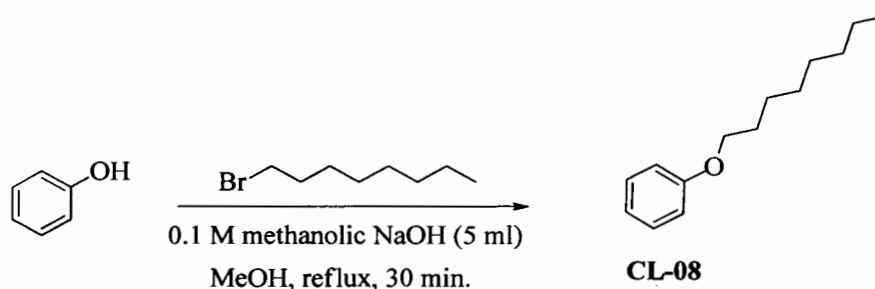
31.80, 29.47, 25.94, 22.79, 14.16; FTIR: (ATR) 3037.38, 2929.05, 2860.01, 1599.44, 1495.63, 1035, 752.08 cm^{-1} .

3.6.4 The synthesized of 5,5'-bis(4-(hexyloxy)phenyl)-5*H*-cyclopenta (1,2-b:5,4-b')dipyridine (CLC-06)



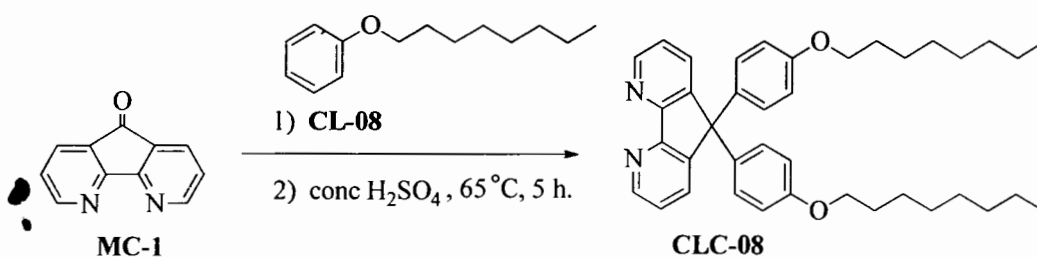
A **MC-1** (0.5 g, 2.8 mmol) and **CL-06** (1.2 ml) were added to round bottom flask. Conc H_2SO_4 (0.8 ml) was slowly added to the mixture with stirring. After that, the mixture was heated to 65 °C overnight. The reaction mixture was cooled to room temperature. Then, water (20 ml) was added to the reaction flask. The initial pH of the medium was adjusted with 1 M NaOH to give the precipitate. The solid was collected by suction filtration and washed with water. This crude product was dissolved in ethyl acetate and dried with Na_2SO_4 . The ethyl acetate was removed by rotary evaporator. Next, crude product was purified by column chromatography on silica gel using pure hexane as eluent to give solid product **CLC-06** (0.55g, 38%); m.p. = 232 °C; ESI-MS calcd for $\text{C}_{35}\text{H}_{40}\text{N}_2\text{O}_2$ ($\text{M} + \text{Na}^+$) 543.2987, found 543.2967; ^1H NMR (300 MHz, CDCl_3) δ 8.70 (d, $J = 4.8$ Hz, 2H), 7.73 (d, $J = 7.8$ Hz, 2H), 7.42 – 7.21 (m, 4H), 7.07 (d, $J = 9.1$ Hz, 3H), 6.76 (d, $J = 9.1$ Hz, 3H), 3.90 (t, $J = 6.7$ Hz, 4H), 1.95 – 1.65 (m, 6H), 1.60 – 1.32 (m, 8H), 1.12 (s, 2H), 0.90 (t, $J = 7.3$ Hz, 6H); ^{13}C NMR (75 MHz, CDCl_3) δ 158.9, 156.9, 149.9, 146.8, 135.48, 133.55, 128.86, 123.40, 114.39, 67.99, 60.9, 31.54, 29.20, 25.70, 22.57, 13.99; FTIR: (ATR) 3061.84, 2928.35, 2866.95, 1605.10, 1505.76, 1396.67, 1243.71, 1161.92, 745.23 cm^{-1} .

3.6.5 The synthesized of n-octyl phenyl ether (CL-08)



Phenol (2 g, 21.25 mmol) was dissolved in MeOH (5 mL), 1 M methanolic NaOH (5 mL) and bromooctane (3 ml). The solution mixtures were refluxed for 1 h in a round bottom flask. Completing reaction was followed by TLC, extracted with ethyl acetate. The combined organic extracts were concentrated on rotary evaporator and the residue was purified by column chromatography using hexane as eluent to get the colorless liquid product **CL-08** (3.02 g, 68%); $^1\text{H NMR}$ (300 MHz, CDCl_3) δ 7.37 - 7.26 (m, 2H), 7.02 - 6.87 (m, 3H), 4.04 - 3.99 (m, 2H), 1.89 - 1.81 (m, 2H), 1.65 - 1.50 (m, 4H), 1.48 - 1.35 (m, 6H), 0.99 - 0.66 (m, 3H); $^{13}\text{C NMR}$ (75 MHz, CDCl_3) δ 158.9, 129.38, 120.44, 114.53, 67.90, 31.83, 29.33, 26.09, 22.66, 14.08; FTIR: (ATR) 2925, 2855, 1600, 1496, 1242, 751 cm^{-1} .

3.6.6 The synthesized of 5,5'-bis(4-(octyloxy)phenyl)-5H-cyclopenta (1,2-b:5,4-b')dipyridine (CLC-08)

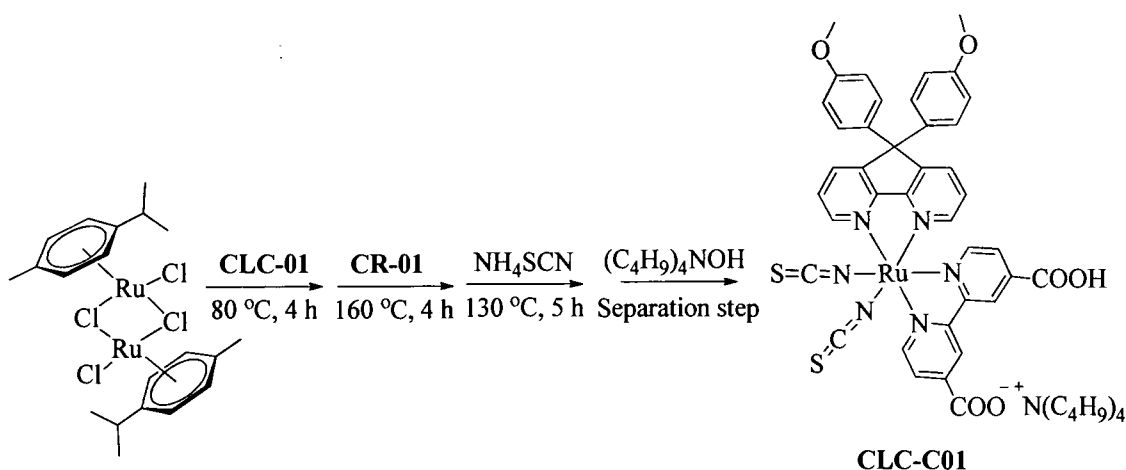


A **MC-1** (0.5 g, 2.8 mmol) and **CL-08** (1.2 ml) were added to round bottom flask. Conc H_2SO_4 (0.8 ml) was slowly added to the mixture with stirring. After that, the reaction was produced by using the same procedure as used for the preparation of **CLC-06**, the **CLC-08** solid product was obtained (0.22g, 13%); m.p. = 218 $^\circ\text{C}$; $^1\text{H NMR}$ (300 MHz, CDCl_3) δ 8.72 (d, $J = 4.8$ Hz, 2H), 7.75 (d, $J = 7.7$ Hz, 2H), 7.34 - 7.23 (m, 4H), 7.08 (d, $J = 8.4$ Hz, 3H), 6.76 (d, $J = 8.3$ Hz, 3H), 3.90

(t, $J = 6.4$ Hz, 3H), 3.51 (s, 1H), 1.83 - 1.73 (m, 4H), 1.60 - 1.27 (m, 20H), 0.88 (t, $J = 6$ Hz, 6H); ^{13}C NMR (75 MHz, CDCl_3) δ 158.9, 158, 140, 146.9, 135.49, 133.53, 128.96, 123.39, 114.39, 67.98, 31.79, 29.32, 29.23, 29.20, 26.03, 22.63, 14.06; FTIR: (ATR) 2932, 2852, 1509, 1399, 1218, 732 cm^{-1} .

3.7 The synthesis a new ruthenium complexes dye

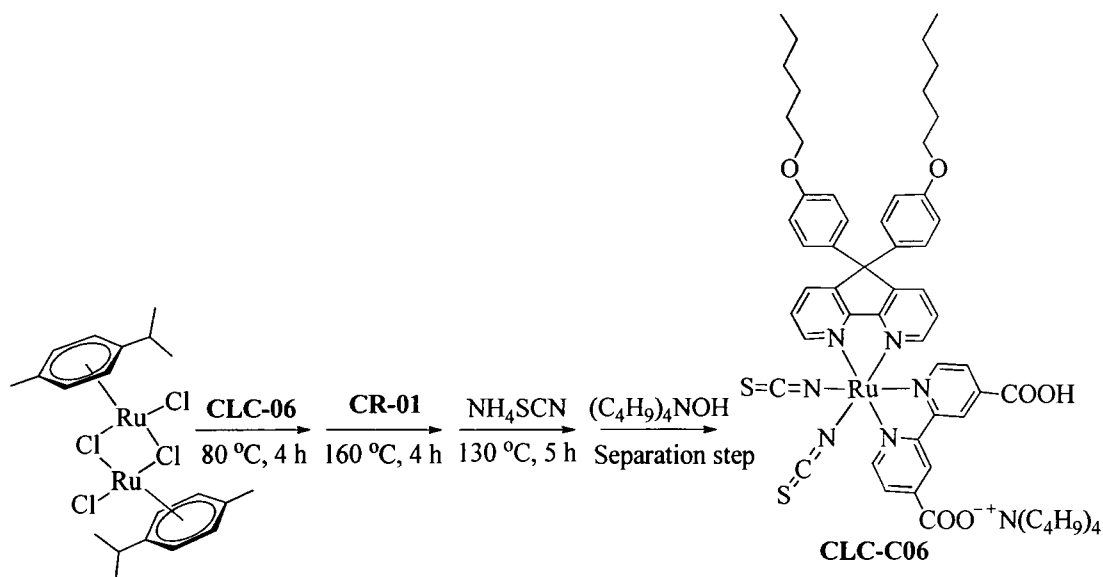
3.7.1 The synthesis of tetrabutylammonium(4-carboxylate-4'-carboxy-2-bipyridine)-5,5'-bis(4-(metyloxy)phenyl-5H-cyclopenta(1,2-b:5,4-b')dipyridine) dithiocyanato ruthenium(II) (CLC-C01)



CLC-01 (0.13 g, 0.32 mmol) and **Ru(cymene)** (0.1 g, 0.16 mmol) in anhydrous DMF were heated at 80 °C for 4 h under nitrogen gas in the dark. Subsequently, the reaction mixture was cooled to room temperature then **CR-1** (0.06 g, 0.24 mmol) was added to the flask and further heated to 160 °C for 4 h. The resulting solution was added by solid NH_4NCS (0.12 g, 1.57 mmol) at room temperature and the reaction mixture was further heated for 5 h at 130 °C. After that DMF was removed by a rotary evaporator under vacuum and water (20 ml) was added to get the precipitate. The purple solid was filtered off, washed with water and diethyl ether and dried in air. The solid mixture compound was dissolved in basic methanol and purified on the sephadex LH-20, columns chromatography twice using methanol as eluent. The first column chromatography was for roughly separation whereas the second column chromatography was for thoroughly separation. The main band was collected, concentrated, and precipitated with HNO_3 to obtain pure **CLC-C01** solid

product (0.15 g, 44%); m.p. > 250 °C; ESI-MS calcd for $C_{55}H_{63}N_7O_6RuS_2$ ($M - H^+$) 1082.3257, found 1082.3480; 1H NMR (300 MHz, CD_3OD) δ 9.69 (d, $J = 9.0$ Hz, 1H), 9.03 (s, 2H), 8.92 (s, 1H), 8.24 (d, $J = 9.0$ Hz, 2H), 8.14 (d, $J = 9.0$ Hz, 2H), 7.84 - 7.80 (m, 2H), 7.78 - 7.70 (m, 1H), 7.44 - 7.36 (m, 1H), 7.21 (d, $J = 7.7$ Hz, 2H), 7.12 (d, $J = 8.1$ Hz, 2H), 6.88 (d, $J = 7.5$ Hz, 4H), 3.72 (s, 6H), 3.30 - 3.22 (m, 8H), 1.68 (s, 8H), 1.53 - 1.31 (m, 8H), 1.21 - 1.04 (m, 12H); ^{13}C NMR (75 MHz, CD_3OD) δ 158, 157, 150, 147, 145, 136, 133, 132, 131, 128, 126, 125, 120, 114, 67, 58, 55, 29.44, 29.19, 28.93, 28.68, 28.42, 25, 24, 20, 14; FTIR: (ATR) 2925, 2873, 2103, 1251, 805 cm^{-1} .

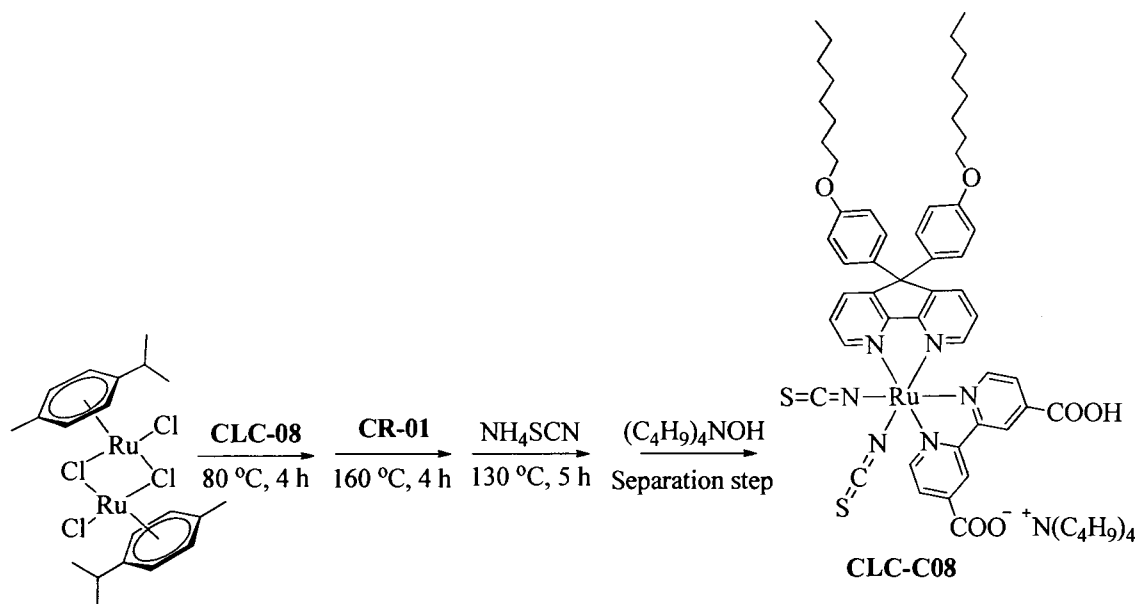
3.7.2 The synthesis of tetrabutylammonium(4-carboxylate-4'-carboxy-2-bipyridine)-5,5'-bis(4-(hexyloxy)phenyl-5H-cyclopenta(1,2-b:5,4-b')dipyridine) dithiocyanato ruthenium(II) (CLC-C06)



CLC-06 (0.18 g, 0.32 mmol) and **Ru(cymene)** (0.1 g, 0.16 mmol) in anhydrous DMF were heated at 80 °C for 4 h under nitrogen gas in the dark. Subsequently, the reaction mixture was cooled to room temperature then **CR-1** (0.06 g, 0.24 mmol) was added to the flask and further heated to 160 °C for another 4 h. The resulting solution was added by solid NH_4NCS (0.12 g, 1.57 mmol) at room temperature and the reaction mixture was further heated for 5 h at 130 °C. After that DMF was removed by a rotary evaporator under vacuum and water (20 ml) was added to get the precipitate. The purple solid was filtered off, washed with water and diethyl

ether. The solid mixture compound was dissolved in basic methanol and purified similar with **CLC-C01** process to obtain pure solid product **CLC-C06** (0.15 g, 39%); m.p. > 250 °C; ESI-MS calcd for $C_{65}H_{83}N_7O_6RuS_2$ ($M + 2H_2O + Na^+$) 1282.4999, found 1281.4573; 1H NMR (300 MHz, CD_3OD) δ 9.65 (s, 1H), 9.06 - 8.89 (m, 3H), 8.22 (t, 2H), 7.71 - 7.69 (m, 3H), 7.46 (s, 1H), 7.17 - 7.07 (m, 4H), 6.84 (d, $J = 8.7$ Hz, 6H), 3.90 (s, 4H), 3.26 (s, 8H), 1.66 (s, 12H), 1.44 - 1.28 (m, 20H), 1.03 - 0.88 (m, 18H); FTIR: (ATR) 2892, 2803, 2100, 1500, 1250, 805 cm^{-1} .

3.7.3 The synthesis of tetrabutylammonium(4-carboxylate-4'-carboxy-2-bipyridine)-5,5'-bis(4-(octyloxy)phenyl)-5H-cyclopenta(1,2-b:5,4-b')dipyridine dithiocyanato ruthenium(II) (CLC-C08)



The **Ru(cymene)** (0.1 g, 0.16 mmol) and **CLC-08** (0.18 g, 0.32 mmol) were dissolved in anhydrous DMF solution. The reaction was heated at 80 °C for 4 h under nitrogen gas in the dark. Then, the reaction mixture was cooled and **CR-1** (0.06 g, 0.24 mmol) was added to the reaction mixture. The reaction was heated at 160 °C for 4 h. After that, the reaction mixture was added by solid NH_4NCS (0.12 g, 1.57 mmol) at room temperature and further heated for 5 h at 130 °C. When reaction was completed, the DMF was removed by a rotary evaporator under vacuum. DI water (20 ml) was added to get the precipitate. The purple solid was filtered off, washed with water and diethyl ether. The crude compound was dissolved by basic methanol and was purified with similar procedure as use for the purification of **CLC-C01** to

obtain pure solid product **CLC-C08** (0.2 g, 50%); m.p. > 250 °C; ESI-MS calcd for $C_{69}H_{91}N_7O_6RuS_2$ ($M - H^+$) 1278.5437, found 1278.5556; 1H NMR (300 MHz, CD_3OD) δ 9.69 (s, 1H), 9.03 (s, 2H), 8.91 (s, 1H), 8.24 (d, $J = 9.0$ Hz, 2H), 8.13 (d, $J = 9$, 2H), 7.82 - 7.77 (m, 2H), 7.71-7.69 (m, 1H), 7.38-7.36 (m, 1H), 7.17 (d, $J = 8.7$ Hz, 2H), 7.09 (d, $J = 8.4$ Hz, 2H), 6.84 (d, $J = 8.7$ Hz, 4H), 3.90 (s, 4H), 3.25 (s, 8H), 1.68 (s, 8H), 1.53 - 1.31 (m, 8H), 1.21 - 1.04 (m, 18H); FTIR: (ATR) 2923, 2853, 2100, 1249, 805 cm^{-1} .

3.8 Fabrication of DSSC devices using N3s as sensitizer

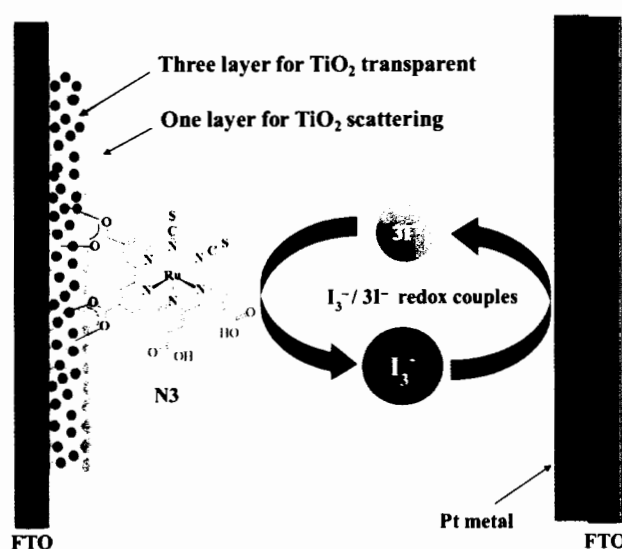


Figure 3.2 The picture of DSSCs based on N3s

3.8.1 Preparation of working electrode of N3 dyes [53]

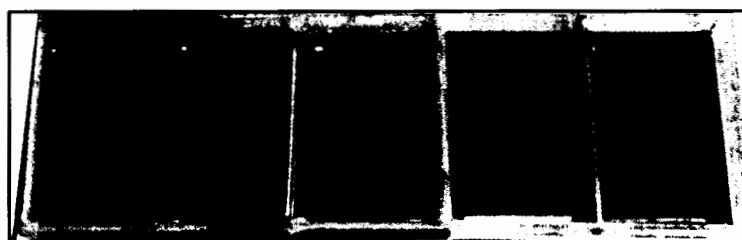
Fluorine-doped tin oxide (FTO) conducting glasses (8 Ω/sq , Solaronix) were used for electrodes. The FTO conducting glasses were immersed in an aqueous solution of 4×10^{-2} M $TiCl_4$ at 70 °C in water saturation for 30 min and then washed with water and ethanol, respectively. The $TiCl_4$ -treated-FTO were coated with 3 layers of a transparent (Ti-Nanoxide 20T/SP, Solaronix) and 1 layer of a scattering (Ti-Nanoxide R/SP, Solaronix) TiO_2 layer by screen planning method, respectively. Then, they were gradually sintered in stepwise at 325 °C for 5 min, at 375 °C for 5 min, at 450 °C for 5 min, at 500 °C for 30 min and was cooled to 80 °C. Prior to dye sensitization, the TiO_2 electrodes were immersed in an aqueous solution of 4×10^{-2} M $TiCl_4$ at 70 °C in a water saturation atmosphere for 30 min. The TiO_2 electrodes were

sintered again at 325 °C for 5 min, at 375 °C for 5 min, at 450 °C for 5 min, at 500 °C for 30 min and then cooled to about 80 °C. The prompted TiO₂ electrodes are shown in Figure 3.3.



Figure 3.3 The picture of burning electrodes

After cooling to about 80 °C, the electrodes were immersed in N3s solution (3×10^{-4} M in ethanol) in the dark at room temperature for 24 h as shown in Figure 3.4.



N3-1 N3-2 N3-3 N3-4 N3-5

Figure 3.4 The picture of N3s dye solution

Then, the electrodes were washed with water and ethanol. They were dried on heater at 50 °C to completed the working electrodes as shown in Figure 3.5.

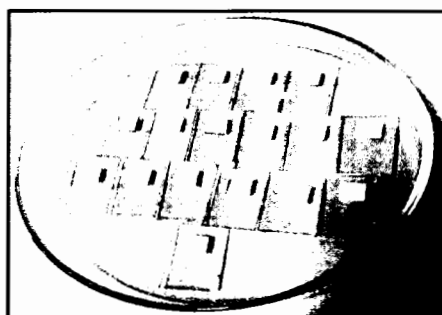


Figure 3.5 The picture of the completed the working electrood

3.8.2 Preparation of counter electrodes

The counter electrodes were prepared by placing a drop of an H_2PtCl_6 solution (18 microliters x 2 times) on an FTO conducting glasses. After that they were heated at 375 °C for 30 min. The counter electrodes are shown in Figure 3.6.



Figure 3.6 The picture of counter electrodes

3.8.3 Preparation of electrolyte

The electrolyte solution was prepared from 0.05 M I_2 , 0.1 M LiI, 0.4 M t-butylpyridine (t-BPy) and 0.6 M tetrapropyl ammonium iodide (TPAI) in 85:15 v/v acetonitrile/valeronitrile solvent.

3.8.4 Assembling of DSSCs

The working electrodes and the counter electrodes were assembled into a sealed sandwich-type cell at 111 °C, 1.30 min (Figure 3.7) by heating a surlyn film as a spacer between the electrodes.

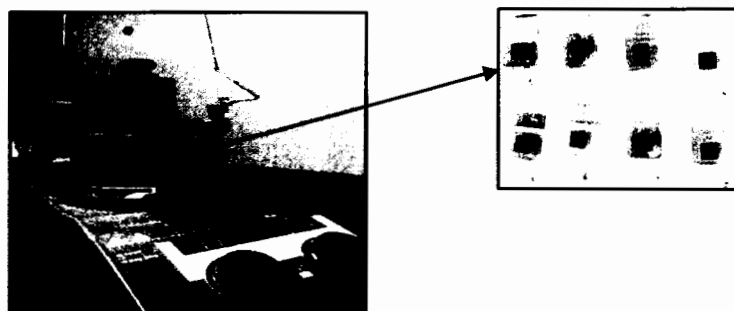


Figure 3.7 The heating step for device assembling

Then the liquid electrolyte was filled through the predrilled hole by a vacuum backfilling as shown in Figure 3.8.

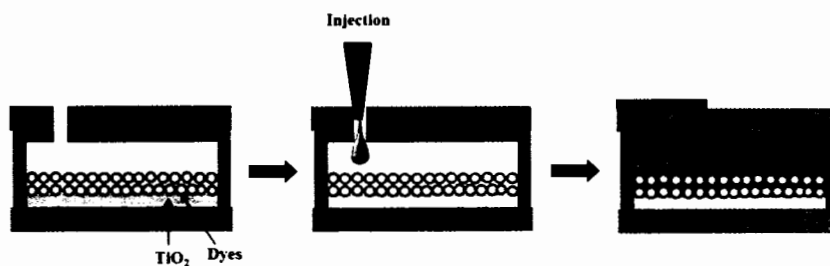


Figure 3.8 Injection step of electrolyte into the cell

Finally, the space left for contacts on both electrodes was stuck with copper film. Then, the cells were painted with silver paint that increased conductivity in the solar cell. Both solar cell electrodes were contacted with copper wire by soldering method to get the completed cells (Figure 3.9).

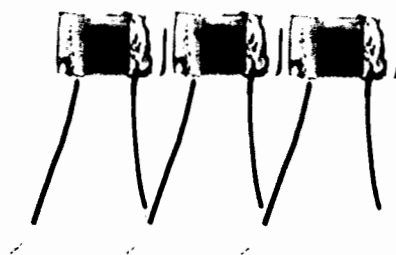


Figure 3.9 The completed dye-sensitized solar cells

3.9 Fabrication of DSSC devices using N719, CLC-C01, CLC-C006 and CLC-C08 as sensitizer [54]

3.9.1 Preparation of working electrodes

The working electrodes of N719, CLC-C01, CLC-C06 and CLC-C08 were prepared without TiCl_4 -treatment. However, the FTO were coated with three layers of transparent (Ti-Nanoxide 20T/SP, Solaronix) and two layers of scattering (Ti-Nanoxide R/SP, Solaronix) TiO_2 which are slightly different from the preparation of N3 (*i.e.*, three transparent layers and one scattering layer). Then, they were gradually sintered in stepwise as similar as the sintered step for N3 preparation (see page 37). The dyes solution of N719, CLC-C01, CLC-C006 and CLC-C08 are shown in Figure 3.10.

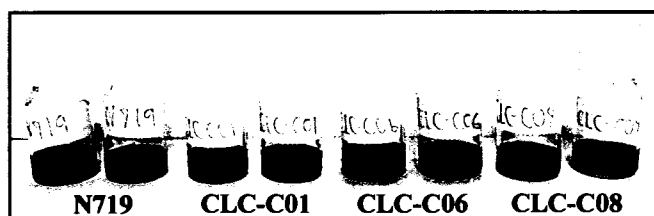


Figure 3.10 The dye solution of N719, CLC-C01, CLC-C06 and CLC-C08

The preparation procedure of counter electrodes, electrolyte and assembling of N719, CLC-C01, CLC-C06 and CLC-C08 are similar to N3s (sections 3.8.3 and 3.8.4).

3.10 DSSCs characterization

3.10.1 Current-voltage (I - V) measurement

The current – voltage (I - V) measurement were carried out with an active area of 0.16 cm^2 by a Keithley 2400 source meter unit under AM 1.5G global sun simulated sunlight (100 mW. cm^{-2}) which was produced by a 150 W Xenon arc lamp (6255 Newport) with an IR-cutoff filter (KG5-Newport).

3.10.2 Incident photon-to-current conversion efficiency (IPCE)

An incident light for IPCE measurement is given by a 150W Xenon arc lamp (6255 Newport) fitted with a monochromator (1/8m Monochromator, 74000 Newport).

4.1.1 Synthesized of di- μ -chloro(*p*-cymene)chlororuthenium(II) (Ru-cymene)

The **Ru-cymene** was synthesized from the $\text{RuCl}_3 \cdot 3\text{H}_2\text{O}$ and α -phellandrene in ethanol solution (Figure 4.2). The product was obtained as the red solid in 76% yield.

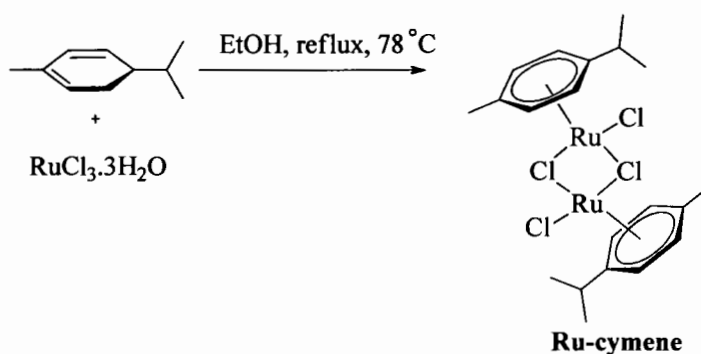


Figure 4.2 The synthesis of Ru-cymene

The **Ru-cymene** was characterized by ^1H NMR (Figure 4.3), ^{13}C NMR, FTIR and MS (APPENDICES, Figure 1). The **Ru-cymene** is a symmetric molecule, so ^1H NMR spectra show only 5 signals. The protons signal corresponding to the protons of phellandrene ring give a chemical shift at 5.49 (3H), 5.35 (3H) ppm. The protons signal at 2.91 (2H), and 1.27 (12H) ppm are assigned to the isopropyl group. The singlet proton at 2.15 (6H) ppm is methyl group.

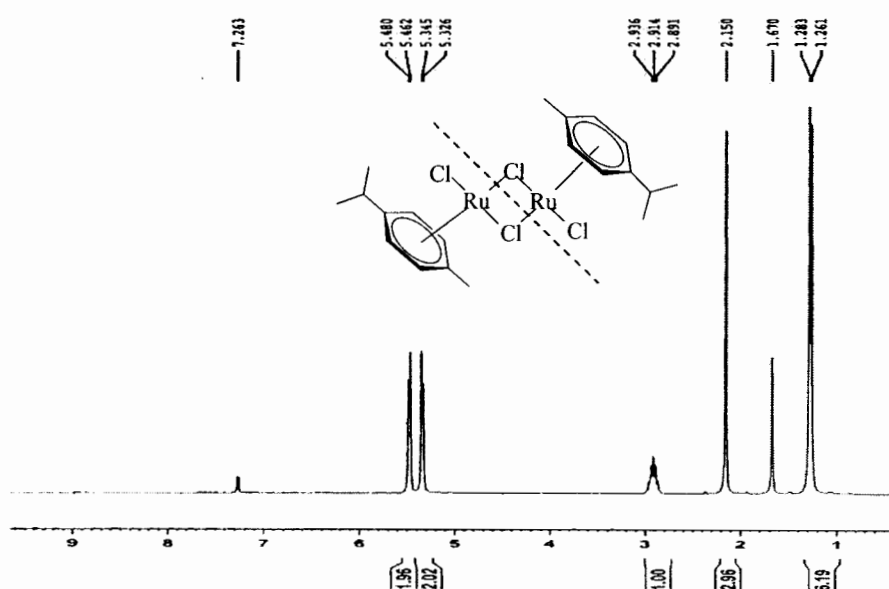


Figure 4.3 The ^1H NMR of Ru-cymene in CDCl_3

4.1.2 Synthesized of 4,4'-dicarboxy-2,2'-bipyridine (CR-1)

The 4,4'-dimethyl-2,2'-bipyridine was oxidized by $\text{Na}_2\text{Cr}_2\text{O}_7$ with H_2SO_4 to get the white solid **CR-01** in 84% yield (Figure 4.4).

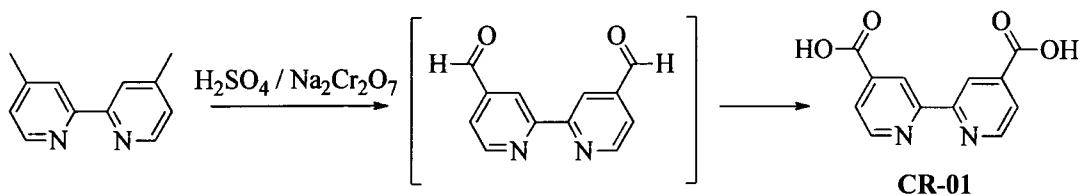


Figure 4.4 The synthesized of **CR-01**

The product was characterized by ^1H NMR (Figure 4.5), ^{13}C NMR, FTIR and MS (APPENDICES, Figure 2). The ^1H NMR spectrum of **CR-01** was shown in Figure 4.6. The **CR-01** is a symmetric molecule as only 3 signals were observed without the proton of the carboxylic groups. The proton signals showed at chemical shift 8.90 (2H), 8.80 (2H) and 7.89 (2H) ppm were assigned to 6 protons of the aromatic pyridine ring. The structure was confirmed with MS at 245.0779 m/z.

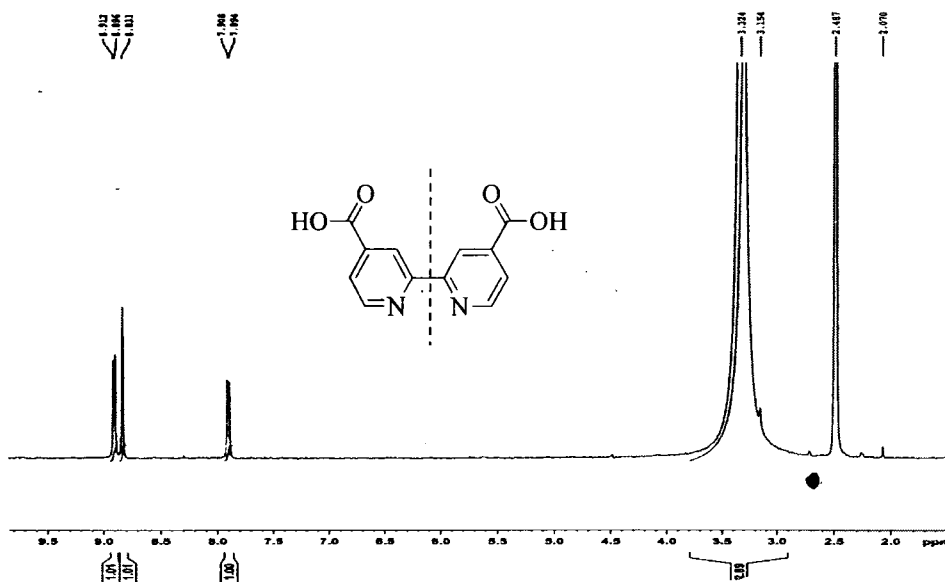


Figure 4.5 The ^1H NMR spectra of **CR-1** in CDCl_3

4.1.3 The synthesized and characterized of N3s dye

N3s were synthesized by the one-pot reaction *via* the reaction of cymene complex as shown in Figure 4.6 [55]. In the first step, the **Ru(cymene)** was reacted with a **CR-01** (2 eq.) in DMF with ligand exchange *via* intermediate **1** and **2**. Then, NH_4SCN (excess) was added to get crude products. The mixture product was purified by column chromatography with sephadex LH-20 and was methanol as an eluent. The main band was variously added by DI water (18-20 mL) and precipitated with 0.01 M HNO_3 to obtain **N3-2** (20%). The **N3-3**, **N3-4** and **N3-5** were synthesized using similar procedure as used for **N3-2**. The product of each reaction set up was obtained in moderate yield (**N3-3**, (30%), **N3-4** (18%) and **N3-5** (22%), respectively). All **N3s** were characterized by ^1H NMR which show exactly the same signals compared with the commercial **N3** (**N3-1**) (see Figure 4.7).

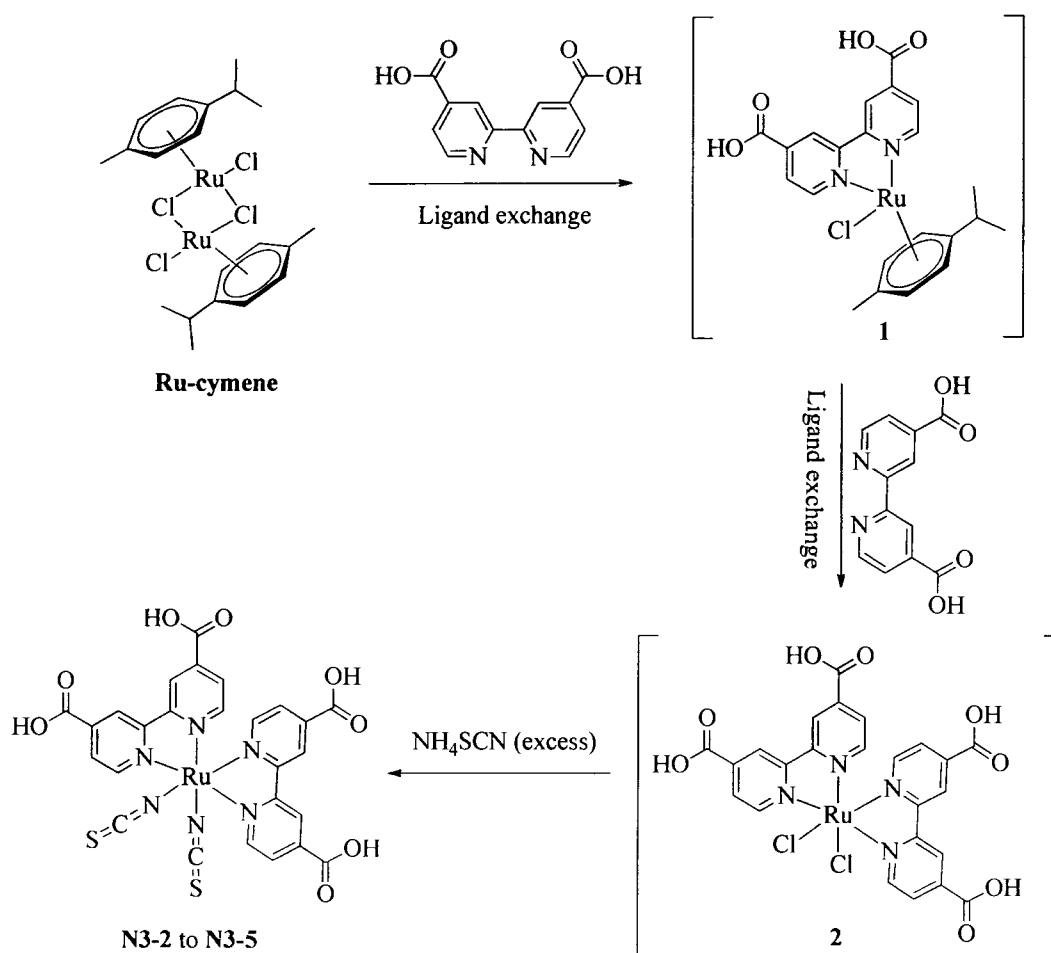


Figure 4.6 The synthetic route of ligand substitution reaction to N3s

The N3s are a symmetric molecule, so only 6 signals of position on the bipyridine ring were observed at chemical shift 9.44 (2H), 9.19 (2H), 9.02 (2H), 8.38 (2H), 7.80 (2H) and 7.60 (2H) ppm.

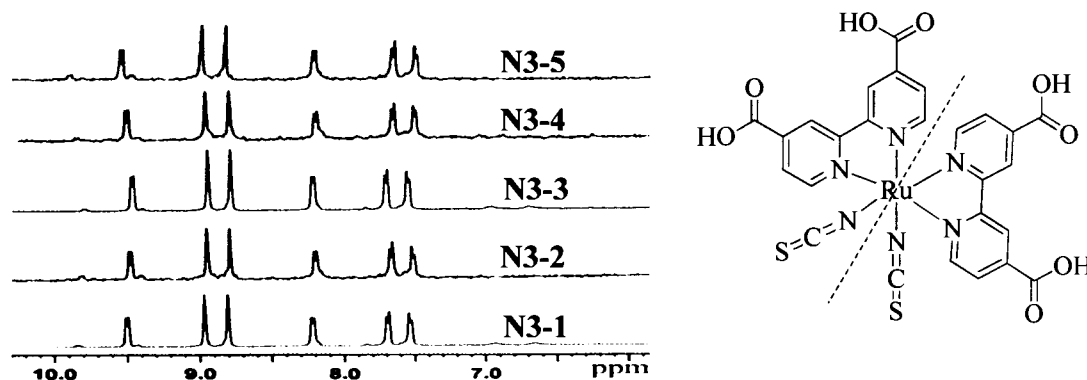


Figure 4.7 The aromatic ^1H NMR of N3s in CD_3OD

4.1.4 The thermal gravimetric analysis (TGA) study of N3s

The TGA was employed to measure the crystallinity and the small molecules that cannot identify by solution NMR technique. The different %weight loss below 100 °C (%WL₁₀₀) was observed (Figure 4.8). The varied %WL₁₀₀ can be explained by the evaporation of water and methanol residuals in complexes (Table 4.1). The order of %WL₁₀₀ are N3-1 > N3-5 > N3-3 > N3-2 > N3-4.

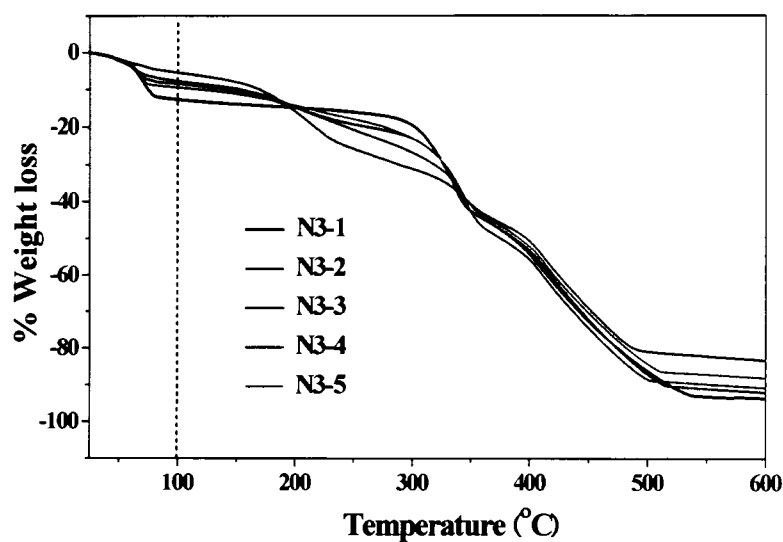


Figure 4.8 The TGA of N3s

Table 4.1 %WL₁₀₀ of N3s from evaporation of water and methanol

Dye	% WL ₁₀₀
N3-1	12.42
N3-2	7.41
N3-3	8.20
N3-4	5.52
N3-5	9.59

4.1.5 The Fourier Transform Infrared study of N3s

The FTIR spectra were measured by Alpha FTIR spectrometer with diamond crystal ATR mode for mid-IR range 4000-550 cm^{-1} . The main FTIR peaks of N3-2 to N3-5 are the same as N3-1, previously reported in the literatures [37, 56] (Figure 4.9). The results show that the higher intensities of hydroxyl to carbonyl ratio in N3s was related to the higher in water and methanol residuals in the complex. The parameters of FTIR are summarized in table 4.2. It was found that, the order of the ratio between hydroxyl (-OH) and carbonyl (-C=O) are in agreement with TGA data.

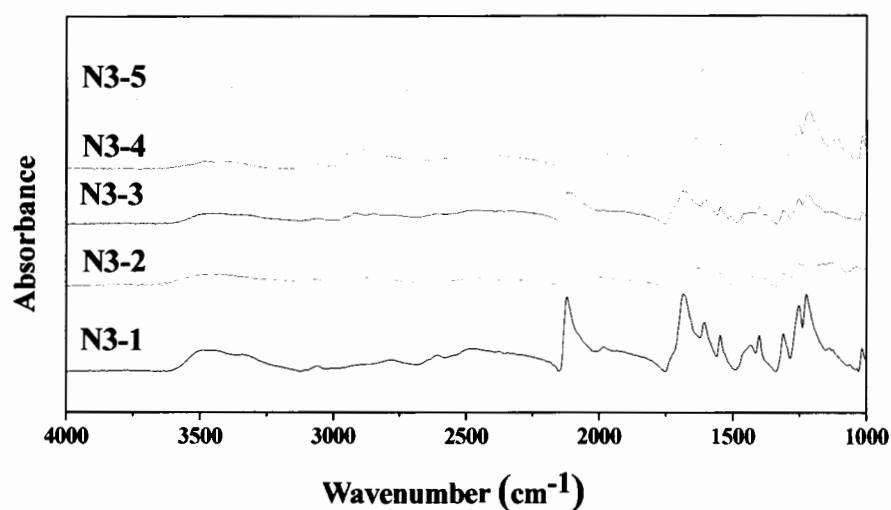
**Figure 4.9 The FTIR spectra for OH/C=O ratio of N3s**

Table 4.2 FTIR data for OH/C=O ratio of N3-1 to N3-5

Complex	OH area (3650-3128 cm^{-1})	C=O area (1756-1620 cm^{-1})	OH/C=O ratio
N3-1	25.10	22.52	1.11
N3-2	11.24	13.18	0.85
N3-3	10.37	11.82	0.87
N3-4	7.80	24.81	0.31
N3-5	15.07	15.66	0.96

4.1.6 Study of the crystallinity and the average roughness (R_a) of N3s

We studied the crystallinity of N3-1 to N3-5 by XRD. The result shows that a similar XRD pattern was observed in Figure 4.10A. The average roughness (R_a) of coated TiO_2 and bare TiO_2 were studied by AFM, shown in Figure 4.10B. The N3s show similar roughness (≈ 85 nm). From this result, it was indicated that the screen printing laminated TiO_2 was good, which lead to the accurately data of DSSCs efficiency.

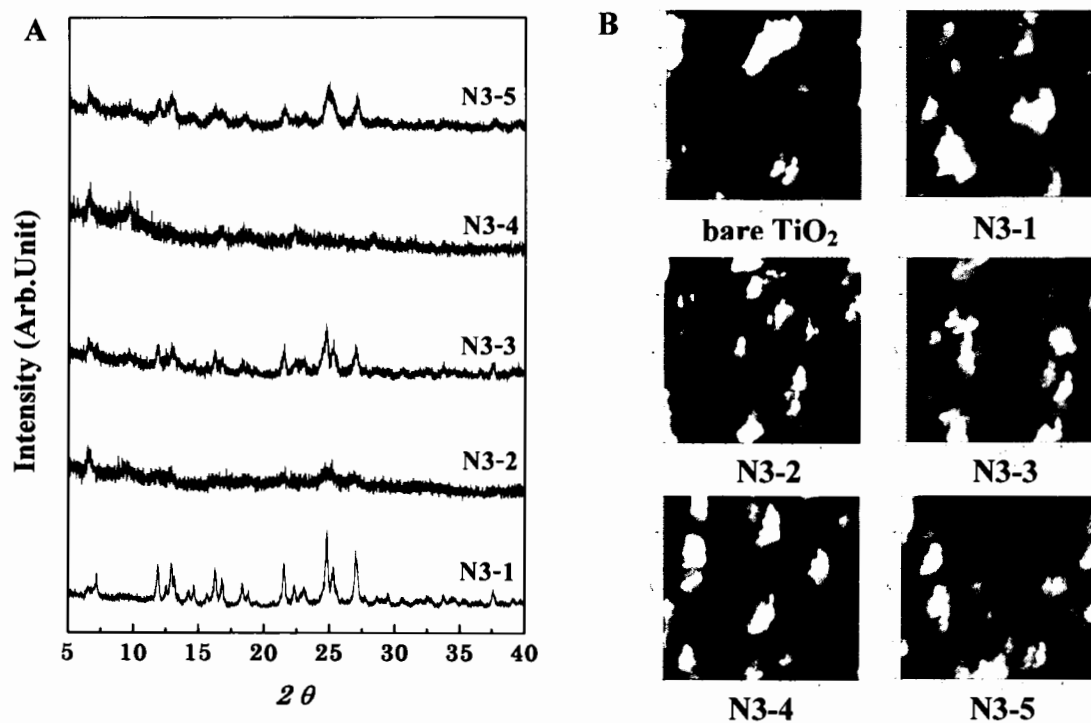


Figure 4.10 A: XRD pattern of N3s, B: AFM of FTO coated on bare TiO_2 and TiO_2 coated by N3s

4.1.7 The power conversion efficiencies study of N3s

The power conversion efficiencies of N3s are shown in Figure 4.11 and summarized in Table 4.3.

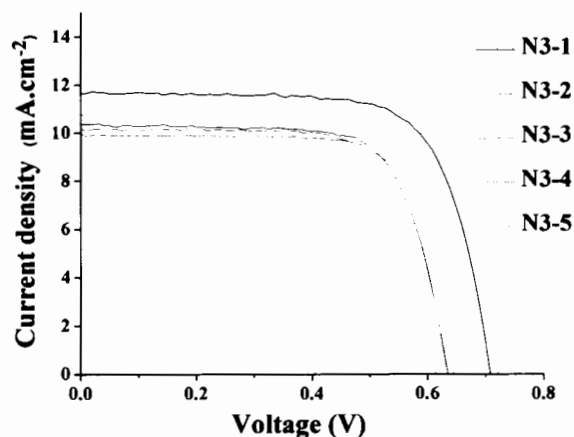


Figure 4.11 The I - V curves of N3s

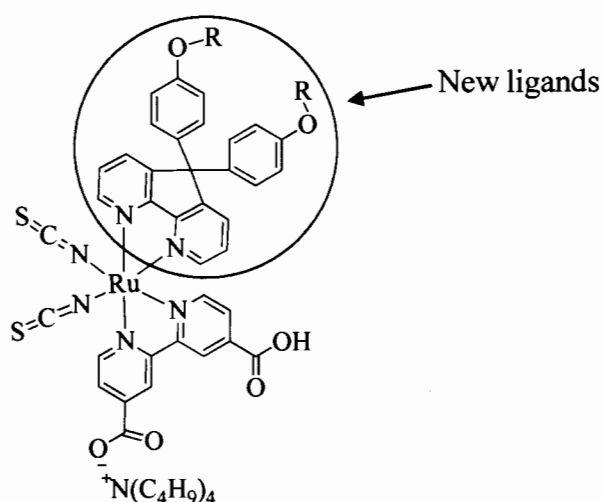
It was found that, the N3s shows varied power conversion efficiency from 4.54% to 5.92%. The N3-1 give the highest efficiency, compared with synthesized complexes (N3-2 to N3-5). Interestingly, the power conversion efficiency shows an agreement with the TGA and FTIR data, higher water and methanol residue give better efficiency. This results clearly showed that N3s have a different amount of water and methanol contents which then affect the solubility in ethanol in devising step leading to a varied dyes absorbed on the TiO_2 surface [57, 58]. Complexes containing more methanol and water improve the N3s solubility that cause dyes molecule to absorb more on the surface TiO_2 leading to high efficiency.

Table 4.3 Photovoltaic efficiencies parameter of the synthesized and commercial N3 dyes

Sample	% η	J_{sc} (mA/cm ²)	ff	V_{oc} (V)	OH/C=O ratio	% WL ₁₀₀
N3-1	5.92	11.64	0.72	0.71	1.11	12.42
N3-2	4.71	9.94	0.73	0.65	0.85	7.41
N3-3	4.73	10.37	0.72	0.64	0.87	8.20
N3-4	4.54	10.16	0.73	0.61	0.31	5.52
N3-5	4.92	10.76	0.72	0.63	0.96	9.59

4.2 Synthesis a new of ruthenium complexes dye using new ligands for DSSCs

This section focuses on the synthesis of new sensitizers with different alkyl chain. The new complexes are named, tetrabutyl ammonium(4-carboxylic acid-4'-carboxylate)-2,2'-bipyridine-5,5'-bis(4-(metyloxy)phenyl-5*H*-cyclopenta-1,2-b:5,4-b'-dipyridine)dithiocyanato ruthenium(II) (CLC-C01), tetrabutyl ammonium(4-carboxylic acid-4'-carboxylate)-2,2'-bipyridine-5,5'-bis(4-(hexyloxy)phenyl-5*H*-cyclopenta-1,2-b:5,4-b'-dipyridine)dithiocyanato ruthenium(II) (CLC-C06) and tetrabutyl ammonium(4-carboxylic acid-4'-carboxylate)-2,2'-bipyridine-5,5'-bis(4-(octyloxy)phenyl-5*H*-cyclopenta-1,2-b:5,4-b'-dipyridine)dithiocyanato ruthenium(II) (CLC-C08) (Figure 4.12). We expected that the different amphiphilic long chains could affect the hydrophobicity in the surface of dye-sensitized and improve DSSC long term stability compared with standard bipyridine ligand N719 dye.



CLC-C01, R = CH₃

CLC-C06, R = CH₂CH₂CH₂CH₂CH₂CH₃

CLC-C08, R = CH₂CH₂CH₂CH₂CH₂CH₂CH₂CH₃

Figure 4.12 The structures of new dyes

The synthetic route of CLC-C01, CLC-C06 and CLC-C08 were designed synthesized process by retrosynthetic analysis as shown in Figure 4.13.

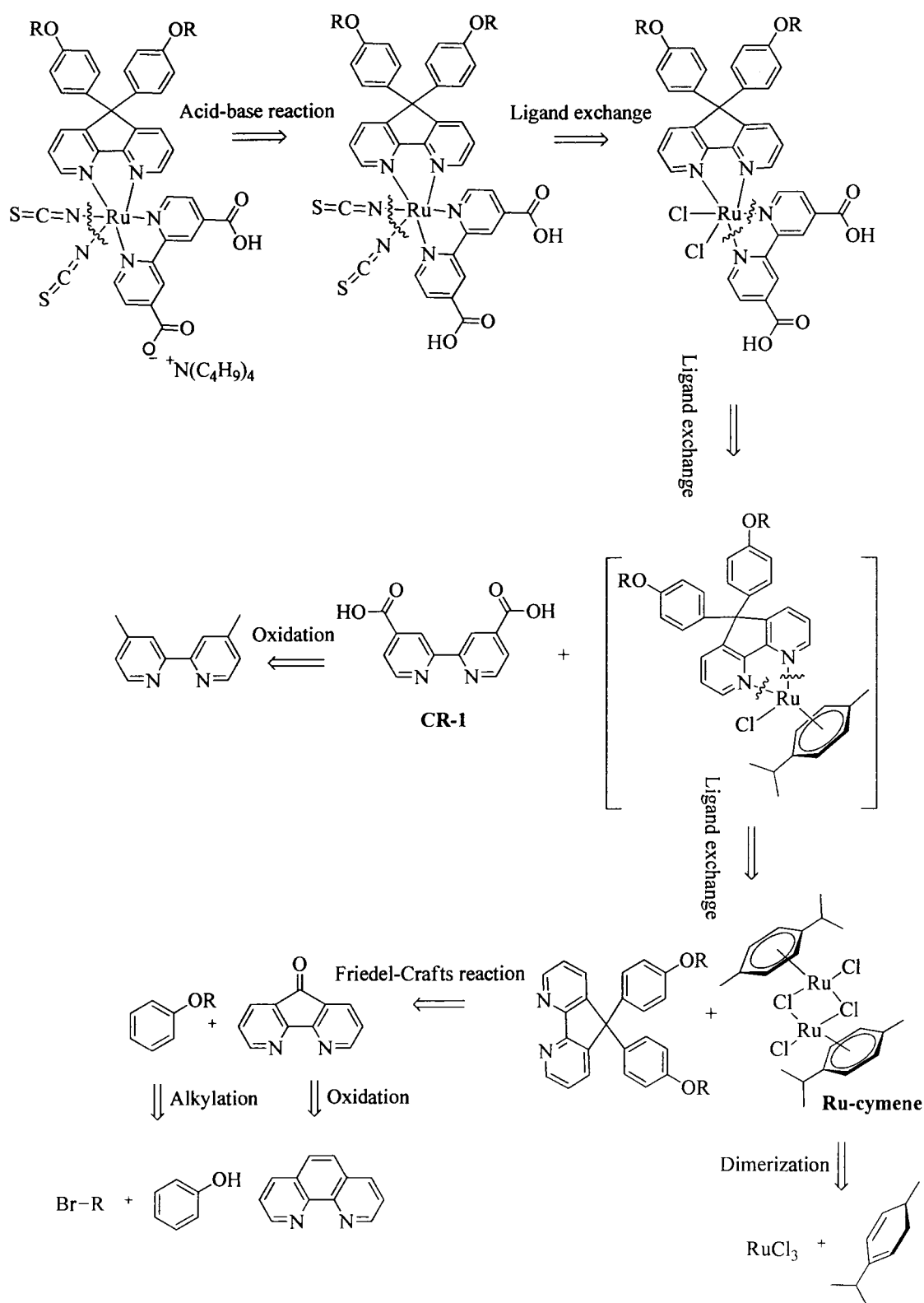


Figure 4.13 The synthetic route of new dyes

The new dyes can be synthesized from one-pot reaction *via* the reaction of **Ru-cymeme** with **CR-1** ligand, a new ligand and NH_4SCN ligand, respectively. The preparation of **Ru-cymeme** and **CR-1** ligand were described in section 3.4.1 and 3.4.2, respectively.

4.2.1 The synthesis of 5,5'-bis(4-methoxyphenyl)-5*H*-cyclopenta(1,2-b:5,4-b')dipyridine (**CLC-01**) ligand

CLC-01 can be prepared from the reaction of anisole with a 4,5-diazafluoren-9-one (**MC-1**). The **MC-1** was synthesized from the oxidation of 1,10-phenanthroline as shown in Figure 4.14.

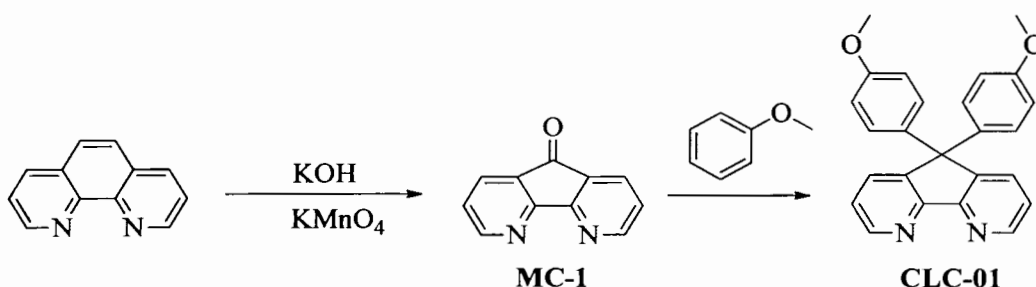


Figure 4.14 The synthesis of **CLC-01**

The mechanism reaction of **MC-1** was presented in Figure 4.15. The reaction occurs *via* the formation of 1,10-phenanthroline-5,6-dione (**2**) as an intermediate. Then, the molecule **2** was converted to molecule **3** by KOH . The carbon dioxide was removed to get alcohol derivative, molecule **4**. The final product **5** was obtained from further oxidation.

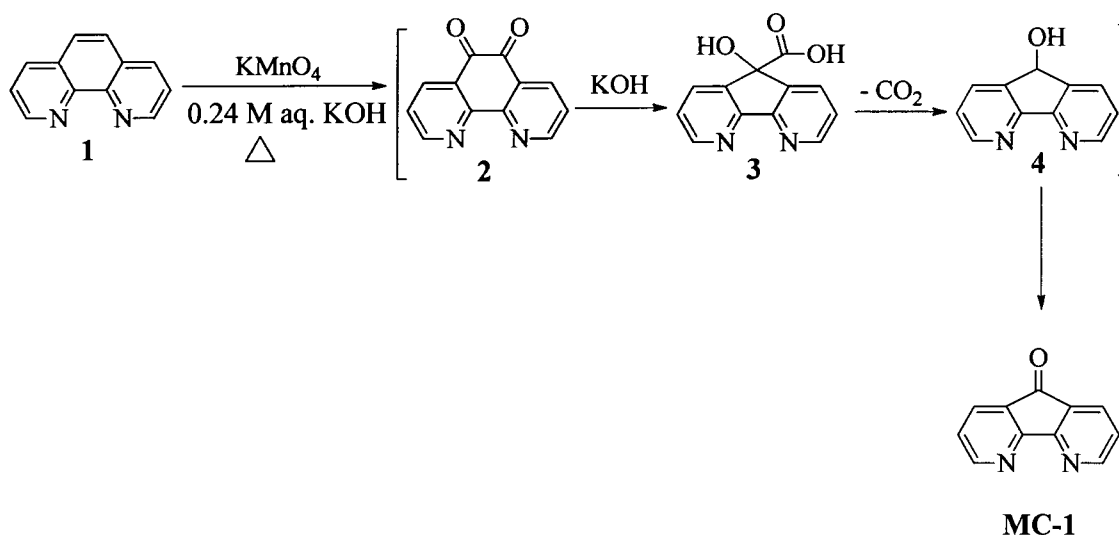


Figure 4.15 The mechanism of MC-1

The chemical structure of MC-1 was confirmed by ^1H NMR, ^{13}C NMR, FTIR and mass spectroscopy (APPENDICES, Figure 3).

The MC-1 is a symmetric molecule, which 3 signals of 6 protons were assigned as the protons of aromatic ring. The signal at chemical shift 8.82 (2H), 8.02 (2H) and 7.35 (2H) ppm are attributed to the proton of *o*-position proton, *m*- position proton and *p*-position proton, respectively (Figure 4.16).

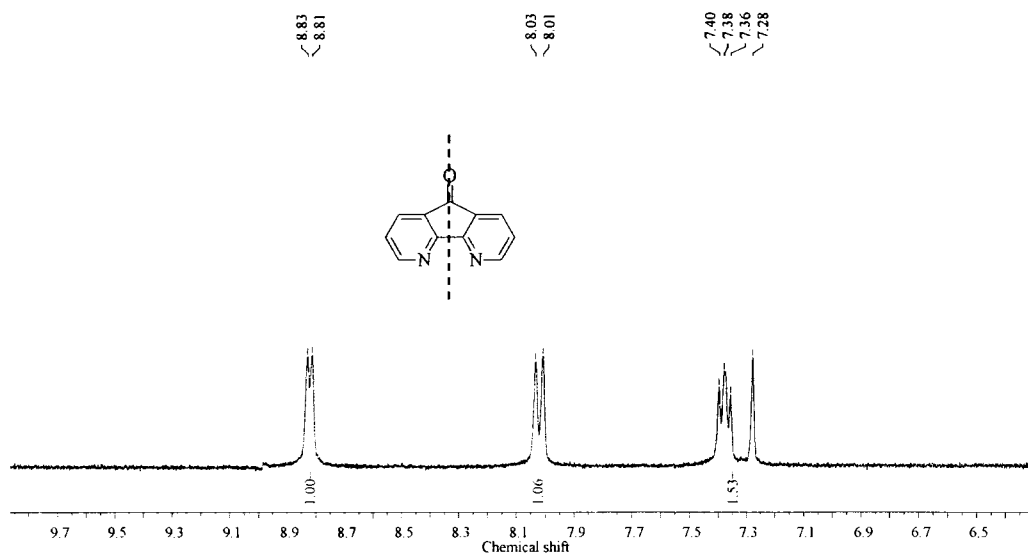


Figure 4.16 The ^1H NMR of MC-1 in CDCl_3

The mechanism for synthesis of **CLC-01** ligand is shown in Figure 4.17. The **CLC-01** was synthesized from the Friedel-Crafts reaction of **MC-1** with anisole in the presence of conc H_2SO_4 .

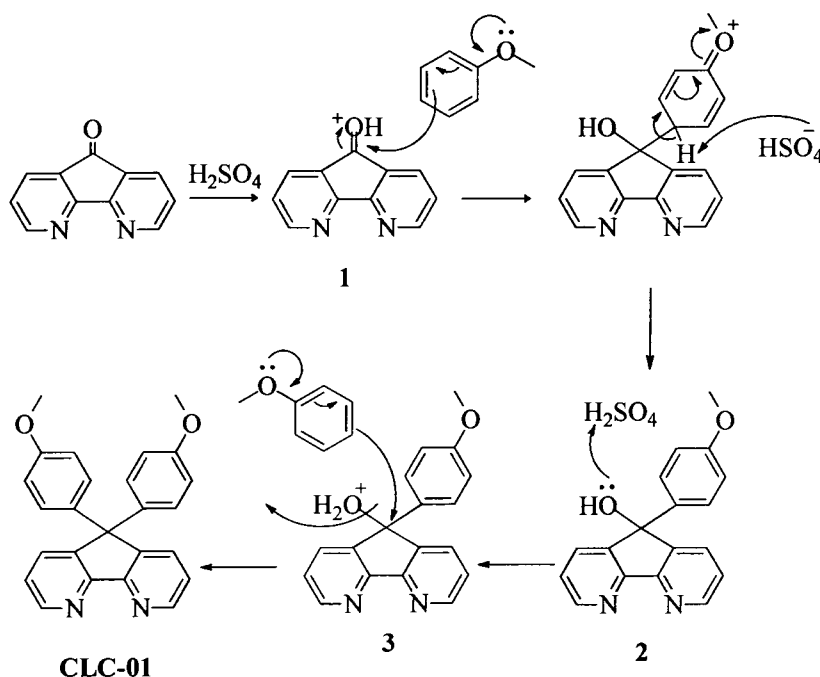


Figure 4.17 The mechanism of **CLC-01** synthesis

^1H NMR spectrum of **CLC-01** is shown in Figure 4.18. The **CLC-01** is a symmetric molecule, which 10 signals of 20 protons are observed at chemical shift 8.87 - 8.59 (2H), 7.86 - 7.67 (2H) and 7.37 - 7.22 (2H), 7.17 - 6.96 (4H) and 6.90 - 6.66 (4H) ppm assigned as aromatic position protons. The methyl protons show at chemical shift 3.77 (6H) ppm.

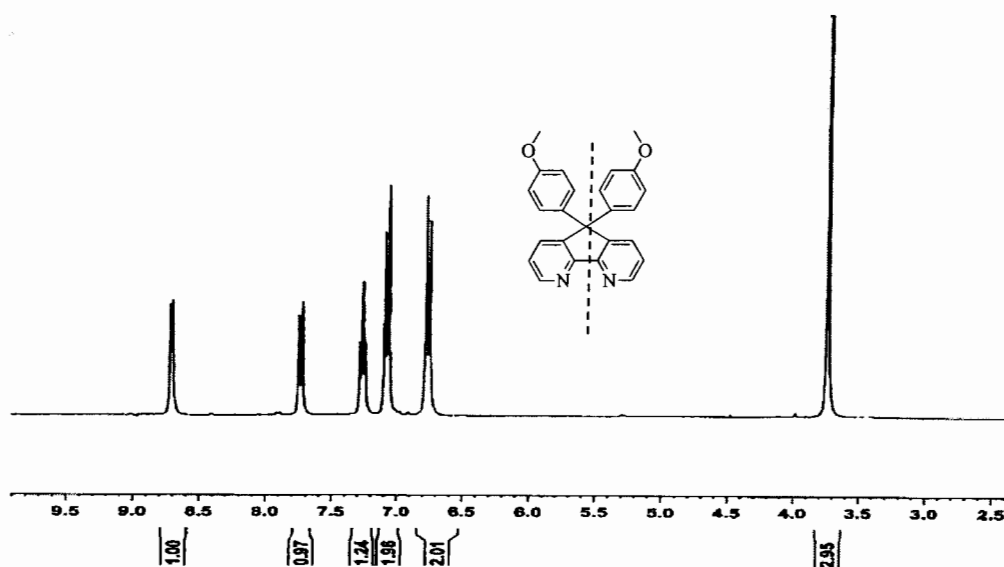


Figure 4.18 The ^1H NMR of the CLC-01 in CDCl_3

4.2.2 The synthesis of 5,5'-bis(4-hexyloxy phenyl)-5H-cyclopenta(1,2-b:5,4-b')dipyridine (CLC-06).

The synthesis procedure of CLC-06 was designed similar to CLC-01 ligand. However, the CLC-06 was synthesized from two steps. In the first step, (hexyloxy)benzene (CL-06) was prepared by Williamson ether of bromohexane with phenol under base condition. The mechanism reacts *via* the $\text{S}_{\text{N}}2$ shown in Figure 4.19. The phenol was converted to phenoxide by methanolic NaOH. Then, the nucleophile attacks to an alkyl group of bromohexane. After that, the mixture was purified by column chromatography on silica gel using pure hexane as eluent to get colorless liquid product.

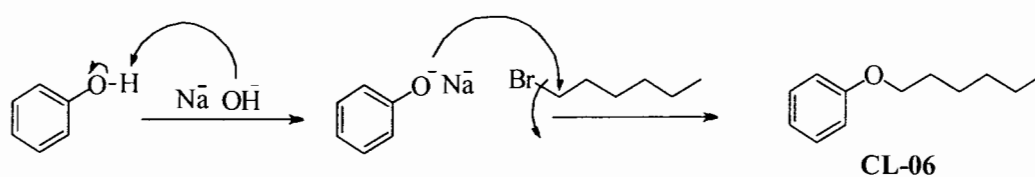


Figure 4.19 The mechanism for synthesis of CL-06

The **CL-06** was characterized by ^1H NMR (Figure 4.20), ^{13}C NMR, FTIR and MS (APPENDICES, Figure 5).

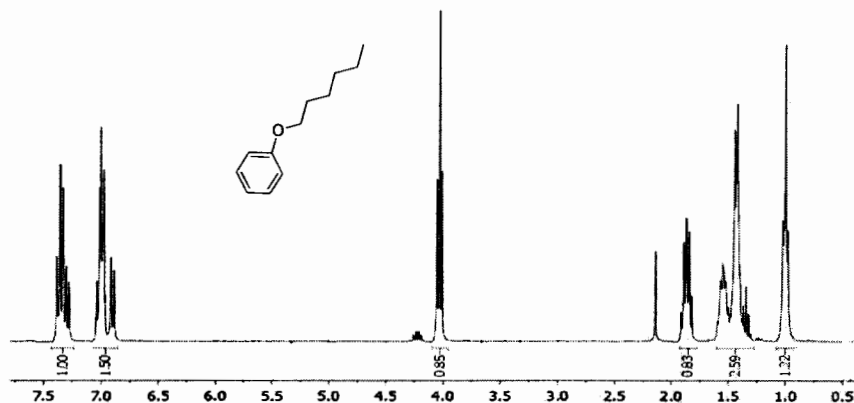


Figure 4.20 ^1H NMR of the **CL-06** in CDCl_3

The signals 18 protons were observed. The protons on aromatic ring shows at chemical shift 7.39-7.28 (2H) and 7.04 - 7.00 (3H) ppm. The chemical shifts at 4.06 to 0.98 ppm were attributed to 13 protons of alkyl long chain position protons.

The second step, the **CL-06** reacts with the **MC-1** by Friedel-Crafts reaction under conc H_2SO_4 as shown in Figure 4.21. The mixture product was purified by column chromatography on silica gel using 5% ethyl acetate: hexane as eluent to obtain white solid product of **CLC-06**. The mechanism for synthesis of **CLC-06** is similar of **CLC-01** (described in Figure 4.17). The **CLC-06** was characterized by ^1H NMR, ^{13}C NMR, FTIR and MS (APPENDICES, Figure 6).

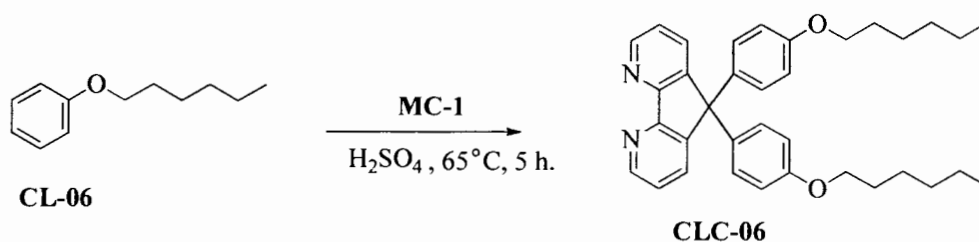


Figure 4.21 Synthesis procedure of the **CLC-06**

The **CLC-06** is a symmetric molecule, so the ^1H NMR spectrum shows 20 protons signal, as shown in Figure 4.22. The proton signals, corresponding to the protons of aromatic position protons, appear at chemical shift 8.71 (2H), 7.73 (2H), 7.28 - 7.23 (2H), 7.05(4H) and 6.75 (4H) ppm. The signals at chemical shift 3.88 to 0.86 were attributed to 13 protons of alkyl long chain position protons.

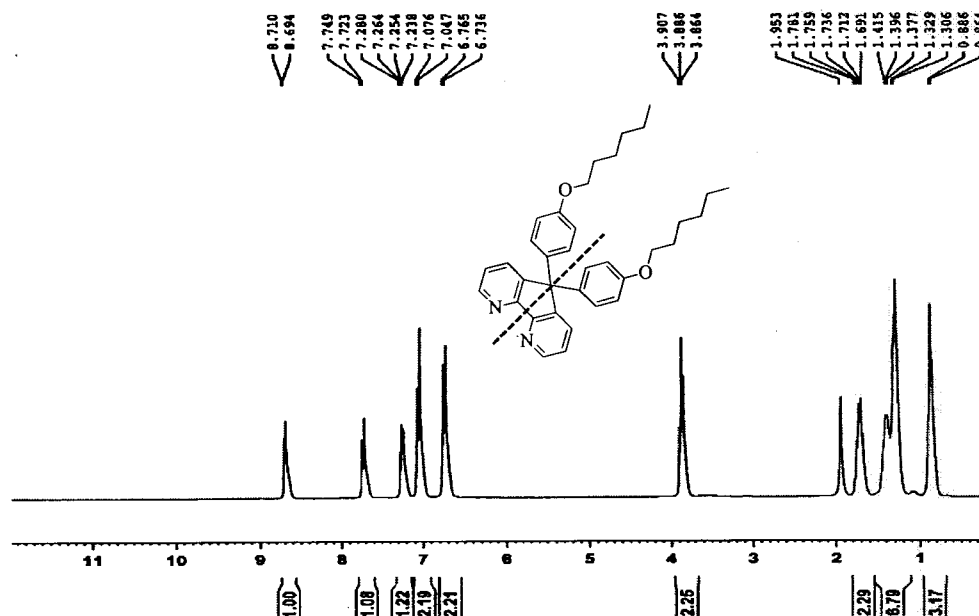


Figure 4.22 ^1H NMR of the CLC-06 in CDCl_3

4.2.3 Synthesis of 5,5'-bis(4-octyloxy phenyl)-5*H*-cyclopenta(1,2-b:5,4-b') dipyridine ligand (CLC-08)

The synthesis procedure of **CLC-08** is similar to **CLC-06** ligand. Starting from the prepared (octyloxy)benzene (**CL-08**) that was synthesized from the alkylation of phenol and n-bromo octane under methanolic NaOH. Then, the mixture was purified by column chromatography on silica gel using pure hexane as eluent to obtain colorless liquid product. The structure of **CL-08** was confirmed by ^1H NMR, ^{13}C NMR and FTIR (APPENDICES, Figure 7). The synthesis procedure of **CLC-08** is similar to **CLC-06** via the Friedel-Crafts reaction of **MC-1** with **CL-08** in the presence of conc H_2SO_4 as shown in Figure 4.23. The ^1H NMR spectrum of **CL-08** is shown in Figure 4.24. The signals at chemical shift 7.37 - 7.26 (2H) and 7.02 - 6.87 (3H) ppm were assigned to aromatic protons. The chemical shifts at 4.04 to 3.99 ppm were assigned to 17 protons of alkyl long chains. The chemical structure of **CLC-08**

was confirmed by ^1H NMR, ^{13}C NMR and FTIR (APPENDICES, Figure 8). The ^1H NMR spectrum of **CLC-08** is shown in Figure 4.25. The **CLC-08** is a symmetric molecule, so only 24 protons signal were observed. The signals at chemical shift 8.72 (2H), 7.75 (2H) and 7.34 - 7.23 (2H), 7.08 (4H), 6.76 (4H) ppm were assigned to aromatic protons. The signals at chemical shift 3.90 to 0.91 ppm were assigned to 34 protons of alkyl long chains.

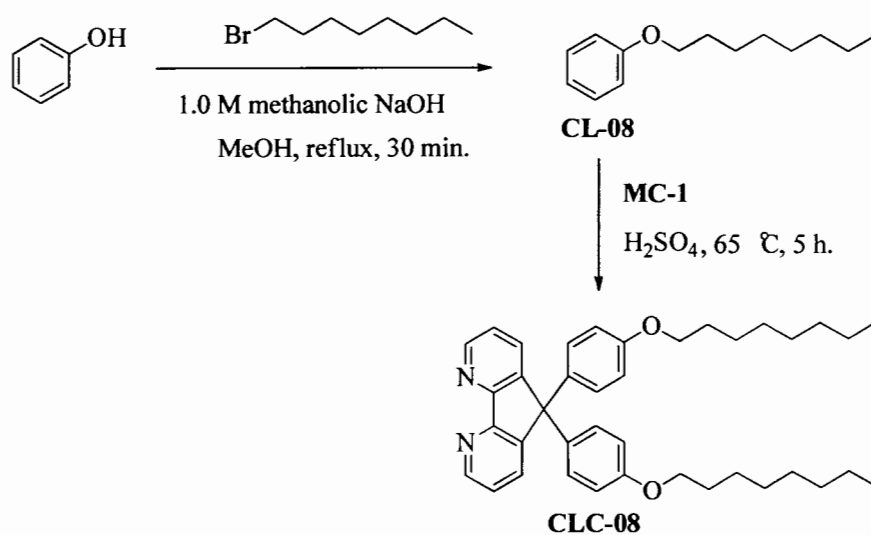


Figure 4.23 The synthesis of **CLC-08**

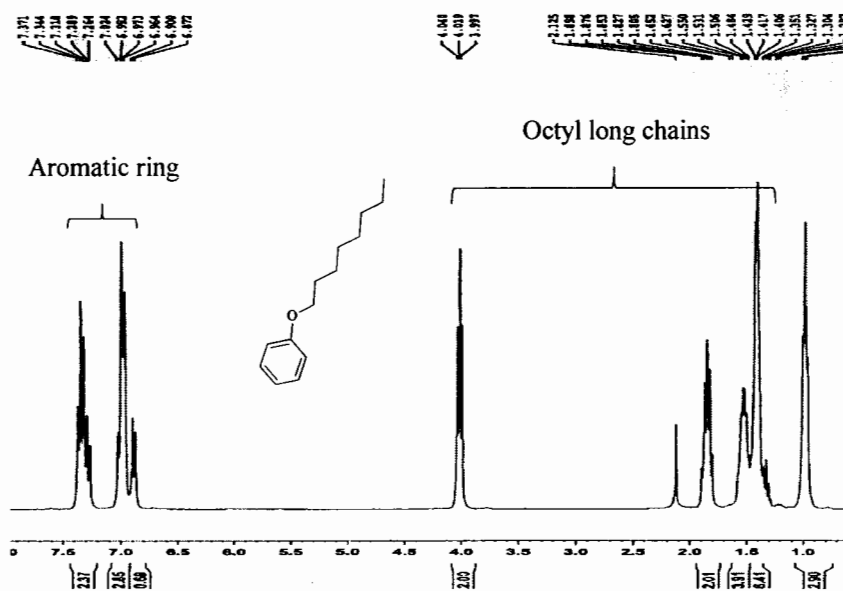


Figure 4.24 The ^1H NMR of the **CL-08** in CDCl_3

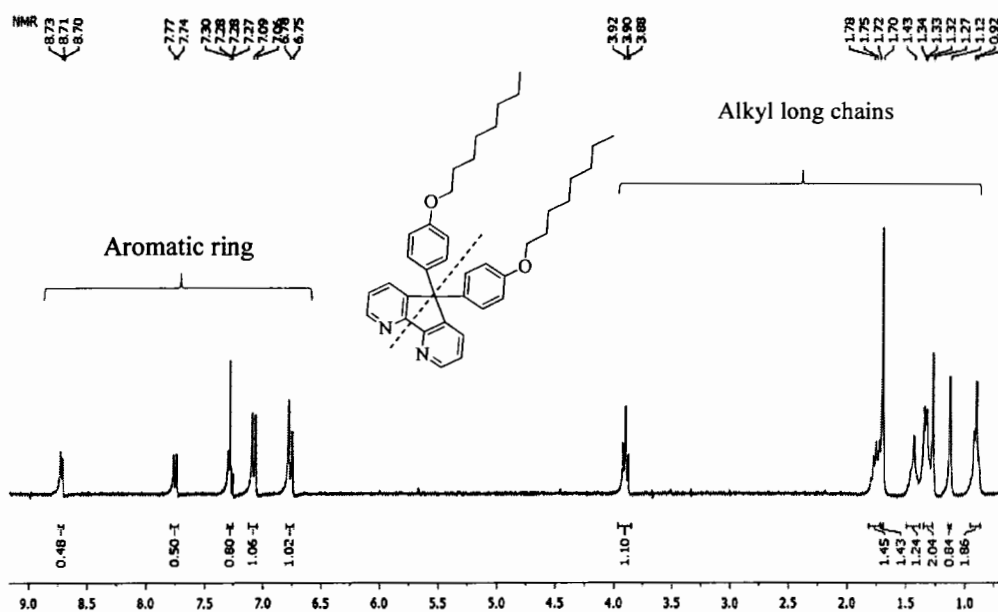


Figure 4.25 The ^1H NMR of the CLC-08 in CDCl_3

4.2.4 The synthesis of tetrabutyl ammonium(4-carboxylate-4'-carboxy-2-bipyridine)-5,5'-bis(4''-(metyloxy)phenyl-5H-cyclopenta(1,2-b:5,4-b')(dipyridine) dithiocyanato ruthenium(II) (CLC-C01)

The CLC-C01 was synthesized by the one-pot reaction *via* the ligands exchange of **Ru(cymene)** (Figure 4.26) [2]. First, the **Ru(cymene)** was reacted with the **CLC-01** ligand and **CR-1** ligand in DMF solution, respectively. Then, NH_4SCN (excess) was added to get the crude products. This crude compound was dissolved in tetra butyl ammonium base and further purified on the sephadex LH-20 column chromatography with methanol as eluent. The main band was collected, concentrated, and precipitated with HNO_3 to obtain **CLC-C01**.

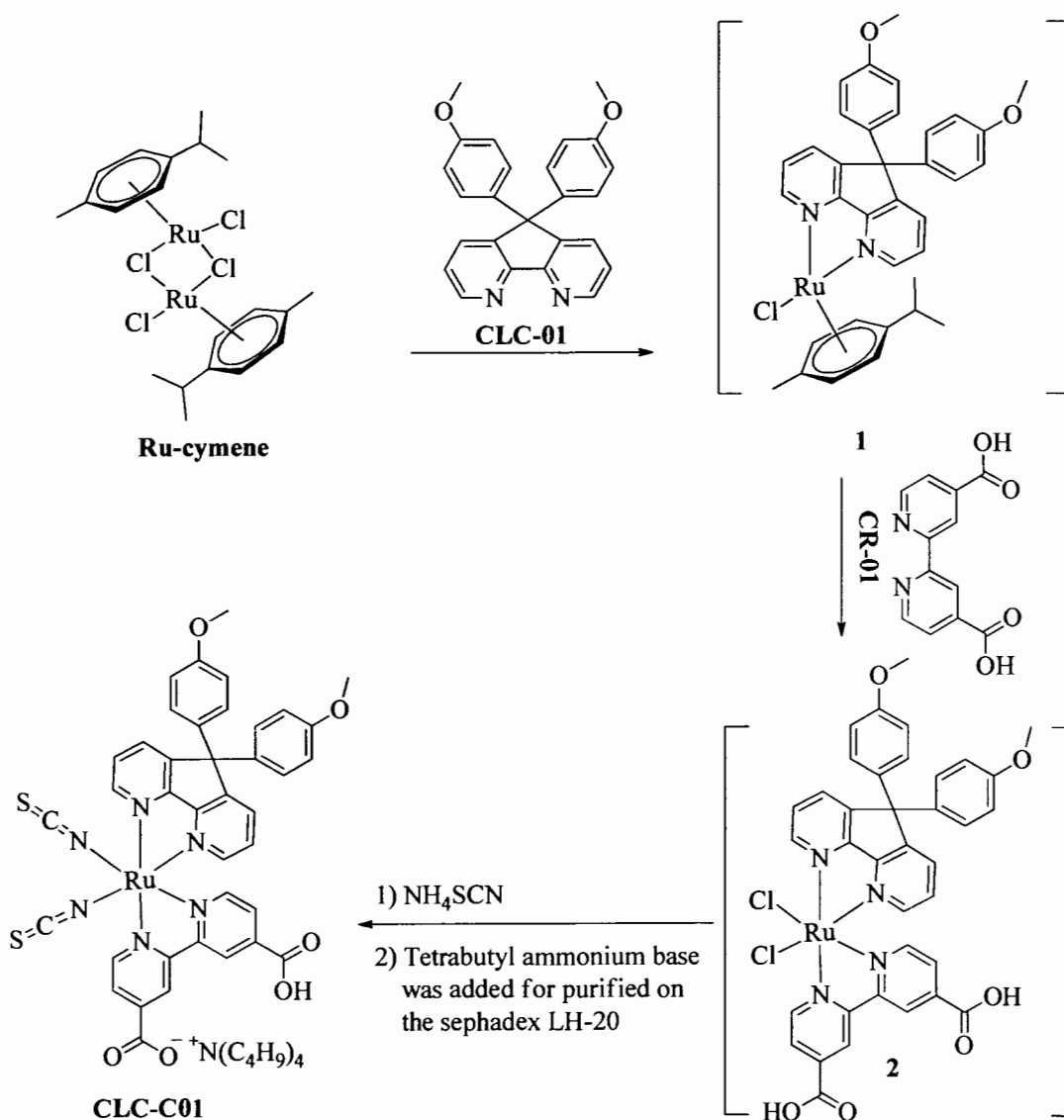


Figure 4.26 The synthesis of CLC-C01 dye

The **CLC-C01** was characterized by ^1H NMR, ^{13}C NMR, FTIR, and MS (APPENDICES, Figure 10). The ^1H NMR spectrum is shown in Figure 4.27. The signals at chemical shift at 9.69 (1H), 9.03 (2H), 8.92 (1H), 8.24 (2H), 8.14 (2H), 7.84 - 7.80 (2H), 7.78 - 7.70 (1H), 7.44 - 7.36 (1H), 7.21 (2H), 7.12 (2H), 6.88 (4H) ppm were assigned to aromatic protons of **CR-01** and **CLC-01** ligands. The signals at chemical shift 3.90 - 3.72 (6H) ppm was assigned to methyl group of **CLC-01** ligand. The proton signal corresponding to 36 protons of tetrabutyl ammonium base show at chemical shift 3.30 to 1.04 ppm.

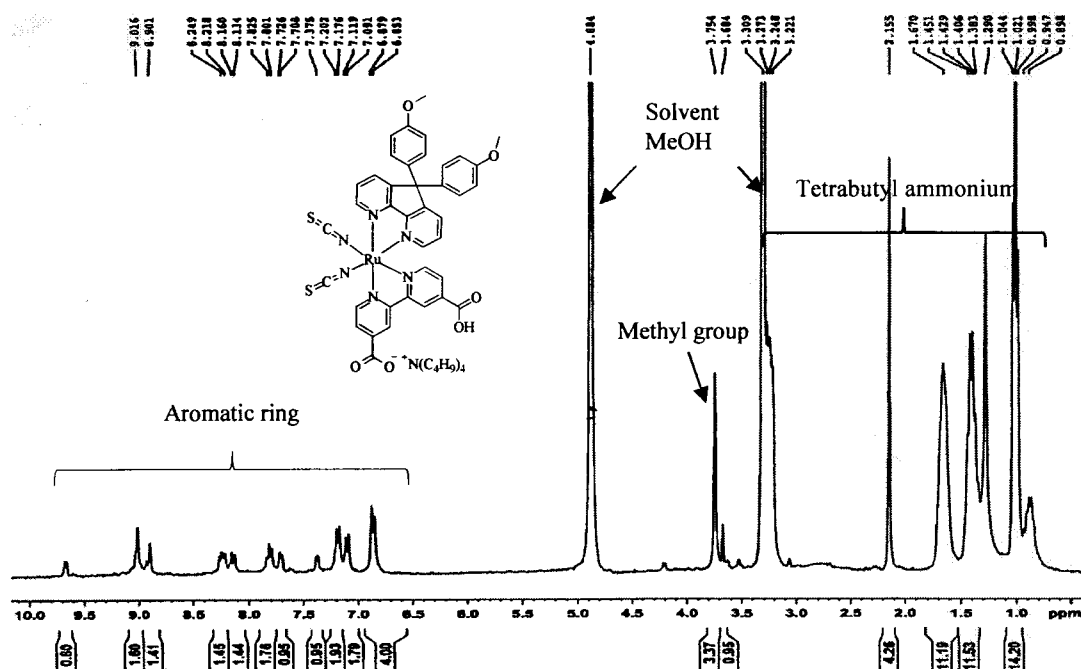
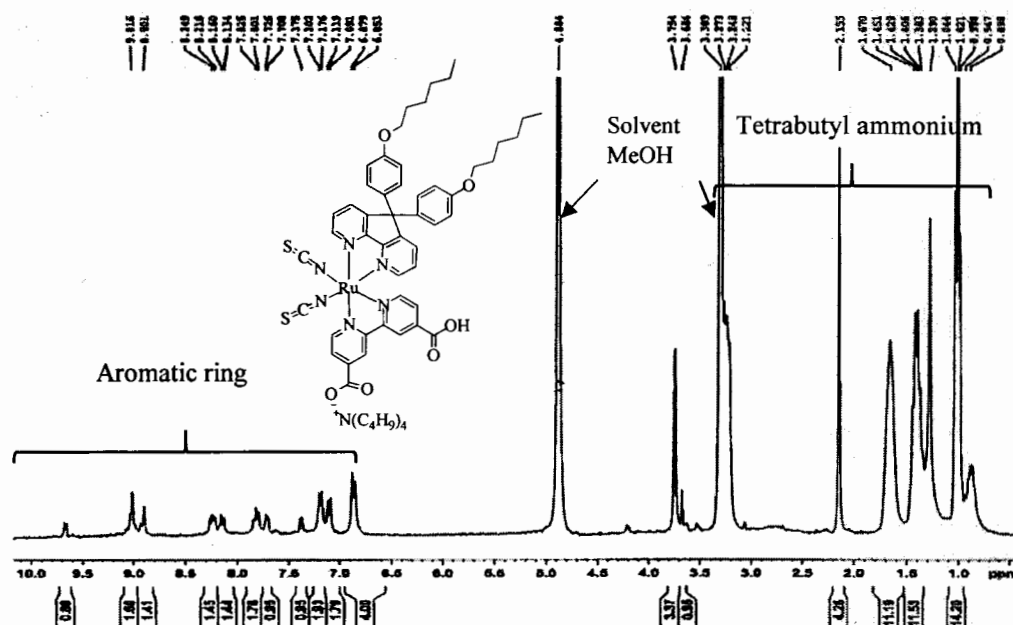


Figure 4.27 The ^1H NMR spectrum of the CLC-C01 in CD_3OD

4.2.5 The synthesis of tetrabutyl ammonium(4-carboxylate-4'-carboxy-2-bipyridine)-5,5'-bis(4''-(hexyloxy)phenyl-5*H*-cyclopenta(1,2-*b*:5,4-*b*')(dipyridine)dithiocyanato ruthenium(II) (CLC-C06)

The synthesis procedure of CLC-C06 is similar to CLC-C01 by the one pot reaction *via* the ligands exchange reaction. The Ru(*cymene*) was reacted with the CLC-06 ligand and CR-1 ligand in DMF solution, respectively. Then, NH_4SCN (excess) was added to the reaction mixture. The mixture product was dissolved in tetrabutyl ammonium base and further purified on the sephadex LH-20 column chromatography with methanol as eluent. The main band was precipitated with HNO_3 acid to obtain CLC-C06. The CLC-C06 was characterized by ^1H NMR, FTIR and MS (APPENDICES, Figure 11). The ^1H NMR spectrums are shown in Figure 4.28. The 20 proton signals of aromatic position protons on CR-01 and CLC-06 ligands were observed at chemical shift at 9.66 (1H), 9.01 (2H), 8.90 (1H), 8.24 - 8.13 (4H), 7.81 (2H), 7.77 (1H), 7.38 (1H), 7.18 (2H), 7.10 (2H) and 6.86 (4H) ppm. The signals at chemical shift 3.75 to 0.89 ppm were attributed to 62 protons of tetrabutyl ammonium base and alkyl long chains of CLC-06 ligands.



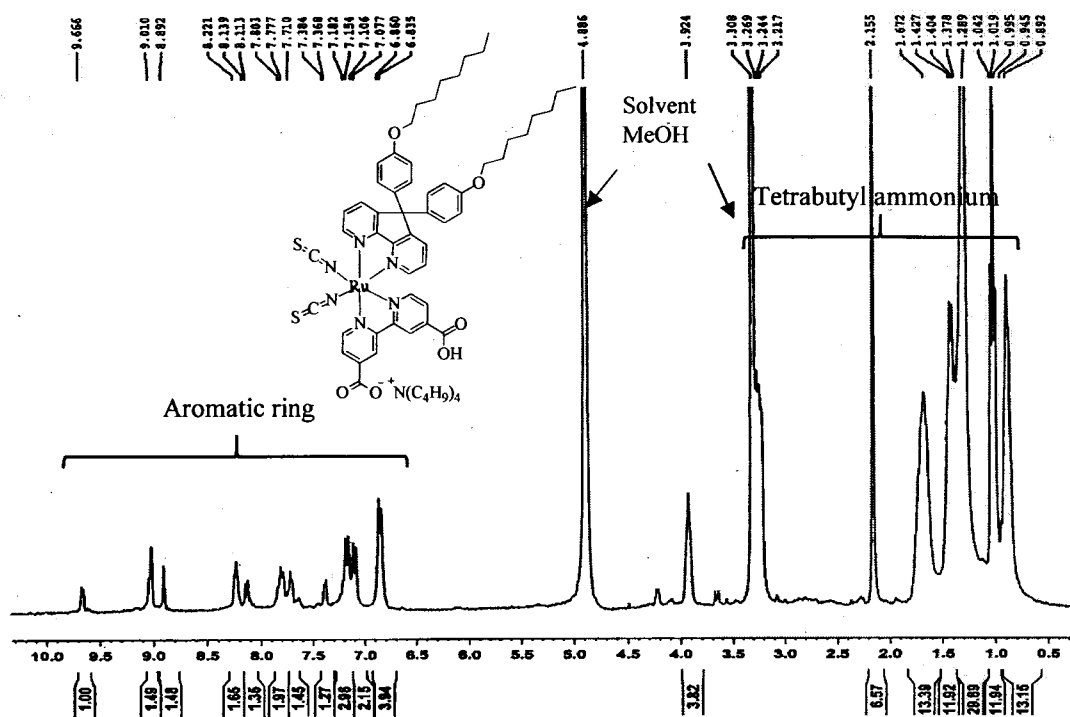


Figure 4.29 The ¹H NMR spectrum of the CLC-C08 in CD₃OD

4.3 Optical properties

The absorption spectra of the ruthenium complexes in ethanol solution are displayed in Figure 4.30 and summarized in Table 4.4. From the result, it was found that the CLC-C01 show two maximum absorption wavelength, from metal-to-ligand charge transfer bands (MLCT) at 382 nm and 521 nm with a molar extinction coefficient of $0.66 \times 10^4 \text{ M}^{-1} \text{ cm}^{-1}$ and $0.60 \times 10^4 \text{ M}^{-1} \text{ cm}^{-1}$, respectively. The MLCT of CLC-C06 was observed at 379 nm, ($\epsilon = 0.68 \times 10^4 \text{ M}^{-1} \text{ cm}^{-1}$) and 521 nm, ($\epsilon = 0.65 \times 10^4 \text{ M}^{-1} \text{ cm}^{-1}$) and CLC-C08 was found at 375 nm, ($\epsilon = 0.63 \times 10^4 \text{ M}^{-1} \text{ cm}^{-1}$) and 519 nm, ($\epsilon = 0.64 \times 10^4 \text{ M}^{-1} \text{ cm}^{-1}$). When compare with the N719, the CLC-C01, CLC-C06 and CLC-C08 sensitizers show similar maximum wavelength as observed in N719 with slightly blue-shifted (by 10 nm) due to the different of d to π^* affected to the molar extinction coefficient. The standard N719 dye shows the absorption band of MLCT at 392 nm, $1.47 \times 10^4 \text{ M}^{-1} \text{ cm}^{-1}$ and at 532 nm, $1.55 \times 10^4 \text{ M}^{-1} \text{ cm}^{-1}$, higher than those about twice new ruthenium complexes.

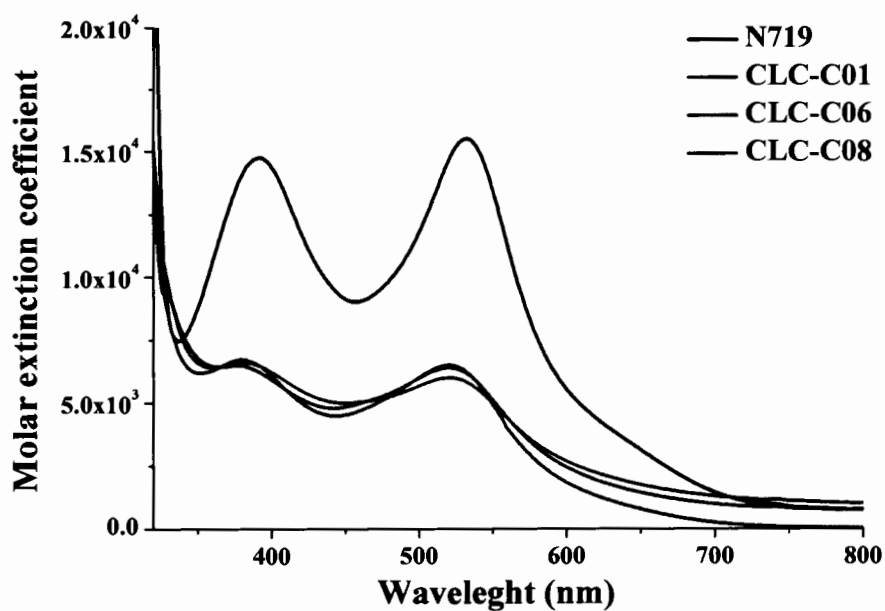


Figure 4.30 UV-Vis spectra of N719, CLC-C01, CLC-C06 and CLC-C08 in ethanol solution

Table 4.4 The absorption of N719, CLC-C01, CLC-C06 and CLC-C08 in ethanol solution

Dye	λ_{\max} (nm)	ϵ ($M^{-1}.cm^{-1}$)
N719	392, 532	1.47×10^4 , 1.55×10^4
CLC-C01	382, 521	0.66×10^4 , 0.60×10^4
CLC-C06	379, 521	0.68×10^4 , 0.65×10^4
CLC-C08	376, 520	0.63×10^4 , 0.64×10^4

4.4 The photovoltaic performance characteristics of DSSCs

4.4.1 Incident photon to current conversion efficiency (IPCE)

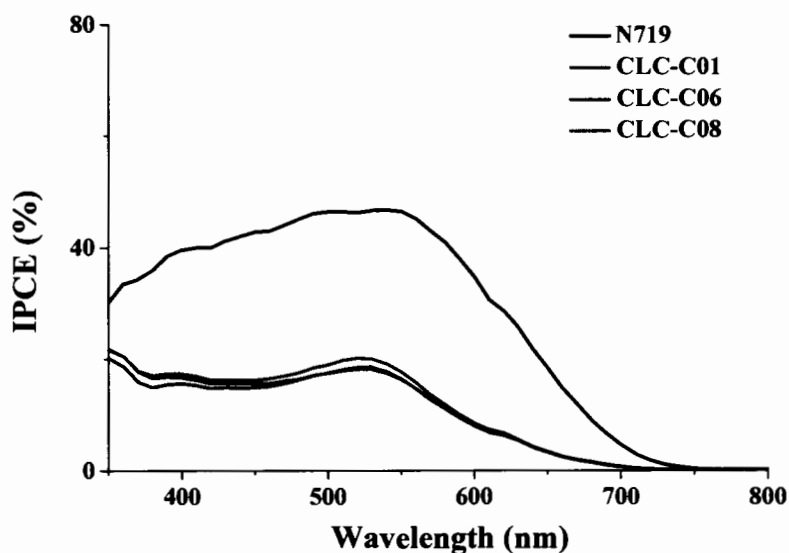


Figure 4.31 Incident photon to current conversion efficiency (IPCE) of N719, CLC-C01, CLC-C06 and CLC-C08

The incident photon to current conversion efficiency (IPCE) of devices based on N719, CLC-C01, CLC-C06 and CLC-C08 are shown in Figure 4.31. The N719 is a high harvesting UV-Vis, therefore effect to high conversion photon-to-current lead to high IPCE. All new dyes show similar IPCE values, the broad IPCE curve covers almost the entire visible spectrum from 350 to 700 nm, reaching maximum of 18-20% at 520 nm. Whereas, N719 show highest IPCE values, the broad IPCE curve covers visible spectrum from 350 to 750 nm, reaching maximum of 46% at 540 nm. Due to the twice lower in UV-Vis absorption spectra of new dyes, as expected, all new dyes give twice lower in IPCE compare to that N719.

4.4.2 The I - V characteristic (η) for DSSCs of N719 and new dyes

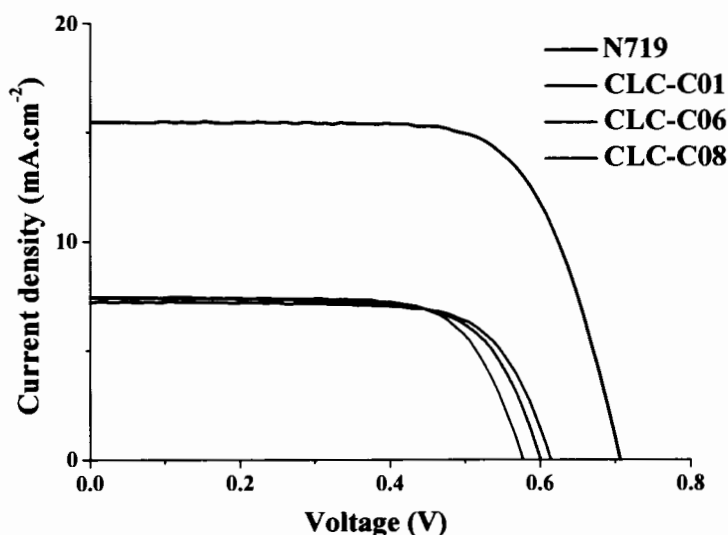


Figure 4.32 The I - V curve of DSSCs based on N719, CLC-C01, CLC-C06 and CLC-C08

The I - V characteristic of the DSSCs is shown Figure 4.32. Overall performance including J_{sc} , V_{oc} , ff and η are summarized in Table 4.5. It was found that, CLC-C01, CLC-C06 and CLC-C08 show efficiency of 3.08%, 3.18% and 3.14%, respectively, compared with N719 of 7.80%. The higher efficiency of N719 can be explained from its small molecule resulting more dye adsorbed on TiO_2 surface improving the J_{sc} leading to high performance. However, the CLC-C06 and CLC-C08 containing of alkyl long chains were found to increase the hydrophobicity in the surface of dye sensitizers that reduce the charge recombination which then improved the V_{oc} when compare with CLC-C01.

Table 4.5 The photovoltaic parameters of N719, CLC-C01, CLC-C06 and CLC-C08

Dye	$\% \eta$	J_{sc} (mA.cm ⁻²)	V_{oc} (V)	ff
N719	7.80	15.59	0.71	0.70
CLC-C01	3.08	7.42	0.58	0.72
CLC-C06	3.18	7.37	0.61	0.70
CLC-C08	3.14	7.19	0.60	0.72

4.5 The photovoltaic performance characteristics for stability test of DSSCs

We studied long term stability (Figure 4.33) and photocurrent density (Figure 4.34) based on CLC-C01, CLC-C06 and CLC-C08 compared with N719 for 1000 h.

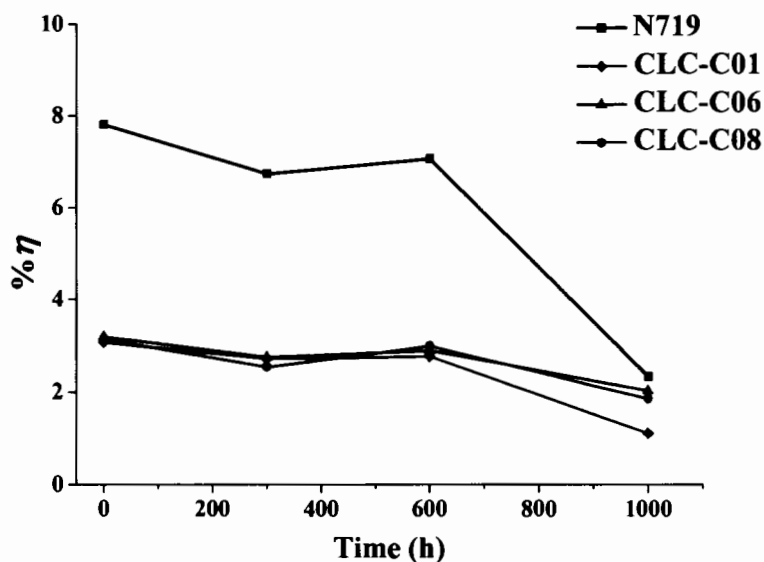


Figure 4.33 The efficiencies variations with aging time (1000 h) for the device based on CLC-C01, CLC-C06, CLC-C08 and N719

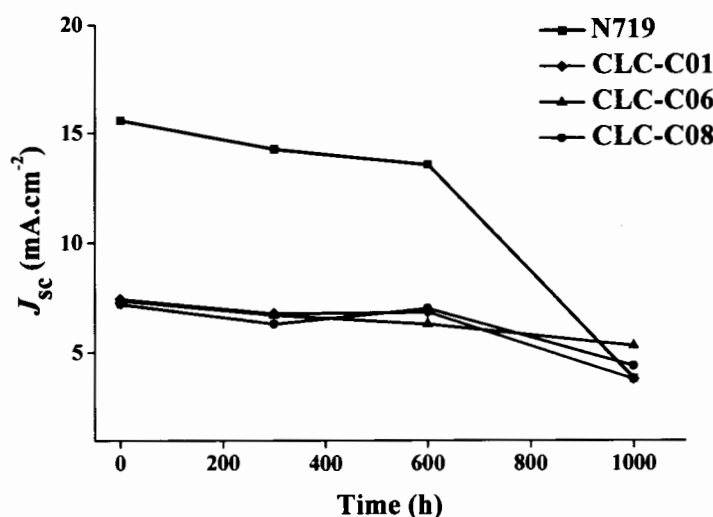


Figure 4.34 Photocurrent density variations with aging time (1000 h) for the device based on CLC-C01, CLC-C06, CLC-C08 and N719

From long term stability, the cell based on **CLC-C01**, **CLC-C06** and **CLC-C08** sensitizer show an excellent photochemical stability when compared with the **N719** sensitizer, measured during 1000 h. From stability test, the **N719** show long term stability up to 600 h, whereas the new dyes show long term stability up to 1000 h. This can be explained by the decrease of efficiency ($\% \eta_{loss}$) and photocurrent density ($\% J_{loss}$) of the DSSCs from each period (see Table 4.6). From 0 to 300 h, all new dyes show small drop in η and J_{sc} ($\% \eta_{loss}$ and $\% J_{loss}$) less than that **N719**. From 0 to 600 h, the **N719**, **CLC-C01**, **CLC-C06** and **CLC-C08** show slightly drop of $\% \eta_{loss}$ and $\% J_{loss}$ (less than 15%). After 600 h, the new dyes show higher stability than **N719**. At 1000 h, the **N719** show a large drop of $\% \eta_{loss}$ and $\% J_{loss}$ (more than 70%). Whereas, the $\% \eta_{loss}$ and $\% J_{loss}$ of new dyes were found that about 36 - 63% and 28 - 49%, respectively. The effect of hydrophobicity was investigated. It was found that, the **CLC-C06** and **CLC-C08** with the alkyl longer chain length compare to **CLC-C01**, show $\% \eta_{loss}$ and $\% J_{loss}$ lower than that **CLC-C01** (methyl), $\% \eta_{loss}$ about of 36 - 41% and $\% J_{loss}$ of 28 - 39%. These results can be explained as the alkyl chains attached to the new dyes, then suppress the charge recombination. In addition, they can inhibit the interaction between the electrolyte and the TiO_2 surface lead to the reduction to desorption of dye on surface TiO_2 which enhanced long term stability in DSSCs.

Table 4.6 The photovoltaic parameters of N719, CLC-C01, CLC-C06 and CLC-C08 for stability test during 1000 h

Dye	Time (h)	Parameters			
		η (%)	$\% \eta_{loss}$	J_{sc} (mA.cm ⁻²)	$\% J_{loss}$
N719	0	7.80	0	15.59	0
	300	6.73	14	14.27	8
	600	7.05	10	13.57	13
	1000	2.33	70	3.82	75
CLC-C01	0	3.08	0	7.42	0
	300	2.72	12	6.76	9
	600	2.76	10	6.84	8
	1000	1.12	63	3.80	49
CLC-C06	0	3.18	0	7.37	0
	300	2.76	13	6.72	9
	600	2.90	9	6.63	10
	1000	2.04	36	5.33	28
CLC-C08	0	3.14	0	7.19	0
	300	2.55	19	6.30	12
	600	2.99	5	7.00	3
	1000	1.86	41	4.40	39

CHAPTER 5

CONCLUSIONS

Novel ruthenium complexes dyes for DSSCs were successfully synthesized from one-pot reaction by ligand substitution reaction. The structural of ligands and ruthenium complexes were characterized by using NMR, FTIR and MS.

First part, the synthetic N3s dye were studied compared with the commercial N3 dye. The N3-1 is commercial dye whereas N3-2 to N3-5 were synthesized from fourth reaction set up. All N3 dyes show exactly the same ¹H NMR in aromatic region. The TGA and FTIR were used for measuring water and methanol residues in N3s. From TGA, the order of %WL₁₀₀ are N3-1 > N3-5 > N3-3 > N3-2 > N3-4. This result correspond to order of hydroxyl (-OH) to carbonyl (-C=O) ratio from FTIR. Then, the N3s were fabricated and studied their power conversion efficiency. It was found that, the power conversion efficiencies observed N3s are varied from 4.54 to 5.92%. The order of power conversion efficiencies are in agreement with the TGA and FTIR data, higher water and methanol residue give higher efficiency. These results clearly seen that the water and methanol residual in the complexes dye show significantly influence in the DSSC performances. The methanol and water containing in the complex improve the N3s solubility that cause dyes absorption more on the TiO₂ surface leading to high efficiency. Moreover, the crystallinity of N3-1 to N3-5 were determined by PXRD. The result shows that all N3s give similar PXRD pattern. The average roughness (R_a) of coated TiO₂ and bare TiO₂ were studied by AFM technique, the N3s show similar roughness (≈ 85 nm).

Second part, a new ruthenium complexes dye with different alkyl long chains, which are methyl (CLC-C01), hexyl (CLC-C06) and octyl (CLC-C08) were synthesized. It was found that, the CLC-C01, CLC-C06 and CLC-C08 show efficiency of 3.08%, 3.18% and 3.14%, respectively, compared with standard N719 (7.80%). The lower power conversion efficiency of these new ruthenium complexes compare to N719 due to their lower molar absorptions coefficient in visible absorption affected from lower light harvesting leading to lower efficiency than of N719.

However, in the long term stability tests, the new dyes show excellent photochemical stability (1000 h) comparing to the standard **N719**. Furthermore, the alkyl long chains on ancillary ligands of **CLC-C06** (hexyl) and **CLC-C08** (octyl) enhance the hydrophobicity at the surface of TiO₂, reducing the charge recombination and prevent the interaction between the electrolyte and surface of TiO₂. As a result, the desorption of dye molecules on TiO₂ surface are low, lead to the increasing of DSSCs stability long term.

The photovoltaic parameters of ruthenium(II) complexes in this study are summarized in Table 5.1 and parameters of stability test are summarized in Table 5.2.

Table 5.1 The photovoltaic parameters of ruthenium(II) complexes

Sample	η (%)	J_{sc} (mA/cm ²)	V_{oc} (V)	ff
N3-1	5.92	11.64	0.71	0.72
N3-2	4.71	9.94	0.65	0.73
N3-3	4.73	10.37	0.64	0.72
N3-4	4.54	10.16	0.61	0.73
N3-5	4.92	10.76	0.63	0.72
N719	7.80	15.59	0.71	0.70
CLC-C01	3.08	7.42	0.58	0.72
CLC-C06	3.18	7.37	0.61	0.70
CLC-C08	3.14	7.19	0.60	0.72

Table 5.2 The photovoltaic parameters of N719, CLC-C01, CLC-C06 and CLC-C08 for stability test during 1000 h

Dye	Time (h)	Parameters			
		η (%)	J_{sc} (mA.cm ⁻²)	V_{oc} (V)	ff
N719	0	7.80	15.59	0.71	0.70
	300	6.73	14.27	0.67	0.70
	600	7.05	13.57	0.72	0.72
	1000	2.33	3.82	0.79	0.77
CLC-C01	0	3.08	7.42	0.58	0.72
	300	2.72	6.76	0.57	0.69
	600	2.76	6.84	0.58	0.69
	1000	1.12	3.80	0.53	0.55
CLC-C06	0	3.18	7.37	0.61	0.70
	300	2.76	6.72	0.63	0.65
	600	2.90	6.63	0.61	0.72
	1000	2.04	5.33	0.61	0.62
CLC-C08	0	3.14	7.19	0.60	0.72
	300	2.55	6.30	0.63	0.64
	600	2.99	7.00	0.60	0.71
	1000	1.86	4.40	0.64	0.66

REFERENCES

REFERENCES

- [1] Green, M. A. "Radiative efficiency of state-of-the-art photovoltaic cells", **Progress in Photovoltaics: Research and Applications**. 20(4): 472-476; June, 2012.
- [2] O'Regan, B. and Gratzel, M. "A low-cost, high-efficiency solar cell based on dye-sensitized colloidal TiO₂ films", **Nature**. 353(6346): 737-740; October, 1991.
- [3] Mathew, S. and et al. "Dye-sensitized solar cells with 13% efficiency achieved through the molecular engineering of porphyrin sensitizers", **Nature chemistry**. 6(3): 242-247; February, 2014.
- [4] Kawashima, T. and et al. "New transparent conductive films: FTO coated ITO", **Thin Solid Films**. 445(2): 241-244; December, 2003.
- [5] Goto, K. and et al. "Heat-resisting TCO films for PV cells", **Solar energy materials and solar cells**. 90(18): 3251-3260; November, 2006.
- [6] Islam, A. and et al. "Synthesis and photophysical properties of ruthenium (II) charge transfer sensitizers containing 4, 4'-dicarboxy-2, 2'-biquinoline and 5, 8-dicarboxy-6,7-dihydro-dibenzo [1, 10]-phenanthroline", **Inorganica Chimica Acta**. 322(1): 7-16; October, 2001.
- [7] Lai, L.-F. and et al. "New fluorenone-containing organic photosensitizers for dye-sensitized solar cells", **Dyes and Pigments**. 98(3): 428-436; September, 2013.
- [8] Tan, H. and et al. "Phenoxazine-based organic dyes with different chromophores for dye-sensitized solar cells", **Organic Electronics**. 14(11): 2795-2801; November, 2013.
- [9] Campbell, W. M. and et al. "Porphyrins as light harvesters in the dye-sensitized TiO₂ solar cell", **Coordination Chemistry Reviews**. 248(13): 1363-1379; July, 2004.
- [10] Sirithip, K. and et al. "Synthesis and characterization of β -pyrrolic functionalized porphyrins as sensitizers for dye-sensitized solar cells", **Tetrahedron Letters**. 54(19): 2435-2439; May, 2013.

REFERENCES (CONTINUED)

- [11] Prompan, P., Wongkhan, K. and Jitchati, R. "Design and Synthesis of Ruthenium(II) Complexes and their Applications in Dye Sensitized Solar Cells (DSSCs)", **Advanced Materials Research**. 770: 92-95; September, 2013.
- [12] Wu, J. and et al. "Progress on the electrolytes for dye-sensitized solar cells", **Pure and Applied Chemistry**. 80(11): 2241-2258; October, 2008.
- [13] Yu, Z. and et al. "Investigation of iodine concentration effects in electrolytes for dye-sensitized solar cells", **The Journal of Physical Chemistry C**. 114(23): 10612-10620; May, 2010.
- [14] Lee, S.-H. A. and et al. "Influence of different iodide salts on the performance of dye-sensitized solar cells containing phosphazene-based nonvolatile electrolytes", **The Journal of Physical Chemistry C**. 114(35): 15234-15242; August, 2010.
- [15] Yu, Q. and et al. "High-efficiency dye-sensitized solar cells: the influence of lithium ions on exciton dissociation, charge recombination, and surface states", **ACS nano**. 4(10): 6032-6038; October, 2010.
- [16] Zeng, W. and et al. "Efficient dye-sensitized solar cells with an organic photosensitizer featuring orderly conjugated ethylenedioxythiophene and dithienosilole blocks", **Chemistry of Materials**. 22(5): 1915-1925; January, 2010.
- [17] Seo, K. D. and et al. "Novel D- π -A system based on zinc porphyrin dyes for dye-sensitized solar cells: Synthesis, electrochemical, and photovoltaic properties", **Dyes and Pigments**. 94(1): 143-149; July, 2012.
- [18] Wu, W. and et al. "Efficient and stable dye-sensitized solar cells based on phenothiazine sensitizers with thiophene units", **Journal of Materials Chemistry**. 20(9): 1772-1779; September, 2010.
- [19] Mikroyannidis, J. A. and et al. "Triphenylamine-and benzothiadiazole-based dyes with multiple acceptors for application in dye-sensitized solar cells", **Journal of Power Sources**. 195(9): 3002-3010; May, 2010.

REFERENCES (CONTINUED)

- [20] Jia, J. and et al. "Synthesis of dendritic triphenylamine derivatives for dye-sensitized solar cells", **Dyes and Pigments**. 96(2): 407-413; February, 2013.
- [21] Wang, Z.-S. and et al. "Thiophene-functionalized coumarin dye for efficient dye-sensitized solar cells: electron lifetime improved by coadsorption of deoxycholic acid", **The Journal of Physical Chemistry C**. 111(19): 7224-7230; April, 2007.
- [22] Hara, K. and et al. "Dye-sensitized nanocrystalline TiO₂ solar cells based on novel coumarin dyes", **Solar Energy Materials and Solar Cells**. 77(1): 89-103; April, 2003.
- [23] Hara, K. and et al. "Oligothiophene-containing coumarin dyes for efficient dye-sensitized solar cells", **The Journal of Physical Chemistry B**. 109(32): 15476-15482; July, 2005.
- [24] Ito, S. and et al. "High-Efficiency Organic-Dye-Sensitized Solar Cells Controlled by Nanocrystalline-TiO₂ Electrode Thickness", **Advanced Materials**. 18(9): 1202-1205; April, 2006.
- [25] Chang, Y. J. and Chow, T. J. "Dye-sensitized solar cell utilizing organic dyads containing triarylene conjugates", **Tetrahedron**. 65(24): 4726-4734; June, 2009.
- [26] Cheng, X. and et al. "Organic dyes incorporating the cyclopentadithiophene moiety for efficient dye-sensitized solar cells", **Dyes and Pigments**. 92(3): 1292-1299; March, 2012.
- [27] Lee, D. H. and et al. "Organic dyes incorporating low-band-gap chromophores based on π -extended benzothiadiazole for dye-sensitized solar cells", **Dyes and Pigments**. 91(2): 192-198; November, 2011.
- [28] Kuang, D. and et al. "Co-sensitization of organic dyes for efficient ionic liquid electrolyte-based dye-sensitized solar cells", **Langmuir**. 23(22): 10906-10909; September, 2007.

REFERENCES (CONTINUED)

- [29] Anderson, H. L. "Building molecular wires from the colours of life: conjugated porphyrin oligomers", **Chemical Communications**. 23: 2323-2330; July, 1999.
- [30] Brückner, C. and Dolphin, D. "2,3-vic-Dihydroxy-meso-tetraphenylchlorins from the osmium tetroxide oxidation of meso-tetraphenylporphyrin", **Tetrahedron Letters**. 36(19): 3295-3298; May, 1995.
- [31] Barea, E. M. and et al. "Porphyrin dyes with high injection and low recombination for highly efficient mesoscopic dye-sensitized solar cells", **The Journal of Physical Chemistry C**. 115(21): 10898-10902; May, 2011.
- [32] Liu, Y. and et al. "N-fused carbazole-zinc porphyrin-free-base porphyrin triad for efficient near-IR dye-sensitized solar cells", **Chemical Communications**. 47(13): 4010-4012; January, 2011.
- [33] Moonsin, P. and et al. "meso-Multi (iodophenyl) porphyrins: synthesis, isolation, and identification", **Tetrahedron Letters**. 52(37): 4795-4798; September, 2011.
- [34] Wang, Z.-S. and et al. "Significant efficiency improvement of the black dye-sensitized solar cell through protonation of TiO₂ films", **Langmuir**. 21(10): 4272-4276; April, 2005.
- [35] Kohle, O. and et al. "The photovoltaic stability of bis(isothiocyanato) ruthenium(II)-bis-2, 2' bipyridine-4, 4'-dicarboxylic acid and related sensitizers", **Advanced Materials**. 9(11): 904-906; October, 1997.
- [36] Nazeeruddin, M. K. and et al. "Engineering of efficient panchromatic sensitizers for nanocrystalline TiO₂ based solar cells", **Journal of the American Chemical Society**. 123(8): 1613-1624; February, 2001.
- [37] Nazeeruddin, M. K. and et al. "Conversion of light to electricity by cis-X₂bis(2, 2'-bipyridyl-4, 4'-dicarboxylate) ruthenium (II) charge-transfer sensitizers (X= Cl⁻, Br⁻, I⁻, CN⁻, and SCN⁻) on nanocrystalline titanium dioxide electrodes", **Journal of the American Chemical Society**. 115(14): 6382-6390; July, 1993.

REFERENCES (CONTINUED)

- [38] Gao, F. and et al. "Enhance the optical absorptivity of nanocrystalline TiO₂ film with high molar extinction coefficient ruthenium sensitizers for high performance dye-sensitized solar cells", **Journal of the American Chemical Society**. 130(32): 10720-10728; July, 2008.
- [39] Grätzel, M. "Recent advances in sensitized mesoscopic solar cells", **Accounts of Chemical Research**. 42(11): 1788-1798; August, 2009.
- [40] Hagfeldt, A. and Grätzel, M. "Molecular photovoltaics", **Accounts of Chemical Research**. 33(5): 269-277; May, 2000.
- [41] Wang, P. and et al. "A stable quasi-solid-state dye-sensitized solar cell with an amphiphilic ruthenium sensitizer and polymer gel electrolyte", **Nature materials**. 2(6): 402-407; May, 2003.
- [42] Ni, J.-S. and et al. "Effects of tethering alkyl chains for amphiphilic ruthenium complex dyes on their adsorption to titanium oxide and photovoltaic properties", **J Colloid Interface Sci**. 386(1): 359-365; November, 2012.
- [43] Schmidt-Mende, L. and et al. "Effect of hydrocarbon chain length of amphiphilic ruthenium dyes on solid-state dye-sensitized photovoltaics", **Nano Lett**. 5(7): 1315-1320; June, 2005.
- [44] Wang, P. and et al. "Stable new sensitizer with improved light harvesting for nanocrystalline dye-sensitized solar cells", **Advanced Materials**. 16(20): 1806-1811; October, 2004.
- [45] Wang, P. and et al. "A high molar extinction coefficient sensitizer for stable dye-sensitized solar cells", **Journal of the American Chemical Society**. 127(3): 808-809; December, 2005.
- [46] Kuang, D. and et al. "High-efficiency and stable mesoscopic dye-sensitized solar cells based on a high molar extinction coefficient ruthenium sensitizer and nonvolatile electrolyte", **Advanced Materials**. 19(8): 1133-1137; April, 2007.
- [47] Paek, S. and et al. "New type of ruthenium sensitizers with a triazole moiety as a bridging group", **Journal of Organometallic Chemistry**. 695(6): 821-826; March, 2010.

REFERENCES (CONTINUED)

- [48] Song, H.-K. and et al. "Synthesis of ruthenium complex and its application in dye-sensitized solar cells", **Journal of Industrial and Engineering Chemistry**. 15(1): 62-65; January, 2009.
- [49] Chen, C. Y. and et al. "A Ruthenium Complex with Superhigh Light-Harvesting Capacity for Dye-Sensitized Solar Cells", **Angewandte Chemie**. 118(35): 5954-5957; September, 2006.
- [50] Chen, C. Y. and et al. "Highly efficient light-harvesting ruthenium sensitizer for thin-film dye-sensitized solar cells", **ACS nano**. 3(10): 3103-3109; September, 2009.
- [51] Pootrakulchote, N. **Investigation on Functionalized Ruthenium-Based Sensitizers to Enhance Performance and Robustness of Dye-Sensitized Solar Cells**. Doctor's Thesis: Swiss Federal Institute of Technology in Lausanne, 2012.
- [52] Jitchati, R. and et al. "Three synthetic routes to a commercial N3 dye", **International Journal of Applied Physics and Mathematics**. 2(2): 107-110; March, 2012.
- [53] Nazeeruddin, M. K. and et al. "Acid-base equilibria of (2, 2'-bipyridyl-4, 4'-dicarboxylic acid) ruthenium(II) complexes and the effect of protonation on charge-transfer sensitization of nanocrystalline titania", **Inorganic Chemistry**. 38(26): 6298-6305; December, 1999.
- [54] Thongkasee, P. and et al. "Carbazole-dendrimer-based donor- π -acceptor type organic dyes for dye-sensitized solar cells: effect of the size of the carbazole dendritic donor", **ACS applied materials & interfaces**. 6(11): 8212-8222; May, 2014.
- [55] Zou, X. and et al. "TiCl₄ pretreatment and electrodeposition time investigations of ZnO photoelectrodes preparation for dye sensitized solar cells", **International Journal of Photoenergy**. 2014: 1-6; June, 2014.
- [56] Gao, R. and et al. "Interface modification effects of 4-tertbutylpyridine interacting with N3 molecules in quasi-solid dye-sensitized solar cells", **Physical Chemistry Chemical Physics**. 13(22): 10635-10640; May, 2011.

REFERENCES (CONTINUED)

- [57] Tian, Z. and et al. “Low-cost dyes based on methylthiophene for high-performance dye-sensitized solar cells”, **Dyes and Pigments**. 87(3): 181-187; November, 2010.
- [58] Kim, J. J. and Yoon, J. “A new ruthenium sensitizer containing dipyriddyamine ligand for effective nanocrystalline dye-sensitized solar cells”, **Inorganica Chimica Acta**. 394: 506-511; January, 2013.

APPENDICES

APPENDIX A
Characterization data

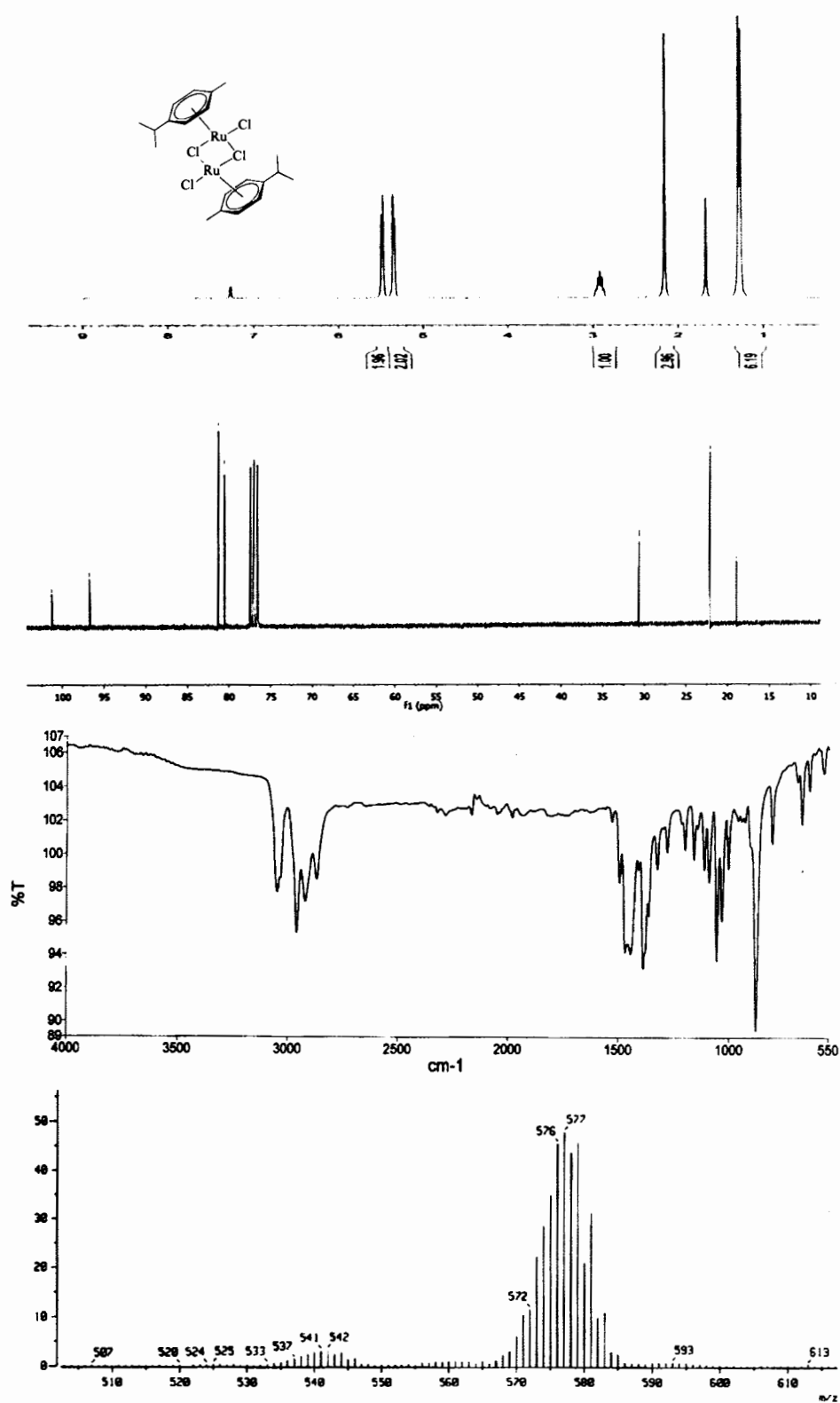


Figure 1 $^1\text{H NMR}$, $^{13}\text{C NMR}$ in CDCl_3 , FT-IR and mass spectra of di- μ -chloro(*p*-cymene)chlororuthenium(II) (Ru-cymene)

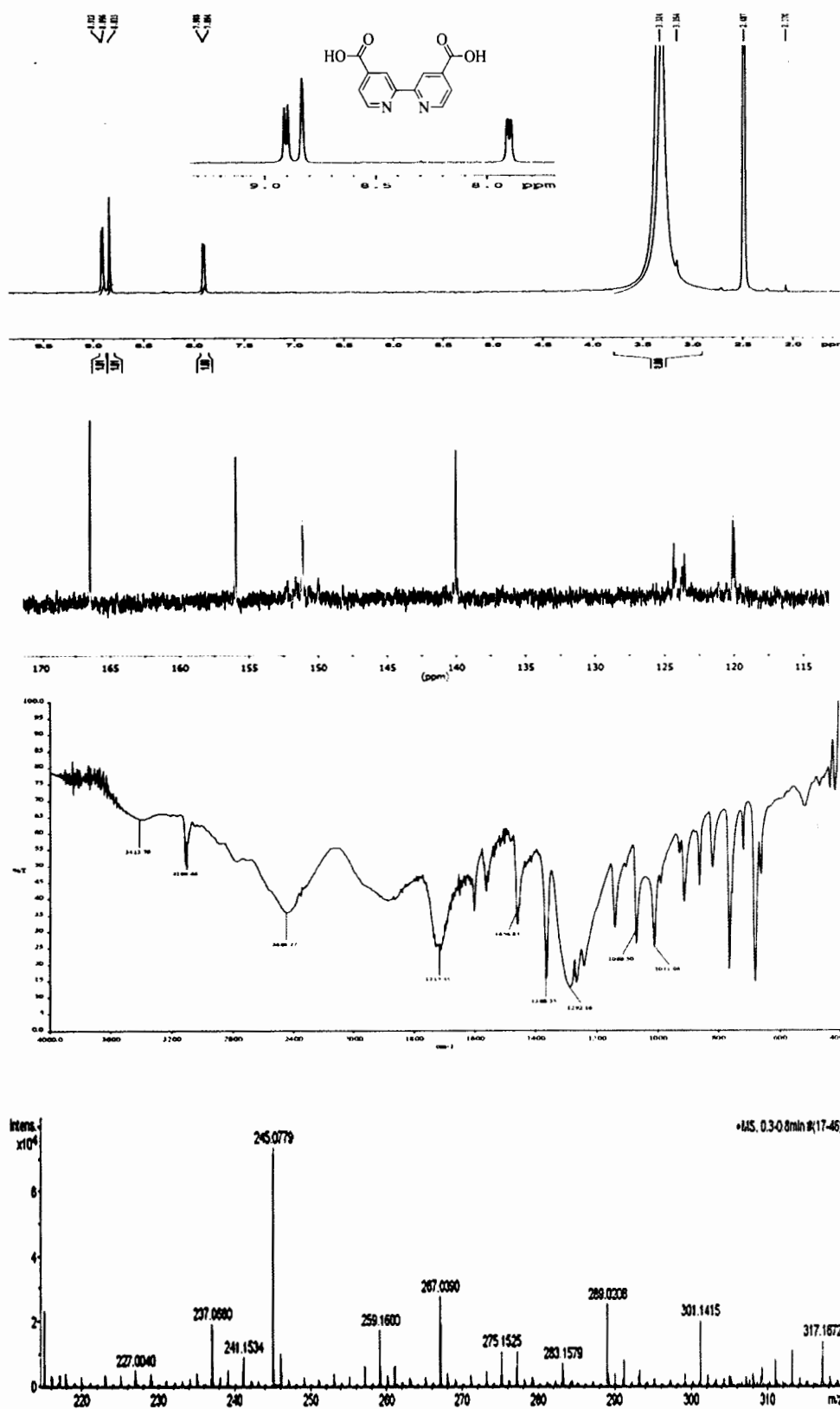


Figure 2 ^1H NMR in CDCl₃, ^{13}C NMR in DMSO-d₆, FT-IR and mass spectra of 4,4'-dicarboxylic-2,2'-bipyridine (CR-01)

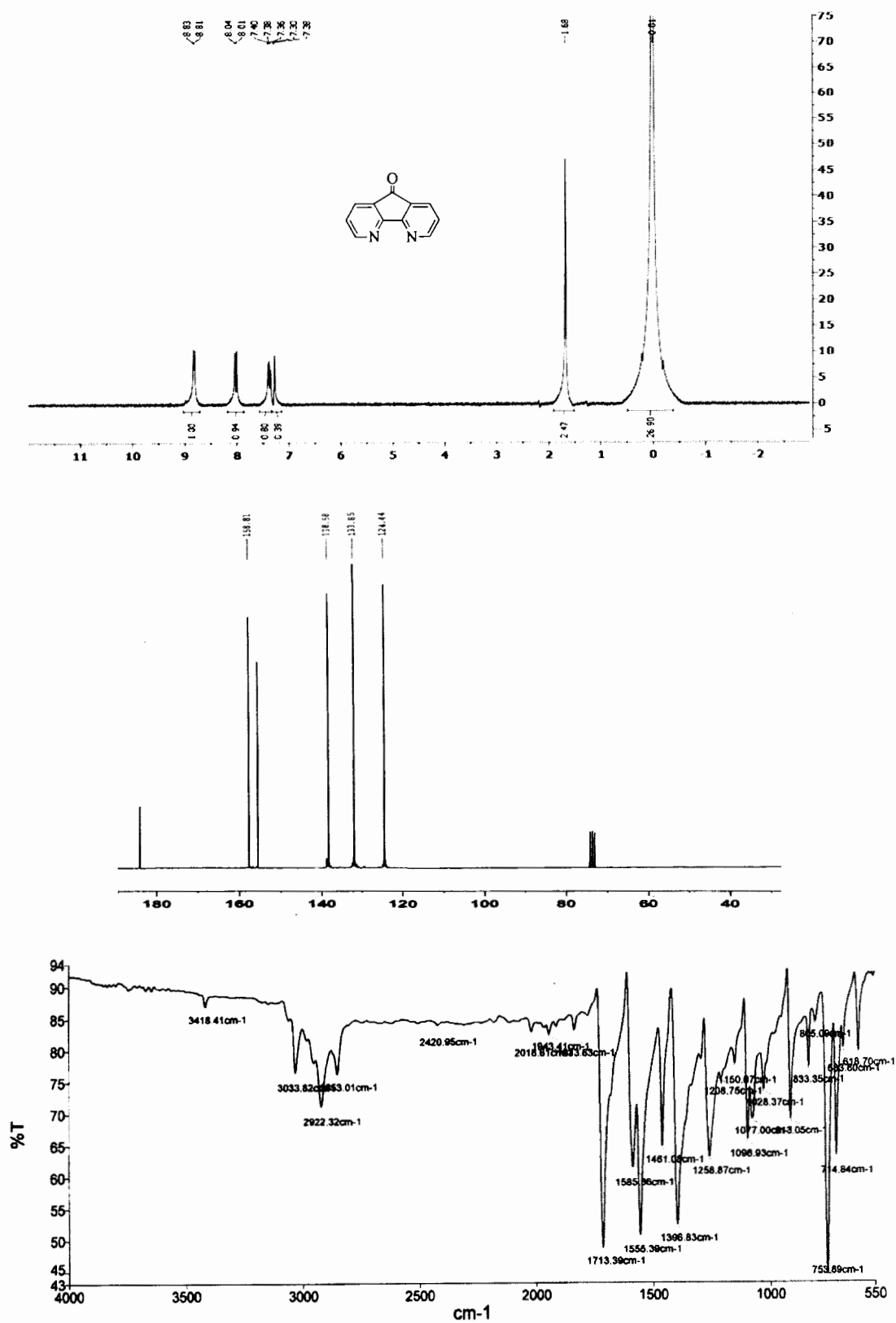


Figure 3 ^1H NMR, ^{13}C NMR in CDCl_3 and FT-IR spectra of 4,5-diazafluoren-9-one (MC-1)

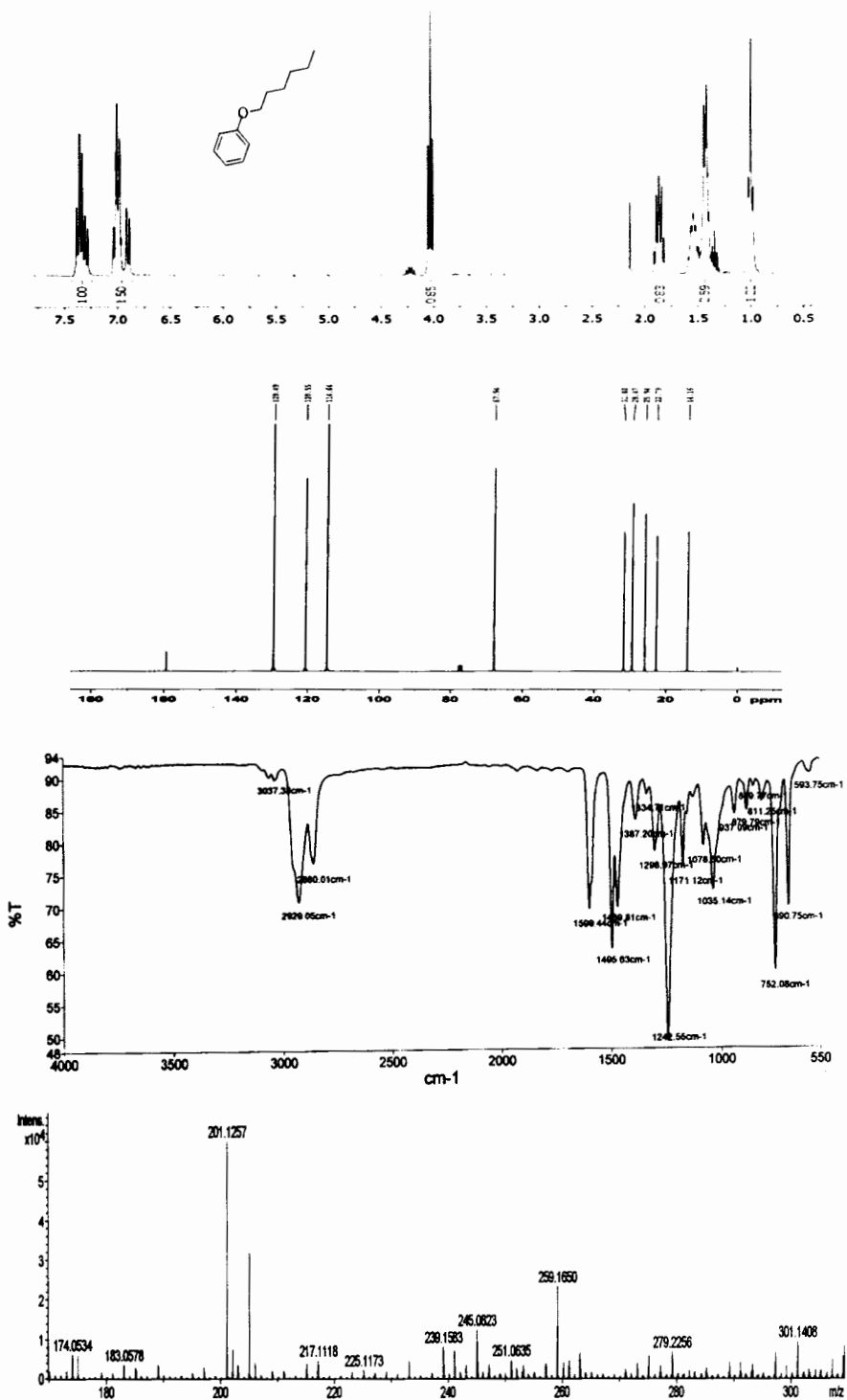


Figure 5 ^1H NMR, ^{13}C NMR in CDCl_3 , FT-IR and mass spectra of (hexyloxy)benzene (CL-06)

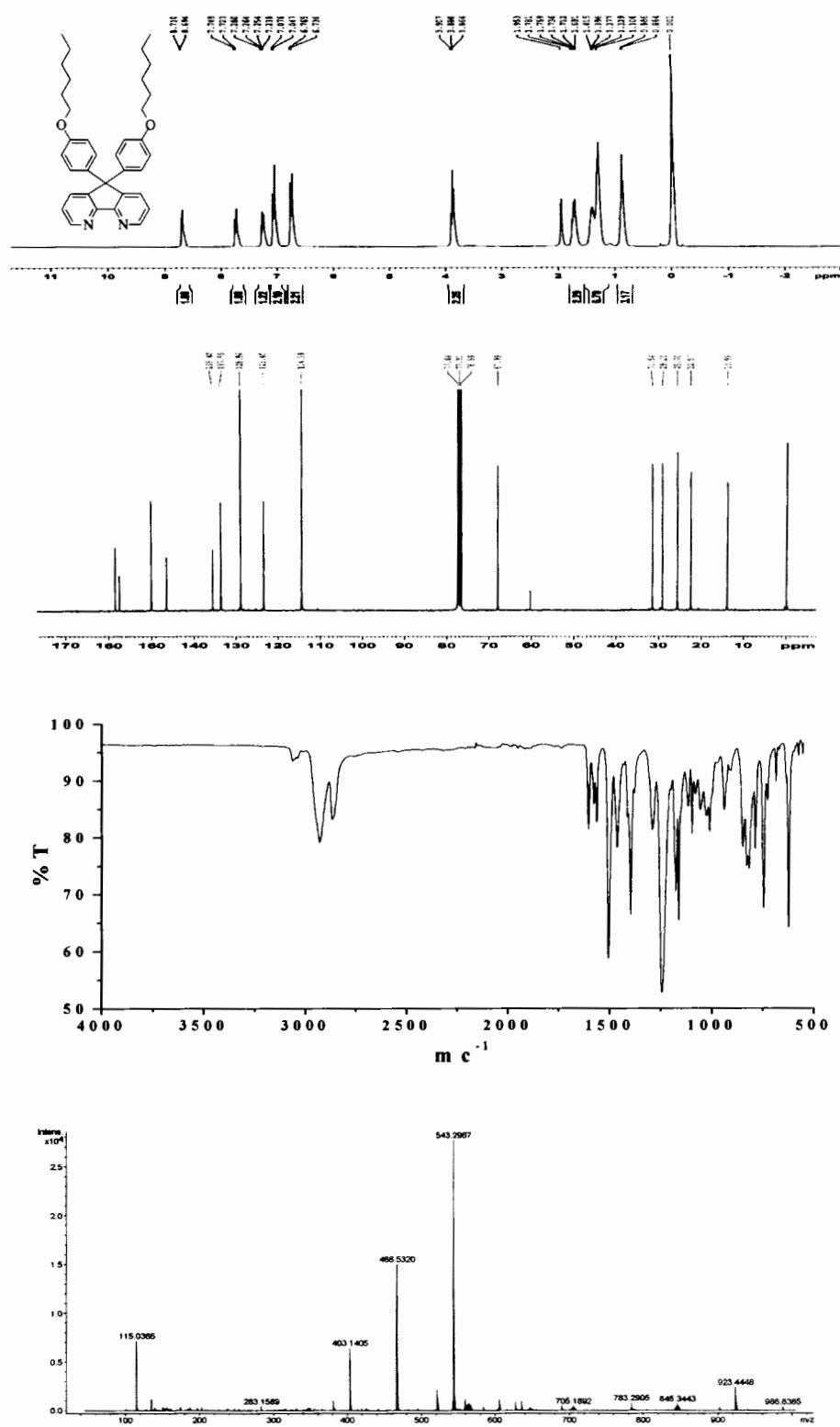


Figure 6 ^1H NMR, ^{13}C NMR in CDCl_3 , FT-IR and mass spectra of 5,5'-bis(4-hexyloxy) phenyl)-5H-cyclopenta(1,2-b:5,4-b')dipyridine (CLC-06)

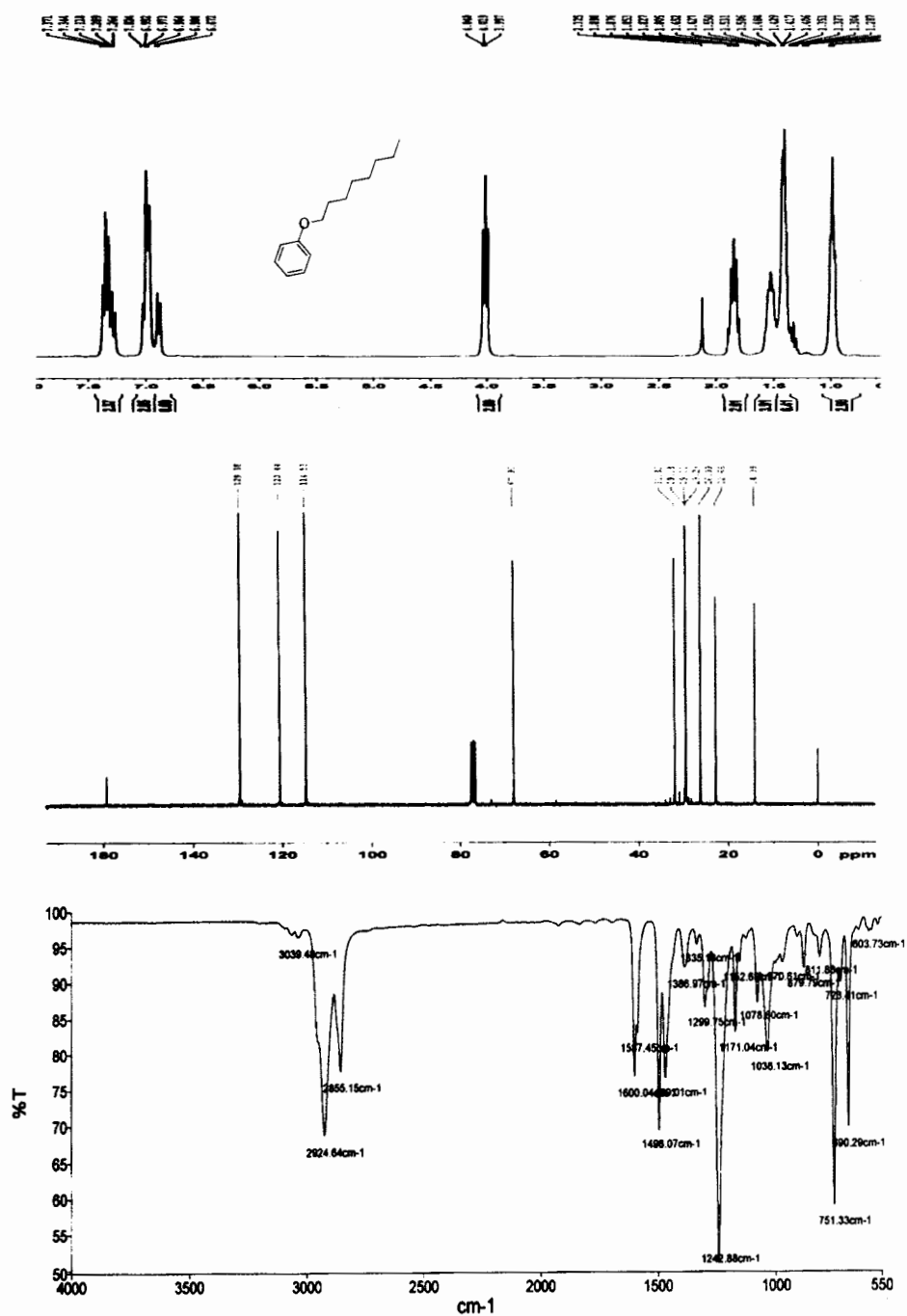


Figure 7 ^1H NMR, ^{13}C NMR in CDCl_3 and FT-IR spectra of (octyloxy)benzene (CL-08)

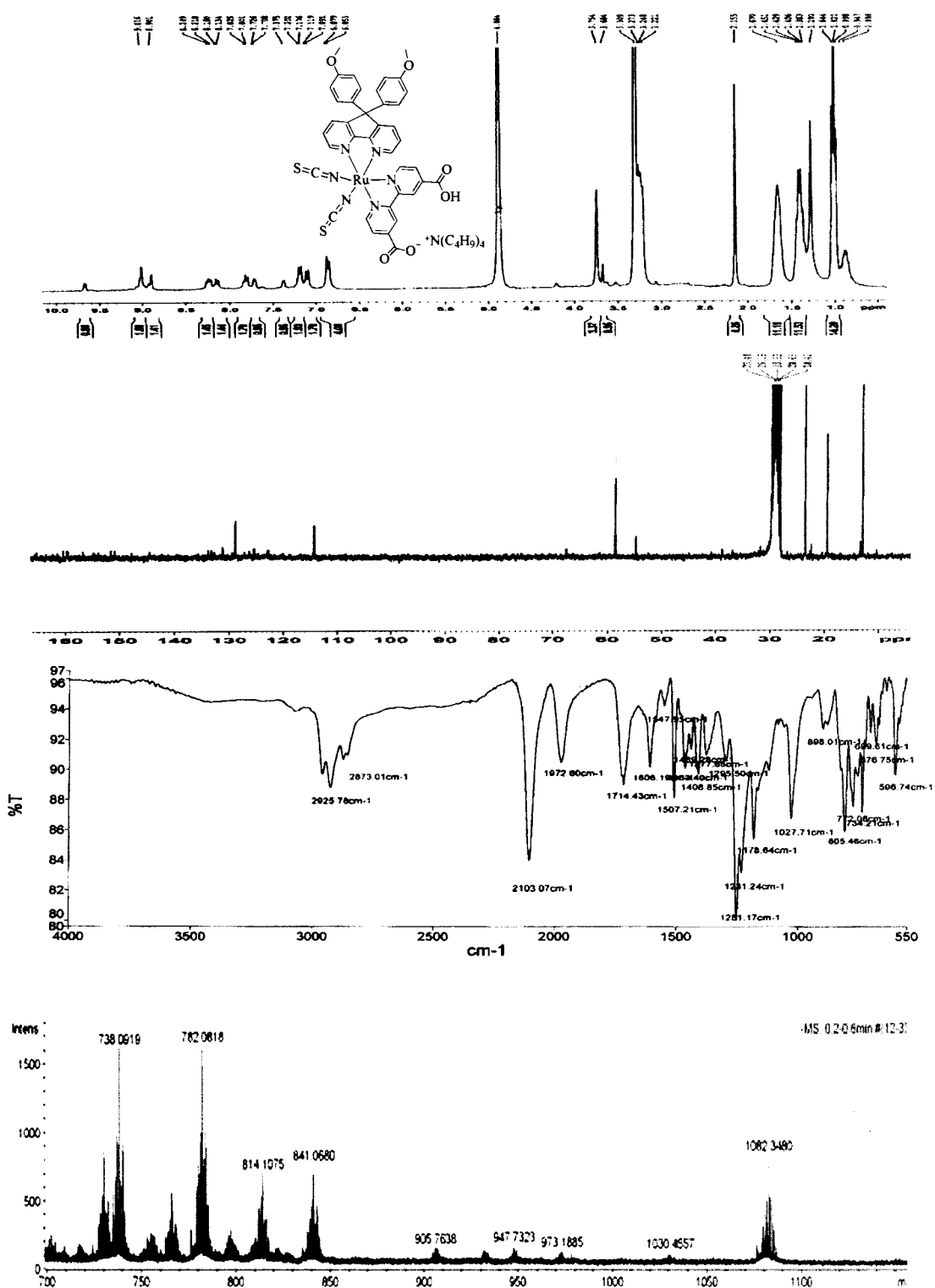


Figure 10 ¹H NMR, ¹³C NMR in CD₃OD, FT-IR and mass spectra and of tetrabutyl ammonium(4-carboxylate-4'-carboxy-2-bipyridine)-5,5'-bis(4''-(metyloxy) phenyl-5H-cyclopenta(1,2-b:5,4-b')(dipyridine) dithiocyanato ruthenium(II) (CLC-C01)

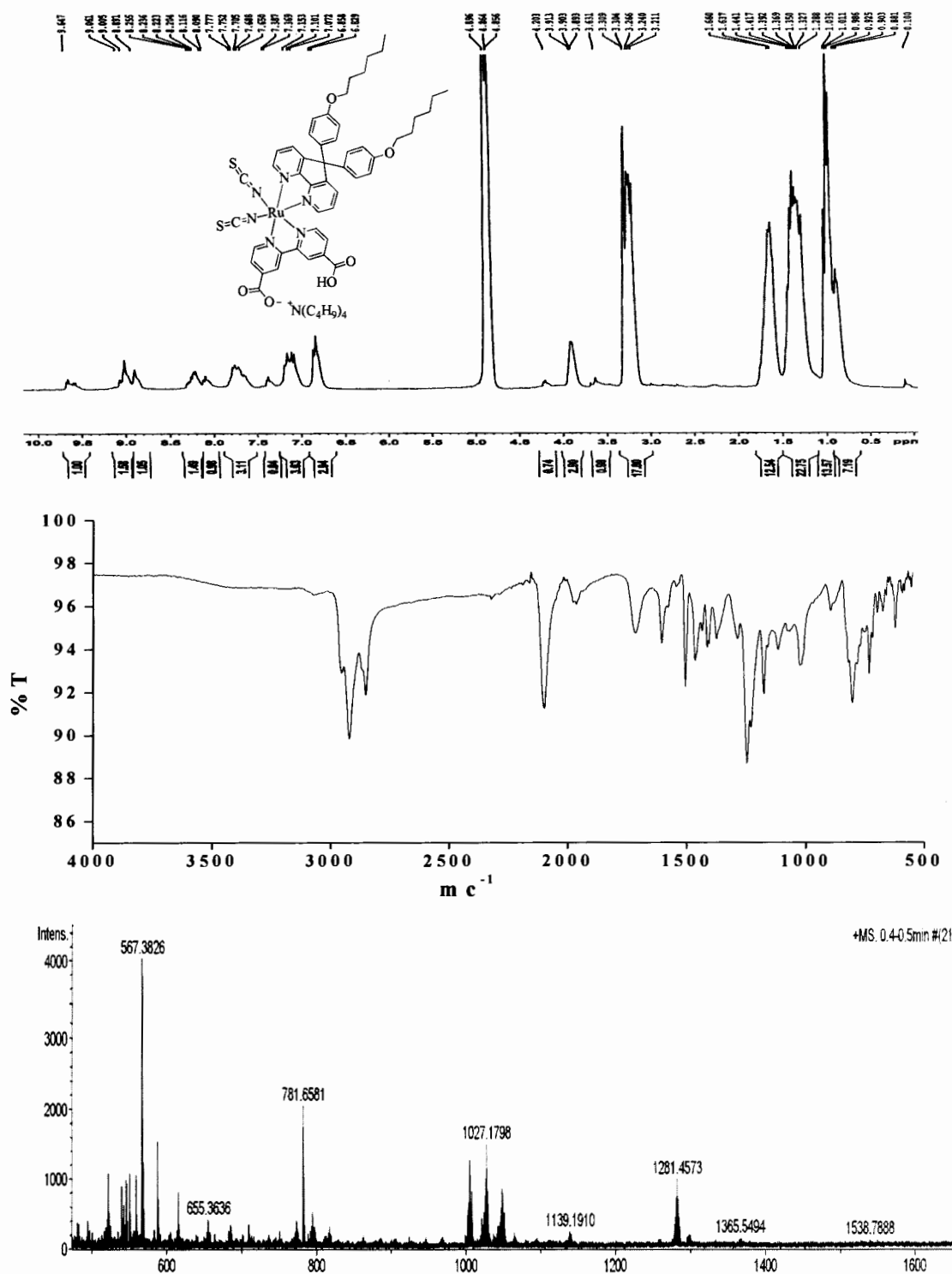


Figure 11 ¹H NMR in CD₃OD, FT-IR and mass spectra of tetrabutyl ammonium(4-carboxylate-4'-carboxy-2-bipyridine)-5,5'-bis(4''-(hexyloxy)phenyl)-5H-cyclopenta(1,2-b:5,4-b')(dipyridine)dithiocyanato ruthenium(II) (CLC-C06)

APPENDIX B
Publications

Comparison of the DSSC efficiency on synthetic N3 dyes

Chonchanok Talodthaisong, Kittiya Wongkhan, Taweesak Sudyoasuk

Sayant Saengsuwan and Rukkiat Jitchati^{a*}

Center for Organic Electronic and Alternative Energy (COEA), Department of Chemistry,
 Faculty of Science, Ubon Ratchathani University, Warinchumrap,

Ubon Ratchathani Province, 34190, Thailand

^arukkiat_j@hotmail.com

Keywords: DSSC; N3; solar cell

Abstract. *Cis*-di(thiocyanato)-bis(4,4'-dicarboxy-2,2'-bipyridine) ruthenium(II) (N3) has been used as the standard complex in the dye-sensitized solar cells (DSSCs). This research studies the N3s which are commercial (N3-1) and synthesized (N3-2 to N3-5) in DSSC as the dyes sensitizer. We found that the varied power efficiencies were observed from 4.54 to 5.92%. The TGA and FT-IR techniques were employed to measure the small molecules that cannot identify by NMR spectra. The results clearly seen that the N3s have a different content in water and methanol residuals which affect the N3s solubility leading to the varied performance in DSSCs.

Introduction

Energy is one of the most important factors to human life. Until now, the main energy source is the fossil fuel which is a non-renewable energy source. It produces a global warming and environmental pollution. To overcome these problems, the renewable and clean energy sources have been developed [1]. Silicon solar energy has been attracted which deploy power conversion efficiencies about 18-25% [2]. However, the synthesis steps of this type require high-purity silicon and skilled manufacturing techniques, which resulted in the construction and installation costs. Therefore, dye-sensitized solar cells (DSSCs) invented by O'Regan and Grätzel in 1991 have been interested as a new generation solar cells because of their low cost, easy preparation, high energy conversion efficiency [3-4]. The ruthenium complexes have been known as the best attractive materials [5-6]. The N3 has been accepted by the scientists around the world as the standard dye in the DSSCs field [7-10]. To deeply understanding, herein, we studied the commercial and synthetic N3s with thermal gravimetric analysis (TGA), Fourier transform infrared spectroscopy (FT-IR), X-ray diffraction (XRD), atomic forced microscopy (AFM) and power conversion efficiencies in DSSCs.

Experimental

The N3s were synthesized according to a recently one pot synthetic protocol [11]. The mixture product was purified by column chromatography with sephadex LH-20 and methanol. The main band was added DI water and precipitated with 0.01 M HNO₃ to obtain N3-2. The N3-3, N3-4 and N3-5 were synthesized similar method but they variously added DI water (18-20 mL). The ¹H NMR and ¹³C NMR in CD₃OD results show that all synthetic N3s show exactly the same spectra compared with commercial N3-1 (figure 1.).

The DSSC devices were fabricated following the literature [12]. The transparent (Ti-Nanoxide 20T/SP, Solaronix) and a scattering (Ti-Nanoxide R/SP, Solaronix) TiO₂ layer were prepared by a screen-printing method on a transparent FTO glass (8 Ω/sq, Solaronix) and then sintered at 450 °C for 30 minutes and cooled to 80 °C. The nanocrystalline TiO₂ films were coated with the dyes by dipping in 3×10⁻⁴ M solutions in ethanol overnight. The dye-coated TiO₂ electrode was incorporated into a thin-layer sandwich-type cell with a Pt-coated FTO as counter electrode, a spacer film, and an organic electrolyte solution to measure the solar cell performance. The Pt counter electrode was

VITAE

NAME	Mr. Chonchanok Talodthaisong
BORN	9 March 1990, Khonkaen, Thailand
EDUCATION	2008-2011, Bachelor's Degree of Science, Ubon Ratchathani University, Chemistry
RESEARCH GROUP	Organometallic and Catalytic Center (OCC)
SCHOLARSHIPS	Science Achievement Scholarship of Thailand (SAST), 2012
PUBLICATIONS	Chonchanok Talodthaisong, Kittiya Wongkhan, Taweesak Sudyoadsuk, Sayant Saengsuwan and Rukkiat Jitchati "Comparison of the DSSC efficiency on synthetic N3 dyes", Advanced Materials Research . 1131: 165-168; December, 2016
PRESENTATIONS	1) 2013 International Workshop on Dielectric Thin Films for Future Electron Devices Science and Technology. Poster presentation in the topic of "Comparison of the DSSC efficiency on synthetic N3 dye" at the University of Tsukuba (Tokyo Campus) Bunkyo-School Building, Tokyo Japan, 2013. 2) The 4 th Thailand International Nanotechnology Conference (Nano Thailand 2014). Oral Presentation in the topic of "Solubility: A Key Factor of N3 DSSCs Efficiencies" at Thailand Science Park Convention Center, Pathumthani, Thailand, 2014. 3) Pure and Applied Chemistry International Conference 2015 (PACCON 2015). Poster Presentation in the topic of "Novel Ruthenium Complexes for Dye Sensitized Solar Cell" at Amari Hotel, Watergate, Bangkok, Thailand, 2015.

